This is a preprint, the final version is subject to change, of the American Mineralogist (MSA)
Cite as Authors (Year) Title. American Mineralogist, in press.
(DOI will not work until issue is live.) DOI: http://dx.doi.org/10.2138/am.2013.4282

4282R2

Far-infrared spectra of synthetic dioctahedral muscovite and muscovite–tobelite series micas: Characterization and assignment of the interlayer I–O_{inner} and I–O_{outer} stretching bands

KIYOTAKA ISHIDA[1*] AND FRANK C. HAWTHORNE[2]

[1*]Department of Environmental Changes, Graduate School of Social and Cultural Studies, Kyushu University, 744 Motooka, Nishi-ku, Fukuoka 819-0395, Japan

[2] Department of Geological Sciences, University of Manitoba, Winnipeg, Manitoba R3T 2N2, Canada

Keywords: Far-infrared spectra, I–O_{inner} stretching band, I–O_{outer} stretching band, dioctahedral mica, muscovite, tobelite

Running title: FIR FOR MUSCOVITE

Written with Microsoft Office Word 2010

*: e-mail: kiyota@scs.kyushu-u.ac.jp

Fax:+81-92-802-5653

ABSTRACT

Far-infrared spectroscopy and X-ray diffraction Rietveld structure refinement for the hydrothermal synthetic muscovite series, (a) $KAl_3(Si_{3-y}Ge_y)O_{10}(OH,OD)_2$, (b) $KGa_3(Si_{3-y}Ge_y)O_{10}(OH,OD)_2$, and (c) $K(Al_{3-x}Ga_x)Ge_3O_{10}(OH,OD)_2$, where x = 0.0–3.0, y= 0.0–3.0, and the muscovite–tobelite series, (d) $[K_{1-A}(NH_4,ND_4)_A]Al_3Si_3O_{10}(OH,OD)_2$ where $_A$ = 0.0–1.0, indicate that there is complete solid-solution in each series. In the 200–50 cm^{-1} far-infrared region, four kinds of bands are observed: two bands due to octahedral deformation coupled with OH deformational vibrations between 240 and 130 cm^{-1}, an in-plane tetrahedral torsional band between 175 and 130 cm^{-1}, an interlayer $I–O_{inner}$ stretching band, and an $I–O_{outer}$ stretching band. The weak broad 140 cm^{-1} band is $K–O_{inner}$ stretching and the strong broad 110 cm^{-1} band is $K–O_{outer}$ stretching in muscovite. The broad 175 cm^{-1} band is $(NH_4/ND_4)–O_{inner}$ stretching and the 140 cm^{-1} broad strong band is $(NH_4/ND_4)–O_{outer}$ stretching in tobelite. With increasing Ga→Al substitution, the $I–O_{inner}$ and $I–O_{outer}$ stretching bands shift to lower frequency, while with increasing Ge→Si substitution, the $I–O_{inner}$ stretching band shifts to higher frequency; the $I–O_{outer}$ stretching bands do not change as a function of composition.

INTRODUCTION

Muscovite is the most common dioctahedral mica and tobelite is its ammonium analogue, where $(NH_4)^+$ ($r \sim 1.7$ Å) substitutes for K^+ ($r = 1.52$ Å) at the [12]-coordinated interlayer site (e.g. Higashi 1982; Harlov et al. 2001; Pöter et al. 2004). At reasonably oxidizing conditions, dehydration of NH_4-bearing micas during prograde metamorphism releases NH_4 which oxidizes to give N_2 and H_2O (Hovis et al., 2004) which are often incorporated as fluid inclusions in higher-grade minerals. Thus micas are of interest as a major player in the nitrogen cycle (Eugster and Munoz, 1966), and as an isotopic indicator of the origin of nitrogen (i.e., abiogenic versis biogenic) in the protolith .

The development of Fourier-Transform InfraRed (FTIR) spectroscopy has made possible the routine measurement of absorption spectra in the frequency range of the far-infrared (FIR): 300–30 cm^{-1}. FIR spectra of muscovite and various clay minerals have been reported by Ishii et al. (1967), Loh (1973), Farmer (1974), Tateyama et al. (1977), Velde (1978), Roth (1978), Fripiat (1982), Velde and Couty (1985), Prost and Laperche (1990), Schroeder (1990), Laperche and Prost (1991), Diaz et al. (2000), Boukilli et al. (2001), Mookherjee and Redfern (2002), Friedrich et al. (2006), and Zhang et al. (2010). The mid-IR spectra of ammonium in both synthetic and natural (NH_4/ND_4)-containing muscovite was described by Vedder (1965), Bokij and

Arkhipenko (1977), Shigorova et al. (1981), Higashi (1982), Shigorova (1982), Voncken et al. (1987), Bastoul et al. (1993), Harlov et al. (2001) and Zhang et al. (2010), and FIR spectra of micas have been reported by Mookherjee et al. (2004). Beran (2002) and Fleet (2003) reviewed FTIR work on micas, including the MIR and FIR regions. Ishida and Hawthorne (2011) reported FIR spectra of synthetic kinoshitalite (a trioctahedral brittle mica) in the range 200–50 cm^{-1}. They assigned three types of bands: (1) $I–O_{inner}$ stretching bands; (2) $I–O_{outer}$ stretching bands; (3) a torsional band of the tetrahedral sheet. Although many spectral studies have assigned the FIR bands in muscovite, no consistent relations have yet been found. The purpose of this paper is to characterize and assign the interlayer $I–O_{inner}$ and $I–O_{outer}$ stretching bands in several synthetic dioctahedral-mica solid-solutions, muscovites and muscovite–tobelite series micas, and to assign the two additional bands which appear in the 240–130 cm^{-1} region.

MATERIALS EXAMINED AND FIR METHOD

Synthesis experiments

Muscovites were synthesized hydrothermally at 435–615°C and 92–280 MPa for 134–1140 h in cold-seal externally heated Tuttle-type vessels (Table 1). The starting mixtures were made from reagent-grade oxides (Al_2O_3, Ga_2O_3, SiO_2, GeO_2) and carbonates (K_2CO_3). The starting materials were mixed and decarbonated by heating for

several hours at approximately 900°C in air, and then sealed in Au capsules (4.3 mm outer-diameter (OD) × 4.0 mm inner-diameter (ID) × 35 mm long) with about 20 wt% distilled H_2O or D_2O (99.9 % in purity). Tobelite components were added as ammonium or ammonium deuteride, 26 % NH_3 or ND_3 solutions in H_2O or D_2O, respectively. Kaolinite from the Lamar Pit, Barth, South Carolina, U.S.A., was used also for synthesis of end-member-composition tobelite.

SEM analysis

Synthesized materials were coated with gold in an evaporative coater and examined using a scanning electron microscope (SEM) model JEOL JSM–5600.

X-ray Rietveld analysis

Rietveld analysis was done as outlined in Ishida and Hawthorne (2011) using Rietan–2000 (Izumi and Ikeda 2000). For synthetic muscovites, the single-crystal data for muscovite GA1 of Brigatti et al. (1998), monoclinic, space group *C2/c*, $2M_1$ polytype with isotropic-displacement parameters, were used as the initial parameters for least-squares refinement. For synthetic muscovite–tobelite solid-solutions, the single-crystal data for polytypes $1M$ and $2M_2$ from Guggenheim (1981) were added to the $2M_1$ data. Three sets of results were averaged from separate Rietveld refinements of

the same sample.

FIR spectroscopy Spectra were recorded in the range 250–30 cm^{-1} with a JASCO FTIR-620 spectrometer equipped with a Hg-lamp power supply, a DLATGS (PE window) detector and a Mylar 12 μm beam-splitter. Each sample was scanned 512 times in an evacuated sample-chamber at a nominal resolution of 4 cm^{-1}.

RESULTS AND DISCUSSION

Products of synthesis

Table 1 shows the materials characterized in this study. Nominal aggregate ionic radii of the tetrahedrally coordinated cations, $<^{[4]}r>$, were calculated from the radii of Shannon (1976) ($^{[4]}$Al = 0.390, $^{[4]}$Ga = 0.47, $^{[4]}$Si = 0.26, $^{[4]}$Ge = 0.390 Å). In the Al- and Ga-bearing Si muscovite series, appreciable amounts of K- and ammonium-bearing feldspar (orthoclase and buddingtonite) and Ga_2O_3 were detected in the products. All micas produced from muscovite starting compositions consisted of 80–95 % $2M_1$ and 20–5 % 1*M* polytypes. The micas produced from muscovite–tobelite solid-solution compositions consisted of up to ~15% 1*M*, ~20% $2M_2$ and ~95% $2M_1$ polytypes. Nearly pure tobelite, mainly $2M_1$ with traces of quartz, was synthesized from kaolinite and ammonium solutions. As estimated from MIR OH/OD and NH_4/ND_4 stretching-band

intensities, micas synthesized from chemical reagents are more than 80% deuterated; micas synthesized from kaolinite are ~60 % deuterated.

SEM

The synthetic muscovite and tobelite crystals obtained in this study are foliate to blocky, up to 10 μm wide and 5 μm thick (Fig. 1). The products that show sharp XRD-patterns are blocky in appearance. The crystallinity of the mica produced tends to be higher with higher nominal Ge content.

X-ray Rietveld refinement

All samples refined contain dominant $2M_1$ polytype and minor 1*M* and/or $2M_2$ polytypes (Fig. 2). Relatively large amounts of Ga_2O_3 and were observed in $K(Al_{3-x}Ga_x)Si_3$-Ms micas, and (NH_4/ND_4)-bearing feldspar is present in the muscovite–tobelite series samples, but the resulting cell-parameters of the dominant micas are sufficient for discussion. Standard deviations for the mean bond lengths involving the T (= <T-O>), M (= <M1-O> and <M2-O>) and I (= <I–O_{inner}> and <I–O_{outer}>) sites are estimated as ±0.03, ±0.05 and ±0.06 Å, respectively; standard deviations of the bond angles are estimated as ±2˚. For the samples which obtained the acceptable structural parameters are given in the CIF file (labeled as CIF in the Tables;

deposit item #########). For the samples with poor structural parameters, <I–O_{inner}>, <I–O_{outer}>, and tetrahedral rotation angles (α) were also given in the Table 1, which are usufull for comparison.

Cell dimensions. The measured cell-dimensions of the synthetic muscovite and muscovite–tobelite series solid-solutions are shown in Figures 3, 4 and 5, respectively. With increasing Ge→Si substitution, the *a*, *b* and *c* parameters increase (Fig. 3). The β angle is fairly constant at ~95.50–95.75° for most of the compositional range (Fig. 3), but is significantly less than these values for low Ge content. In the $K(Al_{3-x}Ga_x)Ge_3$- Ms series, the *a* and *b* parameters increase, and *c* and β are fairly constant (Fig. 4). In these series, up to 2.0 apfu Ga→Al substitution occurs at the octahedrally coordinated M2 site, but has little effect on the *c* and β parameters. In the muscovite–tobelite series, the *b* and *c* parameters increase with increasing interlayer NH_4/ND_4→K substitution (Fig. 5).

Interlayer sites. The relations between the compositions and interlayer-site parameters are shown in Figure 6. With increasing <$^{[4]}r$>, <I–O_{inner}> in both the $KAl_3(Si_{3-y}Ge_y)$- and $KGa_3(Si_{3-y}Ge_y)$-Ms series decreases slightly and <I–O_{outer}> tends to increase. With increasing <$^{[4]}r$>, the difference between <I–O_{outer}> and <I–O_{inner}> becomes larger (Fig. 6a). On the other hand, in the $K(Al_{3-x}Ga_x)Ge_3$-Ms series, <I–O_{inner}> increases slightly and <I–O_{outer}> decreases slightly (Fig. 6d). The basal-oxygen angles, $\angle$O–O–O_{acute} and $\angle$O–O–O_{obtuse}, show similar variations (Figs.

6b and 6e).

Rotation angles (α). With increasing $<^{[4]}r>$, the rotation angles, α, in both the $KAl_3(Si_{3-y}Ge_y)$- and $KGa_3(Si_{3-y}Ge_y)$-Ms series increase, whereas in the $K(Al_{3-x}Ga_x)Ge_3$-Ms series, it decreases with increasing Ga→Al substitution (Figs. 6c and 6f).

FIR spectra

FIR spectra for all muscovites and muscovite–tobelite solid-solutions in the region 250–50 cm^{-1} are shown in Figure 7. Major changes in band intensity, position and band shape are apparent as a function of bulk composition. The higher-frequency bands occur at approximately 250 cm^{-1} in all spectra, and are ascribed to M-O-H/D bending vibrations. The lower-frequency band shows much more varied behaviour. In $^{[6]}$Al-dominant micas, it occurs at ~240 cm^{-1} in $^{[4]}$Ge-free micas (e.g., Fig. 7a,d) and moves to slightly lower frequency (~230 cm^{-1}) with increasing $^{[4]}$Ge-content. In $^{[6]}$Ga-dominant micas, the band occurs at ~230 cm^{-1} in $^{[4]}$Ge-free micas (e.g., Fig. 7b) and moves to lower frequencies (~200 cm^{-1}) with increasing $^{[4]}$Ge-content; moreover, the intensity of this band increases significantly with increasing $^{[4]}$Ge-content (Fig. 7b). In $^{[6]}$Al–$^{[6]}$Ga solid-solution-series micas (Fig. 7c), the lower-frequency band changes from ~240 cm^{-1} in $^{[6]}$Ga-free mica to ~200 cm^{-1} in $^{[6]}$Ga-dominant $^{[4]}$Ge mica, and the

intensity of the band increases strongly with increasing $^{[6]}$Ga-content; these bands are assigned as M–O deformations coupled with (OH/OD)-libration bands. The three dominant bands below 170 cm^{-1} are in-plane torsional bands of the tetrahedron layer (labelled by the arrows in Fig. 7), and $I–O_{inner}$ ($K–O_{inner}$) and $I–O_{outer}$ ($K–O_{outer}$) stretching bands. These bands assignments are the same as those for synthetic kinoshitalite solid-solutions (Ishida and Hawthorne 2011).

With increasing Ga→Al and Ge→Si substitution, the intensities of these $I–O_{inner}$ stretching bands do not change (or increase very slightly) (Figs. 7a, 7b and 7c). Full-width at half-height (FWHH) values for the $I–O_{inner}$ stretching bands are up to ~25 cm^{-1} and do not change with Ga-Al, Ge-Si and interlayer NH_4/ND_4-K substitutions (Fig. 7). On the other hand, with increasing Ge→Si substitution in $KGa_3(Si_{3-y}Ge_y)$-Ms and Ga→Al in $K(Al_{3-x}Ga_x)Ge_3$-Ms series micas, the $I–O_{outer}$ stretching intensities decrease considerably. The $I–O_{outer}$ stretching band FWHHs in $KAl_3(Si_{3-y}Ge_y)$-Ms, $KGa_3(Si_{3-y}Ge_y)$-Ms and $K(Al_{3-x}Ga_x)Ge_3$-Ms series micas also decrease with increasing Ge→Si and Ga→Al substitution. With increasing interlayer NH_4/ND_4→□ substitution, both $K–O_{inner}$ and $K–O_{outer}$ stretching frequencies decrease (Fig. 7d). Ammonium-deuteride exchange also causes a slight downward shift in frequency for the $NH_4/ND_4–O_{outer}$ stretching bands in particular.

M-O-H(I,II)/M-O-D(I,II) bending bands.

With increasing Ga→Al and Ge→Si substitution, the band in the 240–190 cm^{-1} range shifts down in frequency but increases in intensity (Figs. 7b and 7c). Deuteration causes a downward frequency shift of ~10 cm^{-1} for this band. For the micas in these series, Al at the octahedrally coordinated sites is substituted by Ga, causing the downward shift in frequency. The O6–H for O6–D substitution also causes a downward shift in frequency. The 240–190 cm^{-1} bands are assigned as M–O deformations coupled with O6-(H/D) vibrations.

With increasing Ga→Al and Ge→Si substitution, the bands in the 200–150 cm^{-1} range shift down in frequency for the (a) and (b) series, and the bands in the 190–130 cm^{-1} range for the (c) and (d) series shift down in frequency but are unchanged or even increase in intensity (Fig. 7), respectively. Deuteration causes a downward shift in frequency of ~10 cm^{-1} for these bands. This type of band is also assigned as an M-O deformation coupled with O6–(H/D) vibration. Zhang et al. (2010) showed that the 190 cm^{-1} band in muscovite shifts to higher wavenumber (194 cm^{-1}) at 900 K, which supports this assignment. McKeown et al. (1999) assigned this band as an OH–M2–OH bend coupled to an Od_{xz}-translation.

In-plane torsional bands of the T layer.

The relations between the frequencies and the tetrahedron compositions ($<^{[4]}r>$) for the in-plane torsional bands of the tetrahedron layer are exactly in line with those for kinoshitalite (Ishida and Hawthorne 2011): at 166–167 cm^{-1} for the KAl_3Si_3-Ms series ($<^{[4]}r>$ = 0.293 Å), and at 126–129 cm^{-1} for KAl_3Ge_3- end-members ($<^{[4]}r>$ = 0.390 Å), etc. (Figs. 7a and 8a). In the $KGa_3(Si_{3-y}Ge_y)$-Ms series, strong in-plane torsional bands are observed at 127 cm^{-1} in KGa_3Si_3-Ms ($<^{[4]}r>$ = 0.313 Å), and the frequency decreases to 119 cm^{-1} in the KGa_3Ge_3-Ms ($<^{[4]}r>$ = 0.410 Å) end-member (Figs. 7b and 8a). In the $K(Al_{3-x}Ga_x)Ge_3$-Ms series, very large increases in intensity are observed for the in-plane torsional bands, from the weak band at 128–129 cm^{-1} in KAl_3Ge_3-Ms to the strong band at 119 cm^{-1} in the KGa_3Ge_3-Ms ($<^{[4]}r>$ = 0.410 Å) end-members (Figs. 7c and 8b). With increasing Ga (apfu) in the $K(Al_{3-x}Ga_x)Ge_3$-Ms series, the tetrahedral torsional bands shift down in frequency.

$I–O_{inner}$ and $I–O_{outer}$ stretching bands.

The frequencies of the $I–O_{inner}$ and $I–O_{outer}$ stretching bands, ν_B and ν_C, and the mean tetrahedral ionic radii, $<^{[4]}r>$, are shown in Figure 9. The frequency decreases of both the $I-O_{inner}$ and $I-O_{outer}$ stretching bands in the muscovite-tobelite series are due to mass effects for the K→□□□ substitution (Fig. 9a and 9b). With increasing Ge→Si substitution, ν_B increases in both $KAl_3(Si_{3-y}Ge_y)$- and $KGa_3(Si_{3-y}Ge_y)$- Ms series. This

is due to the weaker T–O bond strength caused by the increasing $<^{[4]}r>$, and this strengthens the I-O bond. The ~20 cm^{-1} frequency differences between the $KAl_3(Si_{3-y}Ge_y)$- and $KGa_3(Si_{3-y}Ge_y)$- Ms series are caused by tetrahedral and octahedral cations, Ga or Al: $^{[4][6]}$Al–O bonds are stronger than $^{[4][6]}$Ga–O bonds, and tetrahedral and octahedral oxygens in $^{[4][6]}$Al-O are thus more weakly bonded to other cations than those of $^{[4][6]}$Ga–O because of the valence-sum rule. In the $K(Al_{3-x}Ga_x)Ge_3$-Ms series, ν_B varies by ~15 cm^{-1} from the corresponding values in the Al_3Ge_3- to Ga_3Ge_3-Ms end-members. The I-O_{outer} stretching-band frequencies, ν_C, in the $KAl_3(Si_{3-y}Ge_y)$-Ms series increase slightlywith increasing Ge→Si substitution, but those in the $KGa_3(Si_{3-y}Ge_y)$- Ms series vary little (Fig. 9b). The $\nu_B - \nu_C$ values for $KAl_3(Si_{3-y}Ge_y)$-Ms and $KGa_3(Si_{3-y}Ge_y)$-Ms (31–46 and 27–49 cm^{-1}) are more widely dispersed than those for the $K(Al_{3-x}Ga_x)Ge_3$-Ms micas: 45–51 cm^{-1} (Fig.9c).

The relations of the frequencies of the I–O_{inner} and I–O_{outer} stretching bands, ν_B and ν_C, and the square root of aggregate tetrahedral-cation mass, $\sqrt{(^{[4]}M)}$, are shown in Figure 10. The change from muscovite to tobelite involves a decrease in interlayer K^+ (M = 39, $<^{[12]}r>$ = 1.52 Å) and an increase in interlayer NH_4^+/ND_4^+ (M = 18/24, $<^{[12]}r>$ = ~1.7 Å). Although the ionic radius of the interlayer ammonium ion is larger than that of the K^+ ion, both the I–O_{inner} and I–O_{outer} stretching frequencies shift upward by ~ 40 cm^{-1} due to the smaller mass of ammonium relative to K (Figs. 10a and 10b). Both the

Ge→Si and Ga→Al substitutions cause an increasing ionic radius and atomic mass, and similar variations in the ν_B, ν_C, and $\nu_B-\nu_C$ values as those for Figure 9 are observed (Fig. 10).

The relations between <I–O_{inner}> and the frequencies of the associated bands are shown in Figure 11a. With increasing <I–O_{inner}>, the ν_B decreases, except those for the micas of the muscovite–tobelite series. With increasing Ge→Si and Ga→Al substitution, the I–O_{outer} stretching frequencies decrease, except in the $KAl_3(Si_{3-y}Ge_y)$-Ms series (Figs. 11b). Although <I–O_{outer}> becomes slightly shorter, ν_C decreases in the micas of the series $K(Al_{3-x}Ga_x)Ge_3$-Ms. With increasing difference between <I–O_{outer}> and <I–O_{inner}>, the ν_B-ν_C values increase linearly (Fig.11c). The $\nu_B-\nu_C$ values and α show also a linear relation (Fig. 11d).

ACKNOWLEDGMENTS

The authors are indebted to S. Higashi and Y. Kuwahara for their helpful suggestions. H. Kojitani helped to make CIF files. Infrared spectra were recorded at the Center of Advanced Instrumental Analysis, Kyushu University. We thank A. Beran, M. Mookherjee, and R. Stalder for comments and suggestions which improved the manuscript. K.I. was partly supported by a grant for the Excellent Projects of the Graduate School of Social and Cultural Studies, Kyushu University, and a Grand-in-Aid

for Scientific Research for Y. Kuwahara (No. 23340163). F.C.H. was supported by a Canada Research Chair in Crystallography and Mineralogy, and by a Discovery Grant from the Natural Sciences and Engineering Research Council of Canada.

REFERENCES CITED

Bastoul, A.M., Pironon, J., Mosbah, M., Dubois, M., and Cuney, M. (1993) In-situ analysis of nitrogen in minerals. European Journal of Mineralogy, 5, 233-243.

Beran, A. (2002) Infrared spectroscopy of micas. In A. Mottana, F.P. Sassi, J.B.Thompson Jr., and S. Guggenheim, Eds., Micas: Crystal Chemistry and Metamorphic Petrology, vol. 46, p. 351-369. Reviews in Mineralogy and Geochemistry, Mineralogical Society of America, Chantilly, Virginia.

Bokij, G.B. and Arkihipenko, D.K. (1977) Infrared spectra of oxonium and ammonium ions in layer aluminosilicates. Physics and Chemistry of Minerals, 7, 233-242.

Boukili, B., Robert, J.-L., Beny, J.-M., and Holtz, F. (2001) Structural effects of OH-F substitution in trioctahedral micas of the system: K_2O-FeO-Fe_2O_3-Al_2O_3-SiO_2 -H_2O-HF. Schweizeriche Mineralogische und Petrographische Mitteilungen, 81, 55-67.

Brigatti, M.F., Frigieri, P., and Poppi, L. (1998) Crystal chemistry of Mg-, Fe-bearing muscovites-2M_1. AmericanMineralogist, 83,775–785.

Diaz, M., Farmer, V.C., and Prost, R. (2000) Characterization and assignment of far infrared absorption bands of K^+ in muscovite. Clays and Clay Minerals, 48, 433-438.

Eugster, H.P. and Munoz, J. (1966) Ammonium micas: possible sources of atmospheric ammonia and nitrogen. Science, 151, 683-686.

Farmer, V.C. (1974) Layer silicates. In: Infrared spectra of minerals. Ed. V.C. Farmer, Mineralogical Society London, 331-360.

Fleet, M.E. (2003) Rock-Forming Minerals, vol. 3A, Micas. The Geological Society, London.

Friedrich, F., Gasharova, B., Mathis, Y-L., Nüesch, R., and Weidler, P.G. (2006) Far-infrared spectroscopy of interlayer vibrations of Cu(II), Mg(II), Zn(II), and Al(III) intercalated muscovite. Applied Spectroscopy, 60, 723–728.

Fripiat, J.J. (1982) Application of far infrared spectroscopy of the study of clay minerals and zeolites. In: Developments in sedimentology, 34, 191–210. J.J. Fripiat (ed). Advanced techniques for clay mineral analysis, Elsevier Amsterdam.

Guggenheim, S. (1981) Cation ordering in lepidolite. American Mineralogist, 66, 1221–1232.

Harlov, D.E., Andrut, M., and Pöter, B. (2001) Characterization of tobelite $(NH_4)Al_2[AlSi_3O_{10}](OH)_2$ and ND_4-tobelite $(ND_4)Al_2[AlSi_3O_{10}](OD)_2$ using IR spectroscopy and Rietveld refinement of XRD spectra. Physics and Chemistry of Minerals, 28, 268–276.

Higashi, S. (1982) Tobelite, a new ammonium dioctahedral mica. Mineralogical Journal, 11, 138–146.

Hovis, G.L., Harlov, D., and Gottschalk, M. (2004) Solution calorimetric determination of the enthalpies of formation of NH_4-bearing minerals buddingtonite and tobelite. American Mineralogist, 89, 85-93.

Ishida, K. and Hawthorne, F.C. (2011) Far-infrared spectra of synthetic $^{[4]}[(Al_{2-x}Ga_x)(Si_{2-y}Ge_y)](OH,OD,F)_2$- kinoshitalite: Characterization and assignment of interlayer Ba-O_{inner} and Ba-O_{outer} stretching bands. American Mineralogist, 96, 566–576.

Ishii, M., Shimanouchi, T., and Nakahira, M. (1967) Far infrared absorption spectra of layer silicates. Inorganica Chemica Acta, 1, 387–392.

Izumi, F. and Ikeda, T. (2000) A Rietveld analysis program RIETAN -98 and its application to zeolites. Material Science Forum, 321–324.

Laperche, V. and Prost, R. (1991) Assignment of the far-infrared absorption bands of K in micas. Clays and Clay minerals, 39, 281–289.

Loh, E. (1973) Optical vibrations in sheet silicates. Journal of Physics C: Solid State Physics, 6, 1091–1104.

McKeown, D.A., Bell, M.L., and Etz, E. (1999) Vibrational analysis of the dioctahedral mica: $2M_1$ muscovite. American Mineralogist, 84, 1041–1048.

Mookherjee, M., Redfern, S.A.T. and Zhang, M. (2004) Far-infrared spectra of ammonium layer and framework silicates. Neues Jahrbuch für Mineralogie-Monatshefte, 1, 1–9.

Mookherjee, M. and Redfern, S.A.T. (2002) A high-temperature Fourier transform infrared study of the interlayer and Si–O-stretching region in phengite-2M_1. Clay Minerals, 37, 323–336.

Pöter, B., Gottschalk, M.,and Heirich, W. (2007) Experimental determination of ammonium partitioning among muscovite, K-feldspar,and aquerous chloride solutions. Lithos,74, 67–90.

Prost, R. and Laperche, V. (1990) Far-infrared study of potassium in micas. Clays and Clay minerals, 38, 351–355.

Roth, C. (1978) Effects of exchangeable cations on the far infrared spectra of clay minerals. In 6th International Clay Conference Abstracts with Program, 225.

Schroeder, P.A. (1990) Far infrared, X-ray powder diffraction, and chemical investigation of potassium micas. American Mineralogist, 75, 983-991.

Shannon, R.D. (1976) Revised effective ionic radii and systematic studies of interatomic distances in halides and chalcogenides. Acta Crystallographica, A32, 751–767.

Shigorova, T.A. (1982) The possibility of determining the ammonium content of mica by IR spectroscopy. Geochemical International, 19, 110–114.

Shigerova, T.A., Kotov, N.V., Kotel-nikova, Ye.N., Shimakin, B.M., and Frank-Kamenetsky, V.A. (1981) Synthesis, diffractometry, and IR spectroscopy of micas in the series from muscovite to the ammonium analogue. Geochemical International, 18, 76–82.

Tateyama, H., Shimoda, S., and Sudo, T. (1977) Estimation of K-O distance and tetrahedral angle of K-micas from far-infrared absorption spectral data. American Mineralogist, 62, 534–539.

Vedder, W. (1965) Ammonium in muscovite. Geochimica et Cosmochimica Acta, 29, 221–228.

Velde, B. (1978) Infrared spectra of synthetic micas in the series muscovite-MgAl celadonite. American Mineralogist, 63, 343–349.

Velde, B. and Couty, R. (1985) Far Infrared Spectra of Hydrous Layer Silicates. Physics and Chemistry of Minerals, 12, 347–352.

Voncken, J.H.L., Wevers, J.M., van der Erden, A.M.J., Bos, A., and Jansen, J.B. (1987) Hydrothermal synthesis of tobelite, $NH_4Al_2Si_3AlO_{10}(OH)_2$, from various starting materials and implications for its occurrence in nature. Geologie en Mijnbouw, 66, 259–269.

Zhang, M., Redfern, S.A.T., Salje, K.H., Carpenter, M.A., and Hayward, C.L. (2010) Thermal behavior of vibrational phonons and hydroxyls of muscovite in

dehydroxylation: In situ high-temperature infrared spectroscopic investigations. American Mineralogist, 95, 1444–1457.

Figures captions

FIGURE 1. SEM images of synthetic muscovites and tobelite. **(a)** [1210]Al_3Si_3DMs. **(b)** [1027] Ga_3Ge_3HMs. **(c)** [1102] $Al_{0.5}Ga_{2.5}Ge_3$HMs. **(d)** [1437] $DMs_{00}Tob_{100}$(Kln).

FIGURE 2. Rietveld patterns of synthetic muscovite and tobelite. **(a)** [1027] Ga_3Ge_3HMs and **(b)** [1432] $DMs_{00}Tob_{100}$(Kln). The crosses are the observed data, the solid line is the calculated pattern, and vertical bars mark all possible Bragg reflections (Cu$K\alpha_1$ and Cu$K\alpha_2$) for the $2M_1$ polytype in **(a),** and polytypes $1M$, $2M_1$, and $2M_2$ in **(b)**, respectively. The difference between the observed and calculated patterns is shown at the bottom.

FIGURE 3. Cell parameters of synthetic muscovites. Open circles = $KAl_3(Si_{3-y}Ge_y)$-Ms series. Open squares = $KGa_3(Si_{3-y}Ge_y)$-Ms series. Error bars are in the order of magnitude of the symbols.

FIGURE 4. Cell parameters of synthetic $K(Al_{3-x}Ga_x)Ge_3$-Ms series (solid triangles). Error bars are in the order of magnitude of the symbols.

FIGURE 5. Cell parameters of synthetic muscovite-tobelite series. Solid diamonds = synthesized from chemical reagents. Open diamonds = synthesized from kaolinite. Error bars are in the order of magnitude of the symbols.

FIGURE 6. Variation in interlayer-site parameters as a function of the mean tetrahedral ionic radius or Ga content (apfu). Symbols are as in Fig. 3. **(a)**: <I-O_{inner}> = mean

inner interlayer bond length; <I-O_{outer}> = mean outer interlayer bond length, respectively. **(b)**: ∠O-O-O_{acute} = mean acute interlayer oxygen angle; ∠ O-O-O_{obtuse} = mean obtuse interlayer oxygen angle. (**c**): α = tetrahedron rotation angles. **(d)**: <I-O_{inner}> = mean inner interlayer bond length; <I-O_{outer}> = mean outer interlayer bond length, respectively. **(e)**: ∠O-O-O_{acute} = mean acute interlayer oxygen angle; ∠O-O-O_{obtuse} = mean obtuse interlayer oxygen angle. **(f)**: α = tetrahedron rotation angles.

FIGURE 7. Far infrared spectra of synthetic muscovites and muscovite-tobelite micas. **(a)**: $KAl_3(Si_{3-y}Ge_y)$-Ms series. **(b)**: $KGa_3(Si_{3-y}Ge_y)$-Ms series. **(c)**: $K(Al_{3-x}Ga_x)Ge_3$-Ms series. **(d)**: $\{K_{1-A}(NH_4/ND_4)_A\}Al_3Si_3$-Ms series. One diamond = M-O-H/D deformational bands (I). Two diamonds = M-O-H/D deformational bands (II). Stars = M-O deformasional bands around 250 cm^{-1}. Bands at 250–225 cm^{-1} in Figure 7b include those for Ga_2O_3 in spectra y = 0.5, 1.0, and 2.0. Open symbols = OH-bearing. Solid symboles = OD-bearing. Arrows indicate vibrations in-plane tetrahedral torsional modes (see text). Solid line: OH-forms. Broken line: OD-forms.

FIGURE 8. Relations between frequency and compositions for the in-plane tetrahedron tortional bands. **(a)**: Open circles = $KAl_3(Si_{3-y}Ge_y)$-Ms series. Open squares = $KGa_3(Si_{3-y}Ge_y)$-Ms series. Solid diamonds = $\{K_{1-A}(NH_4/ND_4)_A\}Al_3Si_3$-Ms series. **(b)**: Solid triangles = $K(Al_{3-x}Ga_x)Ge_3$-Ms series.

FIGURE 9. Relations between **(a)** the frequency (= ν_B) and mean tetrahedral ionic radius (= $<^{[4]}r>$) for I-O_{inner} stretching bands, **(b)** the frequency (= ν_C) and mean tetrahedral ionic radius for I-O_{outer} stretching bands, and **(c)** the frequency differences of the I-O_{inner} and I-O_{outer} stretching bands (= ν_B-ν_C) and mean tetrahedral ionic radius. Open circles = $KAl_3(Si_{3-y}Ge_y)$-Ms series. Open squares = $KGa_3(Si_{3-y}Ge_y)$-Ms series. Solid triangles = $K(Al_{3-x}Ga_x)Ge_3$-Ms series. Solid diamonds = $\{K_{1-A}(NH_4/ND_4)_A\}Al_3Si_3$-Ms series.

FIGURE 10. Relations between **(a)** the frequency (= ν_B) and square root of tetrahedral- cation mass (= $\sqrt{(^{[4]}M)}$) for I-O_{inner} stretching bands, **(b)** the frequency (= ν_C) and square root of tetrahedral cation mass for I-O_{outer} stretching bands, and **(c)** the frequency differences (= ν_B-ν_C) of the I-O_{inner} and I-O_{outer} stretching bands and square root of tetrahedral cation mass. Legend as in Figure 9.

FIGURE 11. Relations between **(a)** the frequency (= ν_B) and $<I–O_{inner}>$ for I-O_{inner} stretching bands, **(b)** the frequency (= ν_C) and $<I–O_{outer}>$ for I-O_{outer} stretching bands, **(c)** the frequency differences of I-O_{inner} and I-O_{outer} stretching bands and $<I–O_{outer}>$-$<I–O_{inner}>$ values, and **(d)** the tetrahedral rotation angles (α) and the frequency differences (= ν_B-ν_C) of the I-O_{inner} and I-O_{outer} stretching bands. Legend as in Figure 9.

TABLE 1. Synthetic conditions, Rietveld data and FIR bands assignment for $[K,(NH_4/ND_4)](Al_{3-x}Ga_x)(Si_{3-y}Ge_y)O_{10}(OH/OD)_2$-muscovite and muscovite-tobelite series

Run no.	Symbol(comp.)	*T* (˚C)	*P* (MPa)	Duration *t* (h)	< [4]*r* >† (Å)	< I-O_{inner} >† (Å)	< I-O_{outer} >† (Å)	*a*† (˚)	Band A† (cm^{-1})	Band B† (cm^{-1})	Band C† (cm^{-1})	n_B-n_C† (cm^{-1})	MOH(I) MO+OH libr.(cm^{-1})	MOH(II) MO+OH libr.(cm^{-1})	MOD(I) MO+OD libr.(cm^{-1})	MOD(II) MO+OD libr.(cm^{-1})
	(a) $KAl_3(Si_{3-y}Ge_y)O_{10}(OH,OD)_2$-Ms															
[1344]*	Al_3Si_3DMs	585	250	859	0.293	2.838	3.501	15.4	166	143	110	33	-	-	-	183
[1511]*	Al_3Si_3HMs	565	92	859	0.293	2.825	3.588	18.1	166	142	111	31	-	188	-	-
[999]	$Al_3Si_{2.5}Ge_{0.5}$HMs	610	225	590	0.309	2.843	3.506	15.1	158	148	110	38	-	185	-	-
[1230]*	$Al_3Si_{2.5}Ge_{0.5}$HMs	560	241	547	0.309	2.785	3.540	16.8	-‡	147	110	37	-	183	-	-
[997]*	$Al_3Si_2Ge_1$HMs	610	225	590	0.325	2.865	3.508	14.4	-	150	110	40	233	180	-	-
[1085]*	$Al_3Si_2Ge_1$DMs	595	202	47	0.325	-	-	-	-	149	110	39	-	180	228	-
[1231]CIF**	$Al_3Si_2Ge_1$HMs	560	241	547	0.325	2.842	3.490	14.5	-	150	111	39	229	179	-	-
[994]*	$Al_3Si_{1.5}Ge_{1.5}$HMs	595	192	494	0.341	2.827	3.616	16.1	-	152(155,149)	111	41	229	179	-	-
[1232]*CIF	$Al_3Si_{1.5}Ge_{1.5}$DMs	560	272	544	0.341	2.815	3.535	15.9	-	153(154,151)	112	41	-	-	226	-
[998]*CIF	$Al_3Si_1Ge_2$HMs	610	225	590	0.358	2.766	3.620	19.1	-	154(157,151)	113	41	226	177	-	-
[1086]*	$Al_3Si_1Ge_2$DMs	595	202	47	0.358	-	-	-	-	156	112	44	-	-	228	-
[1233]CIF	$Al_3Si_1Ge_2$HMs	560	272	544	0.358	2.794	3.561	16.8	-	156	115	41	228	176	-	-
[1234]*CIF	$Al_3Si_{0.5}Ge_{2.5}$HMs	560	272	544	0.374	2.774	3.605	18.2	-	158	116	42	228	174	-	-
[995]*CIF	Al_3Ge_3HMs	595	192	494	0.390	2.753	3.650	19.3	128	161	115	46	233	173	-	-
[1087]*	Al_3Ge_3DMs	595	202	47	0.390	-	-	-	129	160	115	45	-	-	221	-
	(b) $KGa_3(Si_{3-y}Ge_y)O_{10}(OH,OD)_2$-Ms															
[1209]*	Ga_3Si_3HMs	435	191	501	0.313	2.780	3.543	14.1	127	127	98(+91)	29	224	175	-	-
[1181]*	$Ga_3Si_{2.5}Ge_{0.5}$HMs	470	265	456	0.329	-	-	-	127	126	98	28	217	170	-	-
[1182]	$Ga_3Si_2Ge_1$HMs	470	265	456	0.345	-	-	-	-	124	97	27	225	164	-	-
[1447]*CIF	$Ga_3Si_2Ge_1$HMs	595	260	833	0.345	2.829	3.461	13.7	126	133	99	34	217	160	-	-
[1142]	$Ga_3Si_{1.5}Ge_{1.5}$HMs	615	245	520	0.361	2.842	3.542	13.4	125	139	99	40	221	154	-	-
[1467]*CIF	$Ga_3Si_{1.5}Ge_{1.5}$HMs	595	280	496	0.361	2.826	3.513	14.8	125	141	98	43	218	158	-	-
[1143]*	$Ga_3Si_1Ge_2$HMs	615	245	520	0.378	-	-	-	123	142	98	44	219	154	-	-
[1207]	$Ga_3Si_1Ge_2$HMs	435	191	501	0.378	2.883	3.768	16.7	122	145	97	48	211	154	-	-
[1491]*CIF	$Ga_3Si_1Ge_2$DMs	555	178	615	0.378	2.808	3.575	16.4	121	146	97	49	-	-	202	-
[1469]*CIF	$Ga_3Si_{0.5}Ge_{2.5}$HMs	600	279	424	0.394	2.788	3.598	17.1	121	143	97	46	205	-	-	-
[1216]*CIF	Ga_3Ge_3HMs	535	110	230	0.410	2.673	3.734	21.5	119	150	97	53	202	-	-	-
[1567]*	Ga_3Ge_3DMs	540	170	641	0.410	-	-	-	118	150	97	53	-	-	195	138
	(c) $K(Al_{3-X}Ga_X)Ge_3O_{10}(OH,OD)_2$-Ms															
[1271]*CIF	$Al_{2.75}Ga_{0.25}Ge_3$HMs	595	214	427	0.390	2.743	3.649	19.6	125	159	114	45	229	171	-	-
[1217]*CIF	$Al_{2.5}Ga_{0.5}Ge_3$HMs	500	216	499	0.390	2.753	3.628	18.9	123	159	112	47	229	-	-	-
[1270]*CIF	$Al_{2.25}Ga_{0.75}Ge_3$HMs	595	214	427	0.390	2.768	3.629	18.6	121	156	110	46	226	-	-	-
[1025]*CIF	$Al_2Ga_1Ge_3$HMs	600	223	430	0.390	2.762	3.621	18.4	121	156	109	47	227	-	-	-
[1088]*	$Al_2Ga_1Ge_3$DMs	595	202	47	0.390	-	-	-	121	155	109	46	-	-	235	-
[1269]*CIF	$Al_{1.75}Ga_{1.25}Ge_3$HMs	595	214	427	0.390	2.768	3.624	18.3	121	154	107	47	226	-	-	-
[1101]*CIF	$Al_{1.5}Ga_{1.5}Ge_3$HMs	550	210	189	0.390	2.751	3.617	18.4	121	154	105	49	213	-	-	-
[1568]*	$Al_{1.5}Ga_{1.5}Ge_3$DMs	540	170	641	0.390	-	-	-	121	154	105	49	-	-	206(211,200)	-
[1267]*CIF	$Al_{1.25}Ga_{1.75}Ge_3$HMs	585	231	447	0.390	2.781	3.616	17.8	121	152	104	48	205	-	-	-
[1026]*CIF	$Al_1Ga_2Ge_3$HMs	600	223	430	0.390	2.765	3.618	18.1	120	151	102	49	205(211,203)	-	-	-
[1089]*	$Al_1Ga_2Ge_3$DMs	595	202	47	0.390	-	-	-	121	151	102	49	-	-	200	-
[1266]*CIF	$Al_{0.75}Ga_{2.25}Ge_3$HMs	585	231	447	0.395	2.748	3.623	18.4	120	149	101	48	205	-	-	-
[1102]*CIF	$Al_{0.5}Ga_{2.5}Ge_3$HMs	550	210	189	0.400	2.768	3.620	18.0	120	149	100	49	202	-	-	-
[1265]*CIF	$Al_{0.25}Ga_{2.75}Ge_3$HMs	580	231	447	0.405	2.778	3.626	17.9	119	149	98	51	202	-	-	-
[1027]*CIF	Ga_3Ge_3HMs	600	223	430	0.410	2.842	3.490	14.5	119	148	97	51	202	-	-	-
[1090]*	Ga_3Ge_3DMs	595	202	47	0.410	-	-	-	119	147	97	50	-	-	195	134
	(d) $\{K_{1-A}(NH_4,ND_4)_A\}Al_3Si_3O_{10}(OH,OD)_2$-Ms–Tob															
[Natural]*CIF	Ms_{100}(UT)§	-	-	-	0.293	2.876	3.348	10.6	167	142	110	32	-	188	-	-
[1579]*	DMs_{100}(UT)	575	216	198	0.293	-	-	-	166	141	109	32	-	-	-	181
[1383]*	$DMs_{75}Tob_{25}$	580	235	352	0.293	2.724	3.846	20.2	168	168/136	136/101	32/35	-	-	-	-
[1382]*	$DMs_{50}Tob_{50}$	580	235	352	0.293	2.997	3.554	13.0	-	174	147/97	27	-	-	-	-
[1381]*	$DMs_{25}Tob_{75}$	580	235	352	0.293	3.029	3.593	13.4	-	174	148/92	26	-	-	-	-
[1438]*CIF	$HMs_{00}Tob_{100}$	570	244	134	0.293	2.929	3.520	13.7	-	175	146(149,143)	29	-	-	-	-
[1426]*	$DMs_{00}Tob_{100}$	505	105	136	0.293	2.980	3.603	14.5	-	174	142	32	-	-	-	-
[1606]*	$HMs_{00}Tob_{100}$(Kln)	545	228	260	0.293	2.925	3.780	13.1	-	178 (180,175)	149	29	-	-	-	-
[1437]*	$DMs_{00}Tob_{100}$(Kln)	570	244	134	0.293	2.790	4.139	13.5	-	175	146 (149,142)	29	-	-	-	-

* FIR spectra were given in Figures. ** CIF = CIFs were deposited.

† < [4]*r* > = nominal mean tetrahedral ionic radius calculated by the mole ratios of the solid starting material's composition. In the (c) series, < [4]*r* > calculated as Al first and then Ge. < I-O_{inner} > = mean bond length between interlayer cations and inner basal oxygen atoms. < I-O_{outer} > = mean bond length between interlayer cations and outer basal oxygen atoms.

a = tetrahedral rotaion angle calculated by the X-ray Rietveld refinement data. Frequencies of the in-plane tetrahedral tortional band (band A), I-O_{inner} stretching band (band B), and I-O_{outer} stretching band (band C). n_B-n_C = frequency difference between I-O_{inner} and I-O_{outer} stretching bands.

‡ Not determined.

§ UT = natural sample. D = deuterated. Kln = kaolinite as the starting material.

TABLE 2a. Rietveld refinement for synthetic $KAl_3(Si_{3-x}Ge_x)O_{10}(OH,OD)_2$-muscovites

Run no.	[1344]	[1511]	[999]	[1230]	[997]	[1231]CIF*	[994]	[1232]CIF	[998]CIF	[1233]CIF	[1234]CIF	[995]CIF
Symbol	Al_3Si_3DMs	Al_3Si_3HMs	$Al_3Si_{2.5}Ge_{0.5}$HMs	$Al_3Si_{2.5}Ge_{0.5}$HMs	$Al_3Si_2Ge_1$HMs	$Al_3Si_2Ge_1$HMs	$Al_3Si_{1.5}Ge_{1.5}$HMs	$Al_3Si_{1.5}Ge_{1.5}$DMs	$Al_3Si_1Ge_2$HMs	$Al_3Si_1Ge_2$HMs	$Al_3Si_{0.5}Ge_{2.5}$HMs	Al_3Ge_3HMs
$<{}^{[4]}r>$ (Å)	0.293	0.293	0.309	0.309	0.325	0.325	0.341	0.341	0.358	0.358	0.374	0.390
Collecting conditions												
2□ scan range (°)	5-110	5-110	5-110	5-110	5-110	5-110	5-110	5-110	5-110	5-110	5-110	5-110
Step interval (°)	0.04	0.02	0.04	0.02	0.02	0.10	0.02	0.10	0.02	0.02	0.02	0.08
Integration times (s)	4	5	4	6	6	5	5	5	7	5	10	10
Agreement indicies from Rietveld refinement												
R_{wp}(%)	22.6	23.9	20.8	20.1	19.6	15.0	14.4	15.9	14.5	15.2	15.6	8.89
R_p(%)	17.7	18.6	16.5	15.4	14.7	11.4	10.7	11.5	10.9	10.2	10.7	5.97
R_e(%)	8.03	7.35	7.19	4.73	5.55	4.77	5.99	4.55	5.12	5.89	4.03	3.03
S	2.81	3.26	2.89	4.26	3.53	3.14	2.40	3.51	2.84	2.58	3.86	2.94
Durbin-Watson d	0.212	0.128	0.224	0.107	0.098	0.889	0.224	0.698	0.159	0.200	0.129	1.13
R_F(%)	3.87	4.04	3.09	2.56	2.14	1.63	1.80	1.71	1.24	1.88	1.36	0.95
Unit-cell parameters												
a( )	5.194(3)	5.202(2)	5.207(3)	5.2120(19)	5.2147(14)	5.213(2)	5.2291(11)	5.226(2)	5.2356(13)	5.238(7)	5.2507(6)	5.2653(5)
b( )	9.003(5)	9.000(4)	9.011(5)	9.017(3)	9.040(3)	9.041(4)	9.075(2)	9.070(4)	9.080(2)	9.0979(12)	9.1206(11)	9.1522(9)
c( )	20.121(11)	20.122(9)	20.293(11)	20.312(8)	20.414(6)	20.414(9)	20.565(4)	20.552(8)	20.677(5)	20.678(3)	20.786(2)	20.919(2)
□(°)	94.71(2)	94.365(16)	95.57(2)	95.772(14)	95.557(10)	95.639(15)	95.652(7)	95.655(13)	95.751(8)	95.687(4)	95.687(4)	95.665(3)
V(^{3})	937.7(9)	939.3(7)	947.7(8)	949.8(6)	957.8(5)	957.5(7)	971.1(4)	969.4(6)	978.0(4)	980.6(2)	990.5(2)	1003.14(17)
$a\sin$□( )	5.176(1)	5.187(1)	5.183(1)	5.186(1)	5.190(1)	5.187(1)	5.204(1)	5.201(1)	5.209(1)	5.213(1)	5.225(1)	5.240(1)
d_{cal}(g/cm^3)	2.701(11)	2.772(11)	2.817(33)	2.892(30)	2.850(6)	2.897(31)	2.997(12)	3.024(12)	3.160(6)	3.138(9)	3.194(18)	3.345(6)
Site-populations												
T1 Ge	-	-	0.16(2)	0.10(2)	0.23(1)	0.24(2)	0.31(1)	0.33(2)	0.47(1)	0.43(1)	0.52(1)	0.65(1)
Al+Si	1.00	1.00	0.84(2)	0.90(2)	0.77(1)	0.76(2)	0.69(1)	0.67(2)	0.53(1)	0.57(1)	0.48(1)	0.35(1)
T2 Ge	-	-	0.00(2)	0.14(2)	0.00(1)	0.07(2)	0.22(1)	0.21(3)	0.30(1)	0.35(1)	0.42(1)	0.63(1)
Al+Si	1.00	1.00	1.00(2)	0.86(2)	1.00(1)	0.93(2)	0.78(1)	0.79(3)	0.70(1)	0.65(1)	0.58(1)	0.37(1)
Average (T sites)												
Ge	-	-	0.08(8)	0.12(2)	0.12(12)	0.16(9)	0.25(4)	0.27(6)	0.36(4)	0.39(4)	0.47(5)	0.64(1)
Al+Si	1.00	1.00	0.92(8)	0.88(2)	0.88(12)	0.84(9)	0.75(4)	0.73(6)	0.64(4)	0.61(4)	0.53(5)	0.37(1)
M1 Al	0.25(2)	0.04(2)	0.16(3)	0.02(2)	0.09(2)	0.07(3)	0.07(1)	0.04(3)	0.12(1)	0.00(1)	0.00(1)	0.01(1)
M2 Al	0.82(2)	1.00(2)	0.89(3)	0.98(2)	0.87(2)	0.88(2)	0.90(1)	0.92(3)	0.95(1)	0.96(1)	0.95(1)	0.93(1)
A K	0.86(2)	0.93(1)	0.83(2)	0.80(1)	0.92(1)	0.90(1)	0.88(1)	0.92(2)	0.89(1)	0.94(1)	0.91(1)	0.92(1)

* CIF = CIFs were deposited.

TABLE 2b. Rietveld refinement for synthetic $KGa_3(Si_{3-x}Ge_x)O_{10}(OH,OD)_2$-muscovites

Run no.	[1209]	[1181]	[1447]CIF*	[1142]	[1467]CIF	[1207]	[1491]CIF	[1469]CIF	[1216]CIF
Symbol	Ga_3Si_3HMs	$Ga_3Si_{2.5}Ge_{0.5}$HMs	$Ga_3Si_2Ge_1$HMs	$Ga_3Si_{1.5}Ge_{1.5}$HMs	$Ga_3Si_{1.5}Ge_{1.5}$HMs	$Ga_3Si_1Ge_2$HMs	$Ga_3Si_1Ge_2$DMs	$Ga_3Si_{0.5}Ge_{2.5}$HMs	Ga_3Ge_3HMs
$< {}^{[4]}r >$ (Å)	0.313	0.329	0.345	0.361	0.361	0.378	0.378	0.394	0.410
Collecting conditions									
2□ scan range (°)	5-110	5-110	5-110	5-110	5-110	5-110	5-110	5-110	5-110
Step interval (°)	0.10	0.10	0.04	0.04	0.04	0.10	0.04	0.04	0.04
Integration times (s	5	5	4	12	4	4	4	4	4
Agreement indicies from Rietveld refinement									
R_{wp}(%)	23.3	30.4	14.5	28.2	12.9	22.9	17.0	10.5	17.4
R_p(%)	18.1	23.2	10.3	21.4	9.44	18.4	12.2	7.32	11.6
R_e(%)	5.45	4.95	5.94	6.28	5.87	5.51	5.65	5.95	5.72
S	4.28	6.13	2.44	4.48	2.19	4.15	3.01	1.76	3.03
Durbin-Watson d	0.837	0.526	0.423	0.174	0.423	0.564	0.397	0.753	0.322
R_F(%)	4.68	15.2	2.14	8.93	1.8	8.92	2.23	1.96	3.73
Unit-cell parameters									
a( )	5.291(5)	5.318(12)	5.3140(8)	5.334(2)	5.3286(6)	5.349(5)	5.3463(14)	5.3574(3)	5.3715(7)
b( )	9.133(9)	9.180(19)	9.2182(14)	9.255(4)	9.2452(11)	9.270(9)	9.276(2)	9.3005(6)	9.3254(13)
c( )	20.148(18)	20.39(4)	20.461(3)	20.570(8)	20.585(2)	20.63(2)	20.713(5)	20.8204(11)	20.933(3)
□(°)	94.13(3)	94.73(4)	95.690(4)	95.693(12)	95.691(4)	95.57(3)	95.680(7)	95.708(2)	95.691(5)
V(^{3})	971.1(16)	992.0(37)	997.3(2)	1010.5(7)	1009.1(2)	1018.1(18)	1022.1(5)	1032.26(10)	1043.4(2)
$a \sin$□( )	5.278(2)	5.300(2)	5.288(1)	5.307(1)	5.302(1)	5.323(1)	5.320(1)	5.331(2)	5.345(1)
d_{cal}(g/cm^3)	3.294(90)	3.338(83)	3.824(40)	4.306(46)	3.918(6)	3.763(27)	4.008(59)	4.081(16)	4.059(46)
Site-populations									
T1 Ga+Ge	0.00(4)	0.18(7)	0.56(2)	0.97(8)	0.67(1)	0.89(9)	0.84(3)	0.91(1)	1.00
Al+Si	1.00(4)	0.82(7)	0.44(2)	0.03(8)	0.33(1)	0.11(9)	0.16(3)	0.09(1)	0.00
T2 Ga+Ge	0.30(6)	0.42(9)	0.52(2)	0.69(7)	0.65(1)	0.50(8)	0.76(3)	0.90(1)	1.00
Al+Si	0.70(6)	0.58(7)	0.48(2)	0.31(7)	0.35(1)	0.50(8)	0.24(3)	0.10(1)	0.00
Average (T sites)									
Ga+Ge	0.15(15)	0.30(12)	0.54(2)	0.83(14)	0.66(1)	0.63(18)	0.80(4)	0.91(1)	1.00
Al+Si	0.85(15)	0.70(12)	0.46(2)	0.17(14)	0.34(1)	0.37(18)	0.20(4)	0.09(1)	0.00
M1 Ga	0.08(3)	0.00	0.00(1)	0.00(3)	0.00(1)	0.00(4)	0.08(1)	0.00(1)	0.00(1)
M2 Ga	0.91(6)	0.86(7)	1.00(1)	1.00(6)	1.00(1)	0.98(5)	0.96(2)	1.00	0.91(1)
A K	0.52(5)	0.72(6)	0.93(1)	1.00(6)	0.83(2)	0.78(5)	0.80(1)	0.92(1)	0.89(1)

* CIF = CIFs were deposited.

TABLE 2c. Rietveld refinement for synthetic $K(Al_{3-x}Ga_x)Ge_3O_{10}(OH,OD)_2$-muscovites

Run no.	[995]CIF*	[1271]CIF	[1217]CIF	[1270]CIF	[1025]CIF	[1269]CIF	[1101]CIF	[1267]CIF	[1026]CIF	[1266]CIF	[1102]CIF	[1265]CIF	[1027]CIF
Symbol	Al_3Ge_3HMs	$Al_{2.75}Ga_{0.25}Ge_3HMs$	$Al_{2.5}Ga_{0.5}Ge_3HMs$	$Al_{2.25}Ga_{0.75}Ge_3HMs$	$Al_2Ga_1Ge_3HMs$	$Al_{1.75}Ga_{1.25}Ge_3HMs$	$Al_{1.5}Ga_{1.5}Ge_3HMs$	$Al_{1.25}Ga_{1.75}Ge_3HMs$	$Al_1Ga_2Ge_3HMs$	$Al_{0.75}Ga_{2.25}Ge_3HMs$	$Al_{0.5}Ga_{2.5}Ge_3HMs$	$Al_{0.25}Ga_{2.75}Ge_3HMs$	Ga_3Ge_3HMs
Collecting conditions													
2□ scan range (°)	5-110	5-110	5-110	5-110	5-110	5-110	5-110	5-110	5-110	5-110	5-110	5-110	5-110
Step interval (°)	0.08	0.10	0.10	0.10	0.10	0.10	0.10	0.10	0.10	0.10	0.10	0.10	0.10
Integration times (s	10	5	5	5	5	5	5	5	5	5	5	5	5
Agreement indicies from Rietveld refinement													
R_{wp}(%)	8.89	12.6	11.7	10.3	9.49	10.8	10.4	12.1	10.2	19.2	9.49	11.5	13.0
R_n(%)	5.97	8.96	8.06	6.78	6.40	7.33	7.05	7.55	7.12	9.63	6.53	7.93	8.95
R_e(%)	3.03	4.54	7.23	4.49	4.23	4.64	4.57	4.44	4.31	4.27	4.47	4.43	4.31
S	2.94	2.78	1.62	2.30	2.24	2.32	2.27	2.72	2.36	4.49	2.12	2.64	3.01
Durbin-Watson *d*	1.13	1.03	1.22	1.15	1.40	1.05	1.12	1.39	1.12	1.17	1.73	1.67	1.09
R_F(%)	0.95	1.98	1.80	1.19	1.44	1.98	1.67	1.42	2.24	2.33	1.38	2.43	2.88
Unit-cell parameters													
a( )	5.2653(5)	5.2748(11)	5.2846(10)	5.2968(7)	5.3060(5)	5.3149(7)	5.3238(6)	5.3343(6)	5.3411(7)	5.3494(9)	5.3575(4)	5.3652(5)	5.3708(6)
b( )	9.1522(9)	9.1666(20)	9.1829(17)	9.2042(13)	9.2196(9)	9.2339(13)	9.2484(11)	9.2664(11)	9.2765(12)	9.2912(16)	9.3051(8)	9.3180(10)	9.3272(11)
c( )	20.919(2)	20.907(4)	20.901(4)	20.891(3)	20.8876(19)	20.886(3)	20.886(2)	20.890(2)	20.8943(25)	20.8967(33)	20.9113(16)	20.9363(19)	20.930(2)
□(°)	95.665(3)	95.678(7)	95.687(6)	95.695(5)	95.701(4)	95.704(5)	95.709(4)	95.715(4)	95.706(5)	95.716(6)	95.717(3)	95.713(4)	95.708(4)
V(^{3})	1003.1(2)	1005.9(4)	1009.3(3)	1013.5(2)	1016.75(16)	1019.9(2)	1023.2(2)	1027.5(2)	1030.1(2)	1034.0(3)	1037.30(15)	1041.46(18)	1043.3(2)
a sin□( )	5.240	5.249(1)	5.259	5.271	5.280	5.289	5.297	5.308	5.315	5.323	5.331	5.339	5.344
d_{cal}(g/cm^3)	3.342(5)	3.409(30)	3.497(1)	3.565(5)	3.624	3.716(17)	3.839	3.846(22)	3.942	4.002	3.983	3.094	4.120
Site-populations													
T1 Ga+Ge	0.65(1)	0.66(2)	0.71(2)	0.72(2)	0.73(2)	0.78(2)	0.84(2)	0.82(2)	0.88(2)	0.90(4)	0.88(2)	0.94(2)	1.00
Al	0.35(1)	0.34(2)	0.29(2)	0.28(2)	0.27(2)	0.22(2)	0.16(2)	0.18(2)	0.12(2)	0.10(4)	0.12(2)	0.06(2)	0.00
T2 Ga+Ge	0.63(1)	0.63(3)	0.67(2)	0.70(2)	0.73(2)	0.75(2)	0.80(2)	0.82(2)	0.85(2)	0.89(4)	0.87(2)	0.93(2)	1.00
Al	0.37(1)	0.37(3)	0.33(2)	0.30(2)	0.27(2)	0.25(2)	0.20(2)	0.18(2)	0.15(2)	0.11(4)	0.13(2)	0.07(2)	0.00
Average (T sites)													
Ga+Ge	0.64	0.65(2)	0.69(3)	0.71(1)	0.73(0)	0.77(2)	0.82(2)	0.82(0)	0.87(2)	0.90(1)	0.88(1)	0.94(1)	1.00
Al	0.37	0.35(2)	0.31(3)	0.29(1)	0.27(0)	0.23(2)	0.18(2)	0.18(0)	0.13(2)	0.10(1)	0.12(1)	0.06(1)	0.00
M1 Ga	-	0.00(1)	0.00(0)	0.00(9)	0.00(8)	0.00(1)	0.00(2)	0.00 (1)	0.00(1)	0.00(2)	0.00(2)	0.00(1)	0.00(1)
Al	0.01(1)	-	-	-	-	-	-	-	-	-	-	-	-
M2 Ga	-	0.06(2)	0.15(2)	0.27(1)	0.35(1)	0.46(2)	0.55(2)	0.64(2)	0.70(2)	0.75(4)	0.81(2)	0.91(2)	0.97(1)
Al	0.93(1)	0.94(2)	0.85(2)	0.73(1)	0.65(1)	0.54(2)	0.45(2)	0.36(2)	0.30(2)	0.25(4)	0.19(2)	0.09(2)	-
A K	0.92(8)	0.94(1)	0.95(1)	0.94(1)	0.96(1)	0.96(1)	1.00(3)	0.98(1)	1.00(1)	1.00(2)	0.98(1)	1.00(2)	1.00(2)

* CIF = CIFs were deposited.

TABLE 2d. Rietveld refinement for synthetic muscovite-tobelite series, $[K_{1-A}(NH_4,ND_4)_A]Al_2(AlSi_3)O_{10}(OH,OD)_2$

Run no.	[Natural]CIF*	[1383]	[1382]	[1381]	[1438]CIF	[1426]	[1606]	[1437]
Symbol	Ms_{100}(UT)	$DMs_{75}Tob_{25}$	$DMs_{50}Tob_{50}$	$DMs_{25}Tob_{75}$	$HMs_{00}Tob_{100}$	$DMs_{00}Tob_{100}$	$HMs_{00}Tob_{100}$(Kln)	$DMs_{00}Tob_{100}$(Kln)
Collecting conditions								
2□ scan range (°)	5-110	5-110	5-110	5-110	5-110	5-110	5-110	5-110
Step interval (°)	0.04	0.10	0.10	0.10	0.04	0.04	0.04	0.04
Integration times (s	10	5	5	5	12	4	4	4
Agreement indicies from Rietveld refinement								
R_{wp}(%)	14.0	24.9	23.0	24.5	23.7	25.4	26.3	26.2
R_p(%)	10.5	19.5	18.5	19.4	17.5	19.6	20.3	20.5
R_e(%)	9.59	7.15	6.92	6.59	7.64	5.49	6.97	5.56
S	1.46	3.49	3.33	3.71	3.11	4.62	3.77	4.71
Durbin-Watson *d*	0.642	0.724	0.716	0.754	0.307	0.212	0.116	0.105
R_F(%)	1.95	7.60	4.20	5.49	3.84	3.63	8.03	7.32
Unit-cell parameters								
a( )	5.1932(14)	5.224(5)	5.209(5)	5.205(5)	5.198(4)	5.200(6)	5.214(4)	5.214(4)
b( )	9.012(2)	9.007(9)	9.023(9)	9.025(10)	9.021(7)	9.043(10)	9.032(6)	9.024(6)
c( )	20.080(5)	20.32(2)	20.41(2)	20.50(2)	20.743(14)	20.696(23)	20.623(15)	20.688(14)
□(°)	95.752(6)	93.20(3)	93.86(4)	93.94(4)	95.36(3)	93.89(4)	93.68(3)	93.59(2)
V(^{3})	935.0(4)	954.6(17)	957.1(16)	960.7(17)	968.4(12)	971.0(19)	969.2(12)	971.5(11)
asin□( )	5.166(1)	5.215(1)	5.197(2)	5.192(1)	5.175(1)	5.188(4)	5.203(1)	5.204(1)
d_{cal}(g/cm^3)	2.707(30)	2.663(24)	2.656(28)	2.594(24)	2.586(4)	2.503(41)	2.599(19)	2.555(5)
Site-populations								
M1 Al	0.00(1)	0.33(5)	0.18(6)	0.09(7)	0.27(3)	0.00(5)	0.72(4)	0.78(3)
M2 Al	0.93(1)	0.85(3)	0.93(4)	0.90(5)	0.85(3)	0.89(4)	0.82(3)	0.69(3)
A K	0.92(1)	0.80(5)	0.27(4)	0.06(4)	-	-	-	-
NH_4/ND_4	-	0.20(5)	0.73(4)	0.94(4)	0.90(4)	0.77(6)	0.13(7)	0.20(6)

* CIF = CIFs were deposited.

1210A13SI3DMs

5 µm

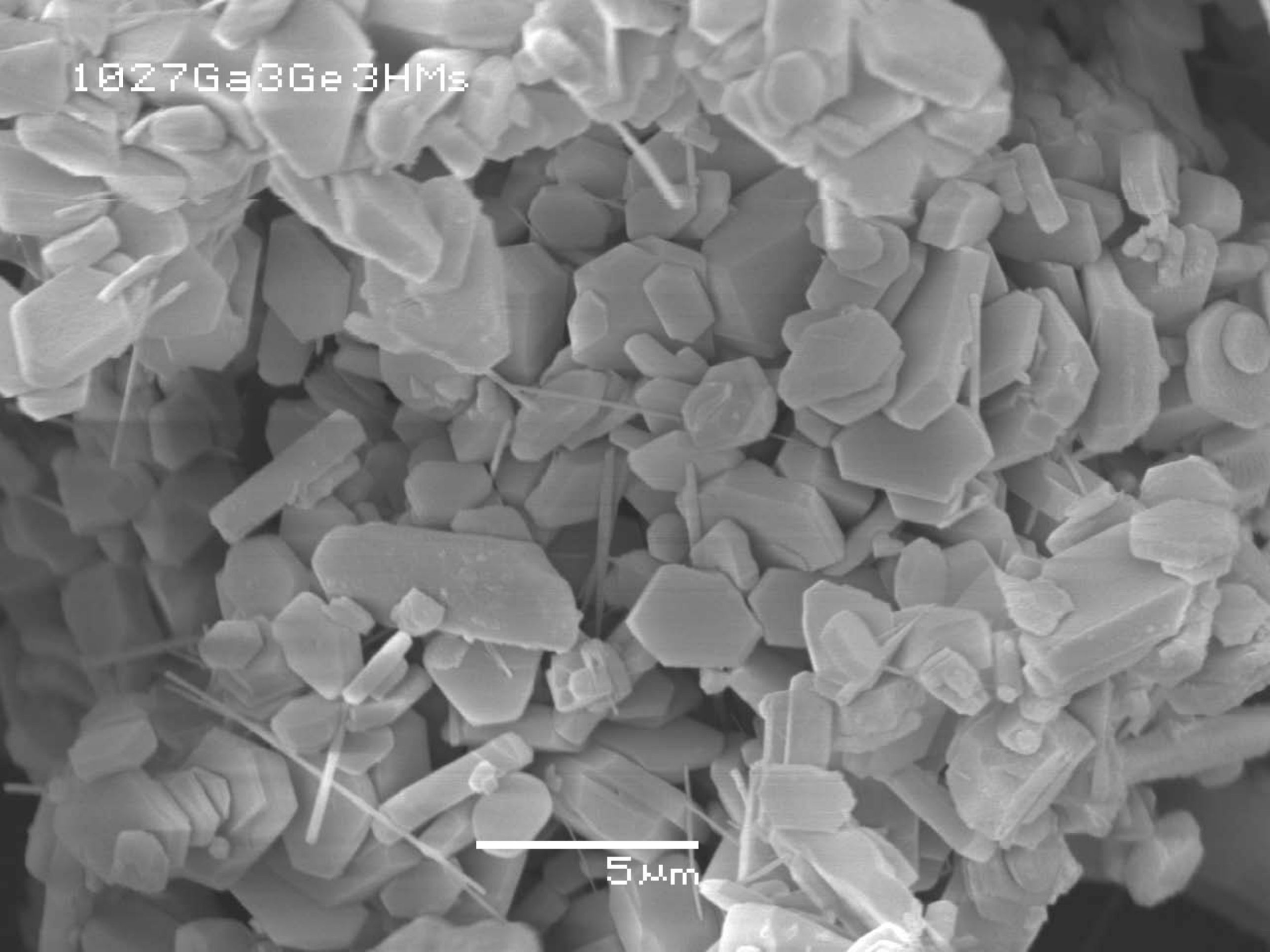
1027Ga3Ge3HMs
5 µm

1102A10.5Ga2.5Ge3HMs

5 µm

DTob100Ms00

2 µm

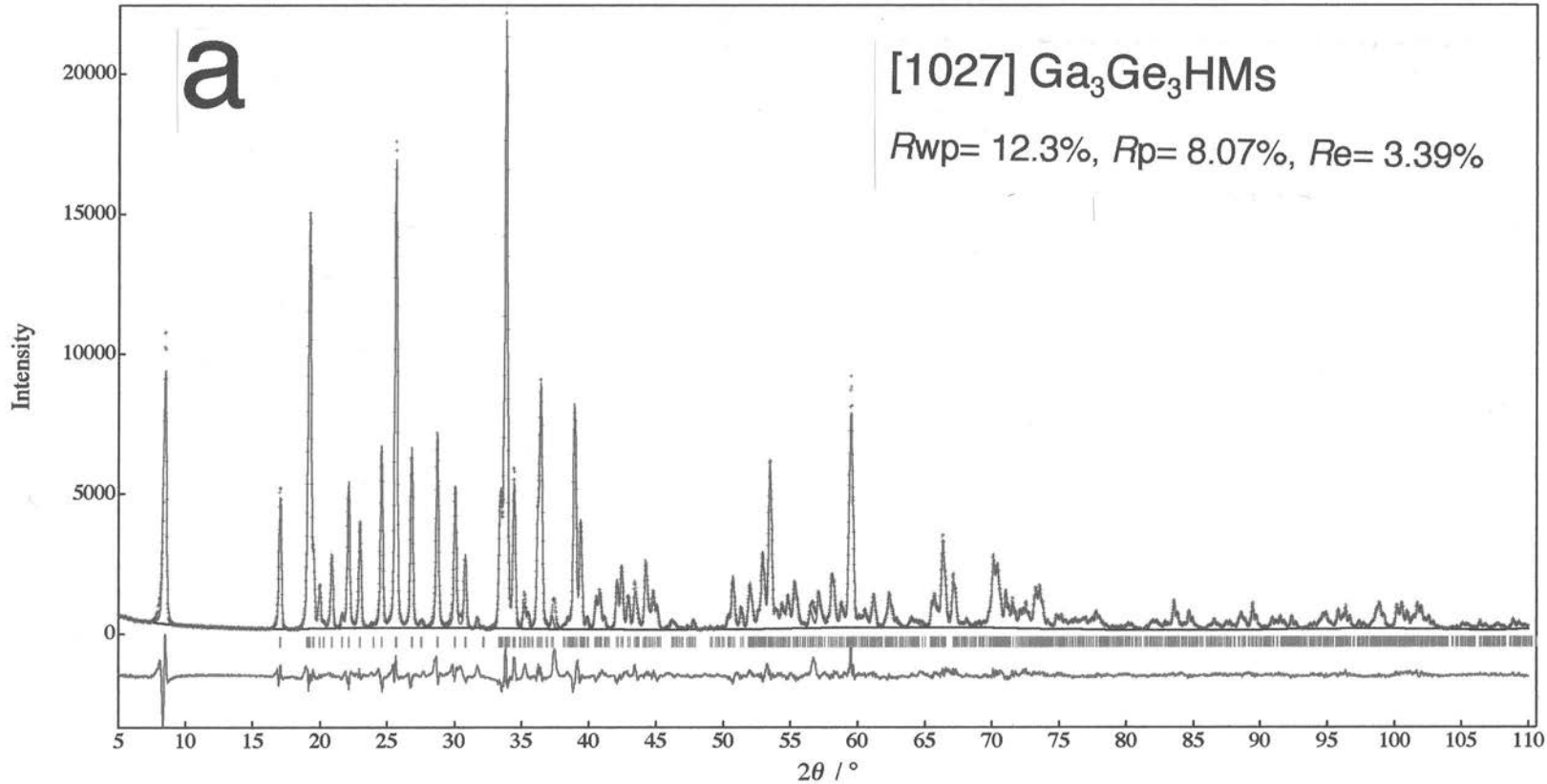
a
[1027] Ga_3Ge_3HMs
*R*wp= 12.3%, *R*p= 8.07%, *R*e= 3.39%
Intensity
20000
15000
10000
5000
0
5
10
15
20
25
30
35
40
45
50
55
60
65
70
75
80
85
90
95
100
105
110
2θ / °

Fig. 2a

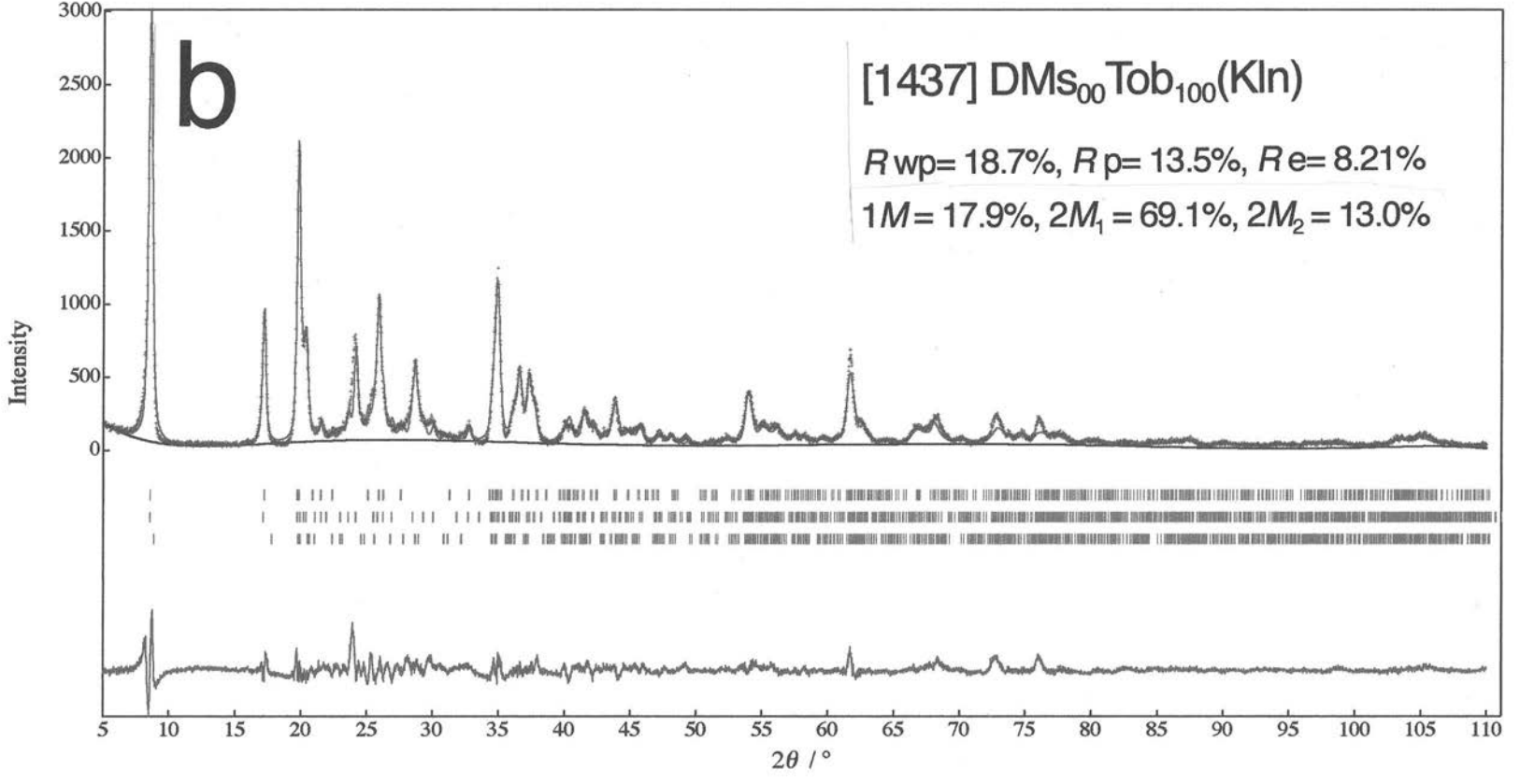
b
[1437] DMs00Tob100(Kln)
Rwp= 18.7%, Rp= 13.5%, Re= 8.21%
1M= 17.9%, 2M1 = 69.1%, 2M2 = 13.0%
Intensity
3000
2500
2000
1500
1000
500
0
5
10
15
20
25
30
35
40
45
50
55
60
65
70
75
80
85
90
95
100
105
110
2θ / °

Fig. 2b

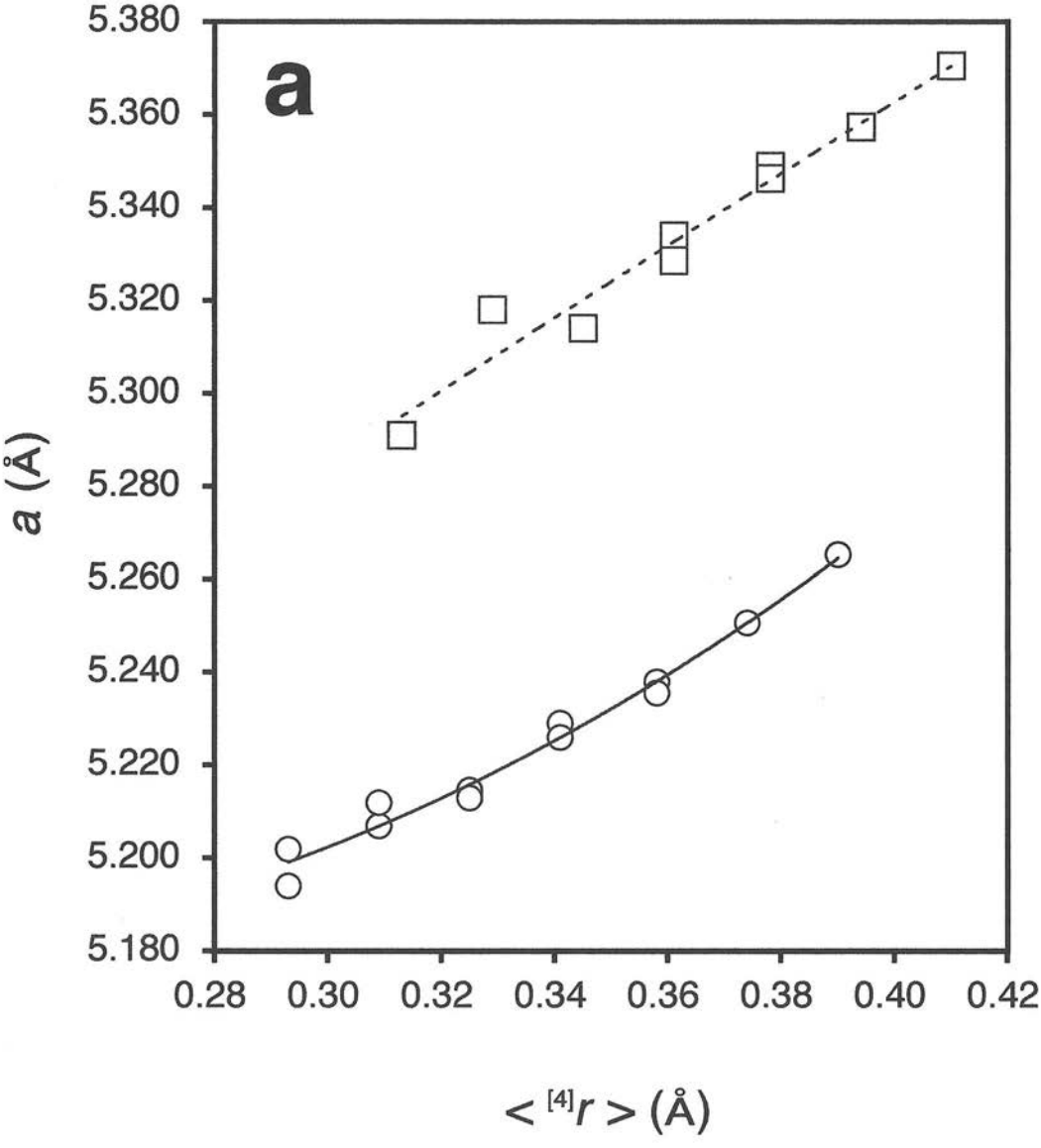
a
5.380
5.360
5.340
5.320
5.300
5.280
5.260
5.240
5.220
5.200
5.180
a (Å)
0.28
0.30
0.32
0.34
0.36
0.38
0.40
0.42
< [4]r > (Å)

Fig. 3a

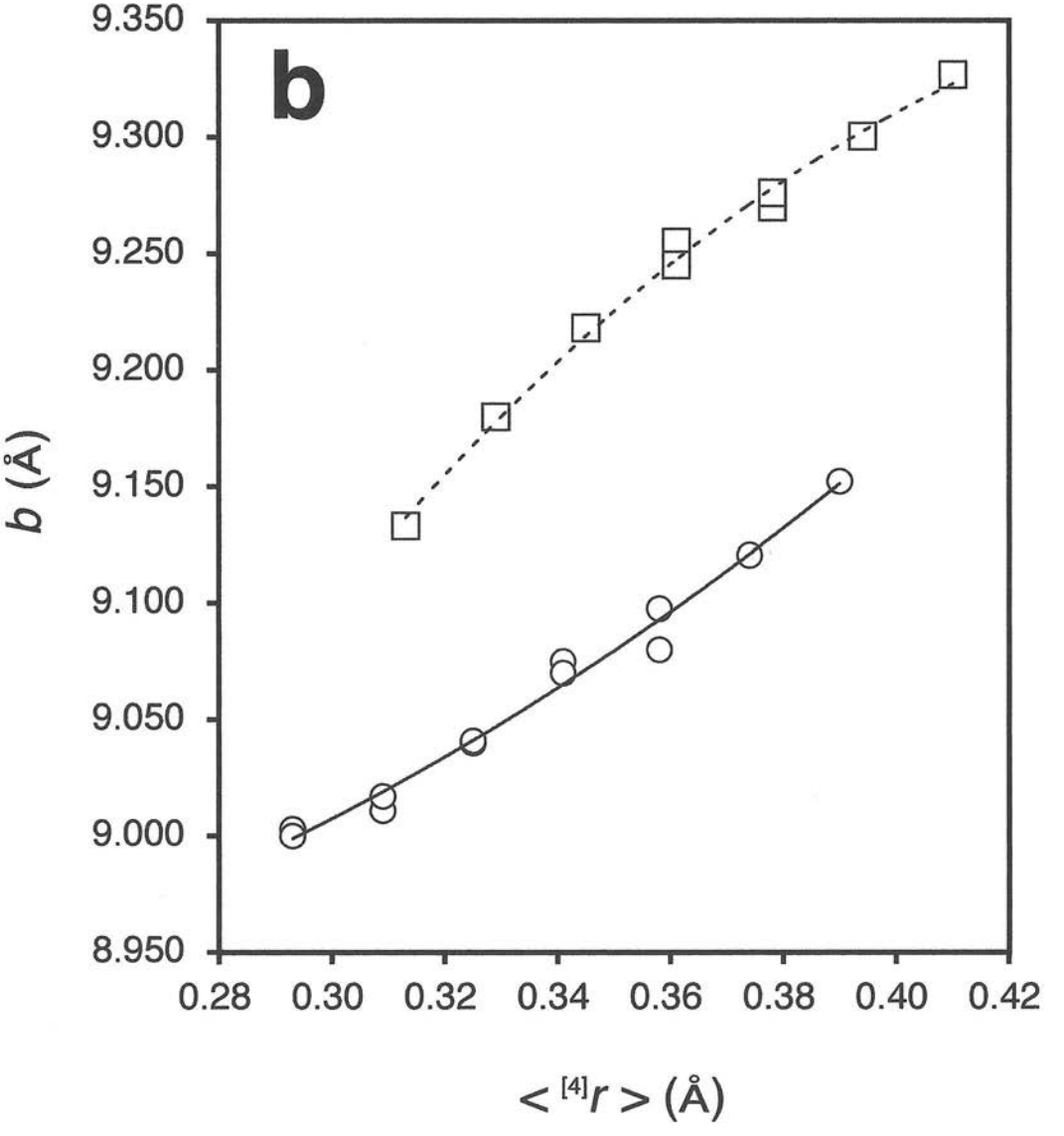
b
9.350
9.300
9.250
9.200
9.150
9.100
9.050
9.000
8.950
b (Å)
0.28
0.30
0.32
0.34
0.36
0.38
0.40
0.42
< [4]r > (Å)

Fig. 3b

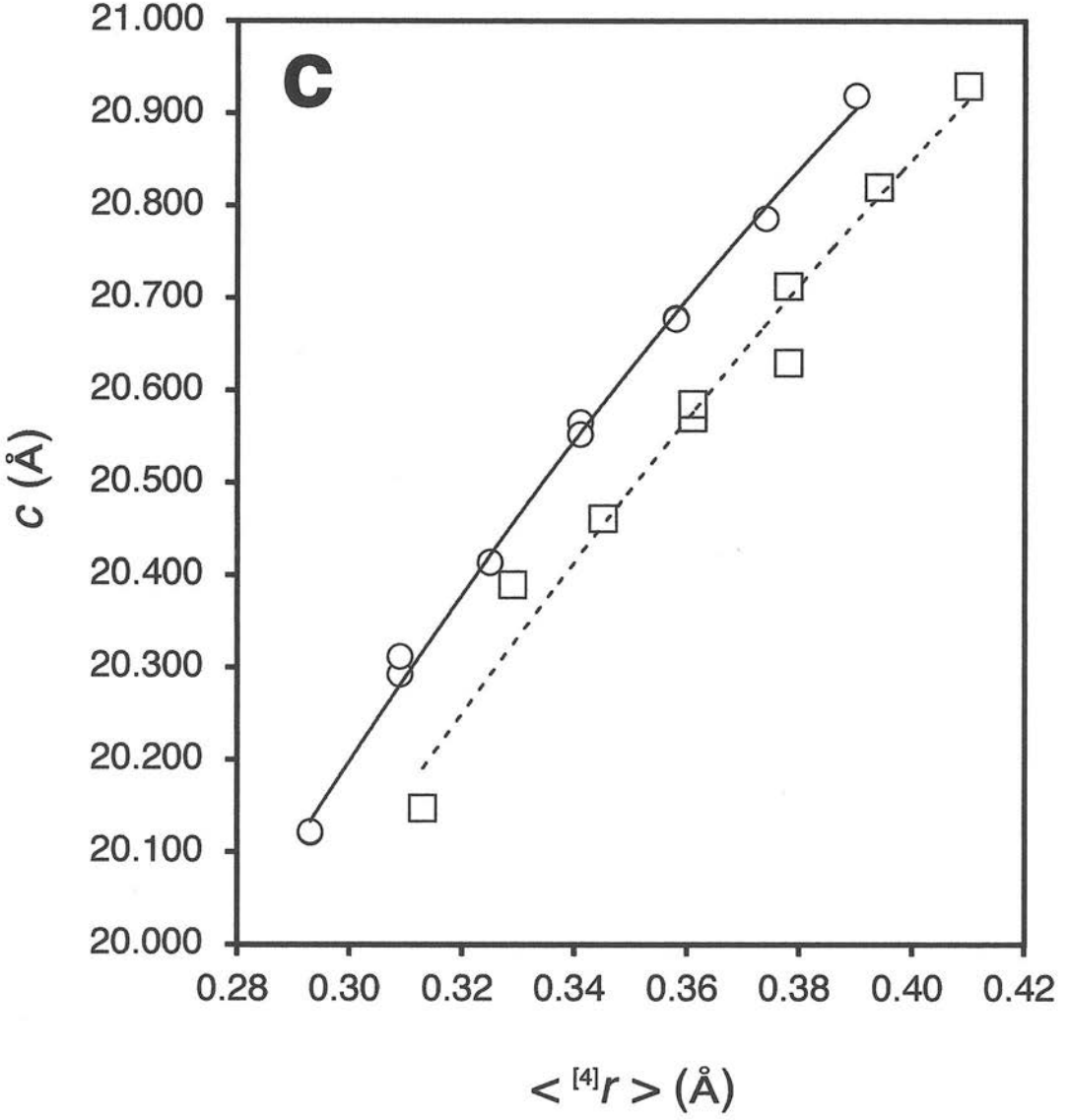
c
21.000
20.900
20.800
20.700
20.600
20.500
20.400
20.300
20.200
20.100
20.000
c (Å)
0.28
0.30
0.32
0.34
0.36
0.38
0.40
0.42
< [4]r > (Å)

Fig. 3c

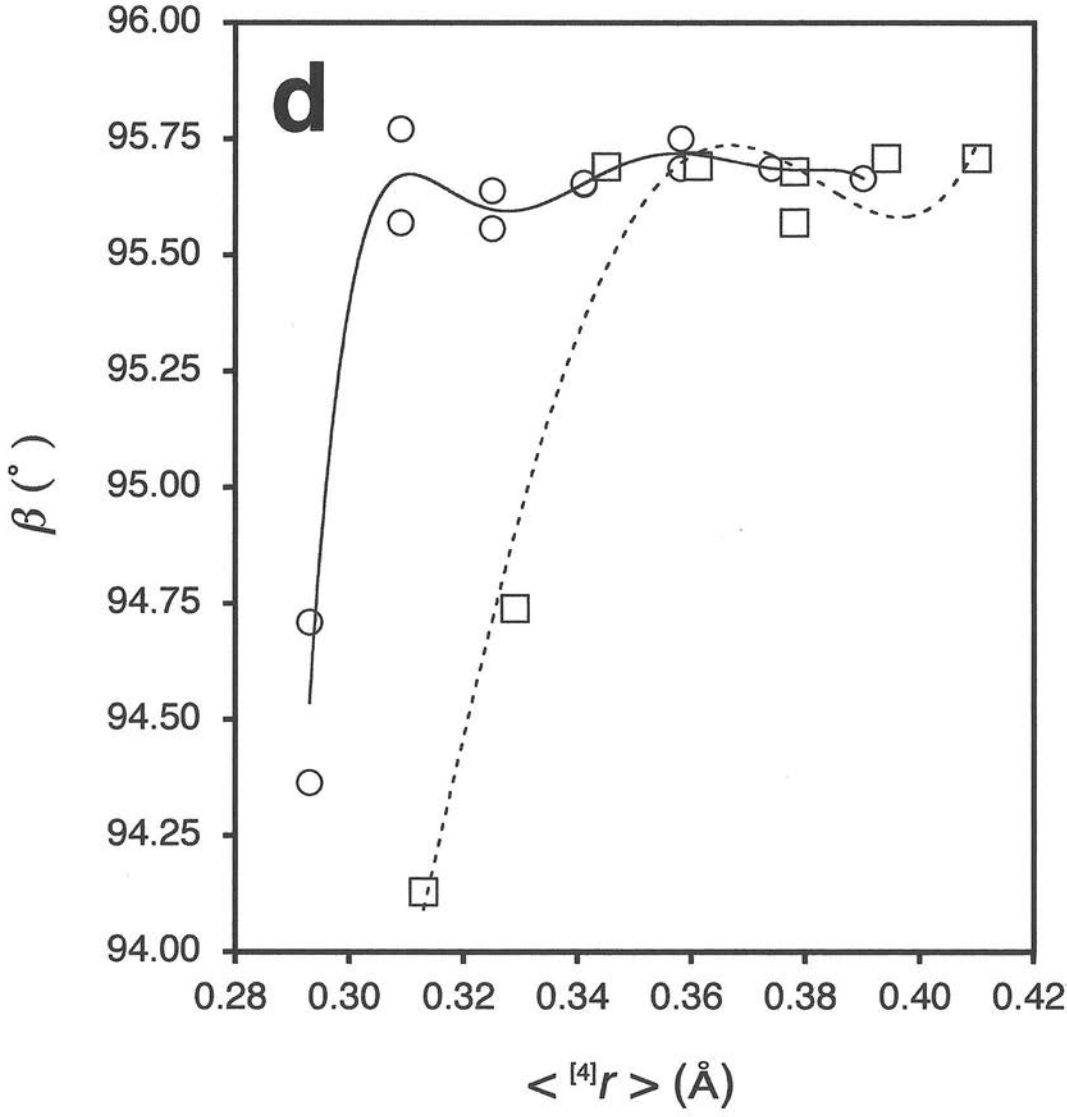
d
96.00
95.75
95.50
95.25
95.00
94.75
94.50
94.25
94.00
β (°)
0.28
0.30
0.32
0.34
0.36
0.38
0.40
0.42
< [4]r > (Å)

Fig. 3d

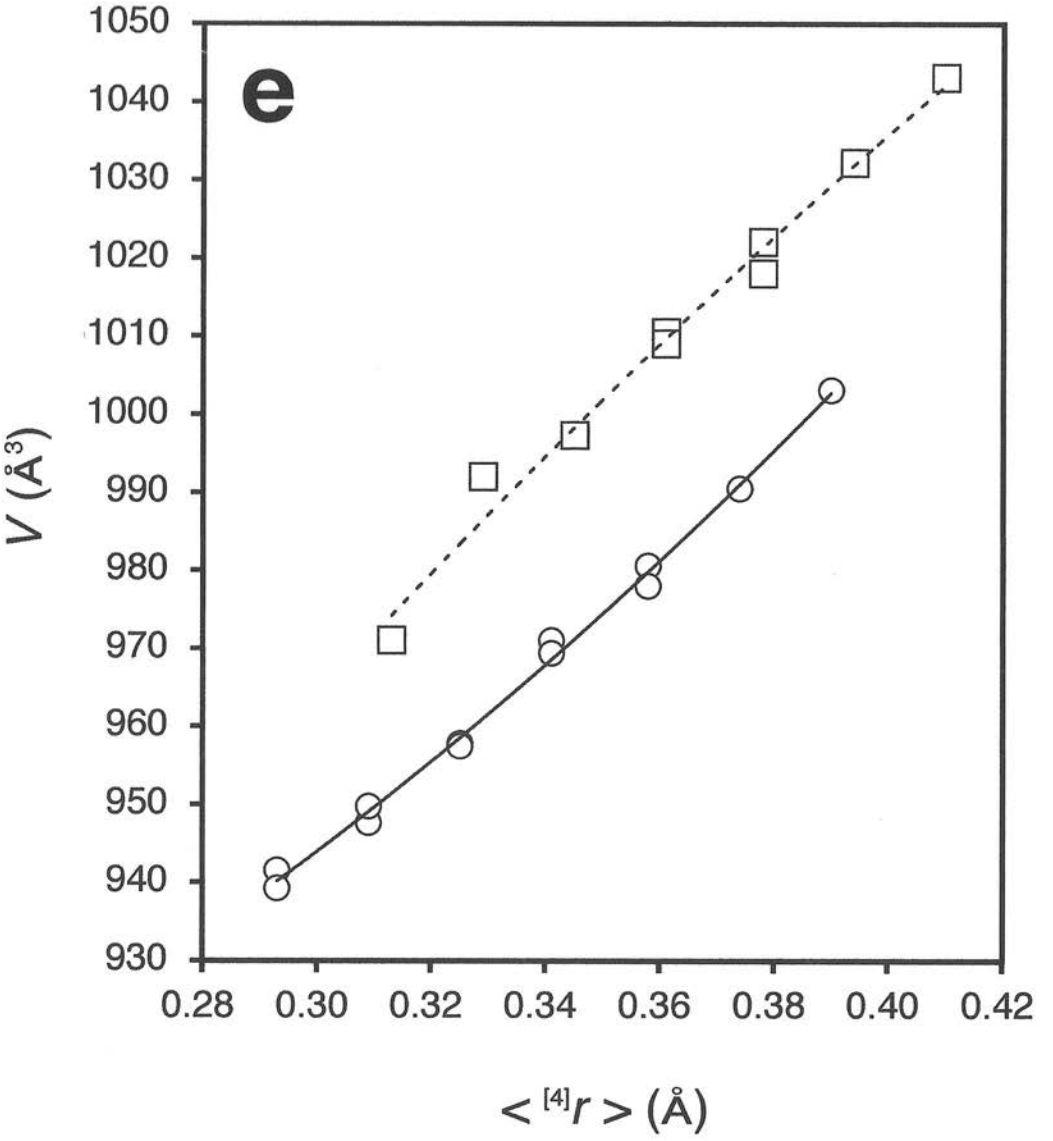
e
1050
1040
1030
1020
1010
1000
990
980
970
960
950
940
930
V (Å3)
0.28
0.30
0.32
0.34
0.36
0.38
0.40
0.42
< [4]r > (Å)

Fig.3e

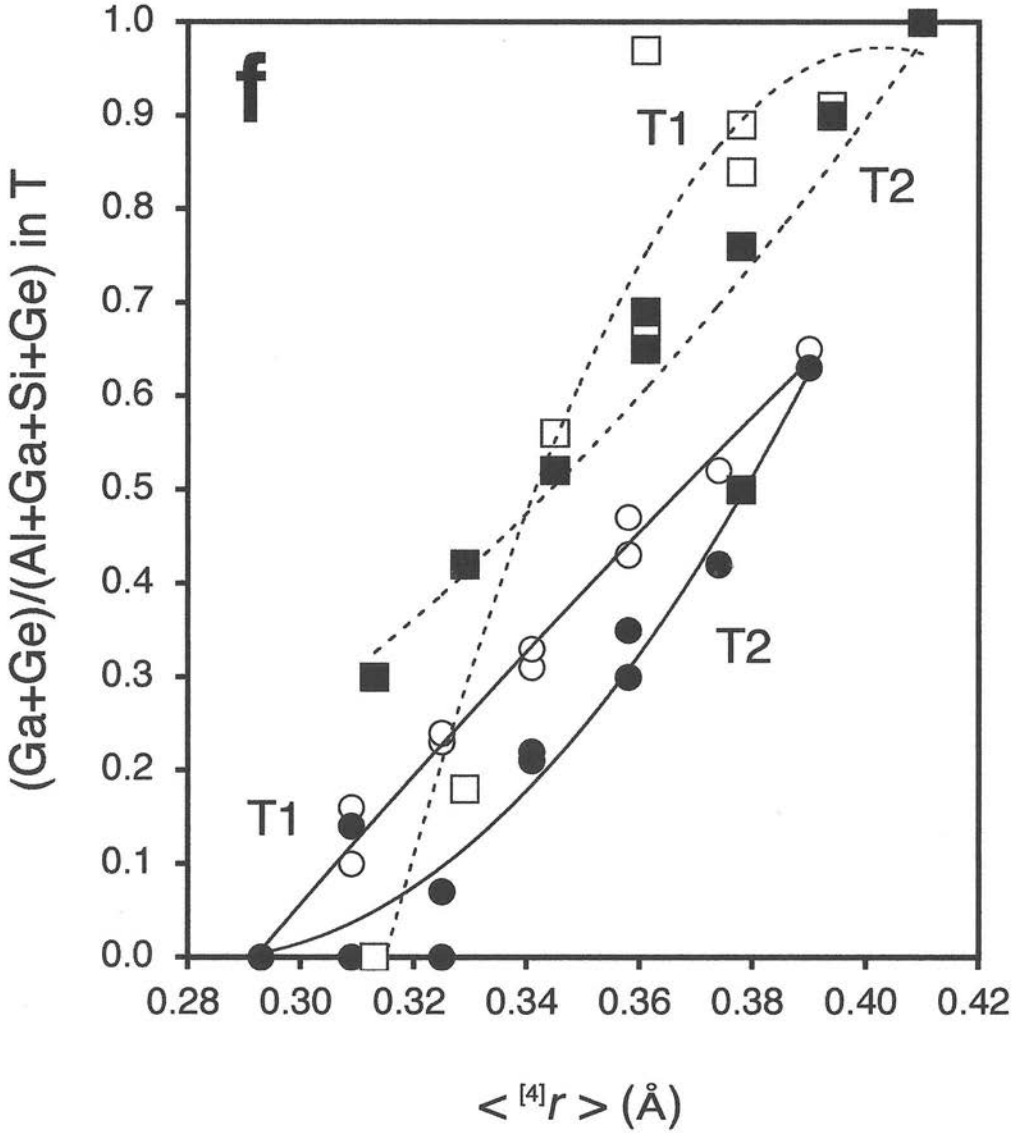
f
T1
T2
T2
T1
(Ga+Ge)/(Al+Ga+Si+Ge) in T
1.0
0.9
0.8
0.7
0.6
0.5
0.4
0.3
0.2
0.1
0.0
0.28
0.30
0.32
0.34
0.36
0.38
0.40
0.42
< [4]r > (Å)

Fig. 3f

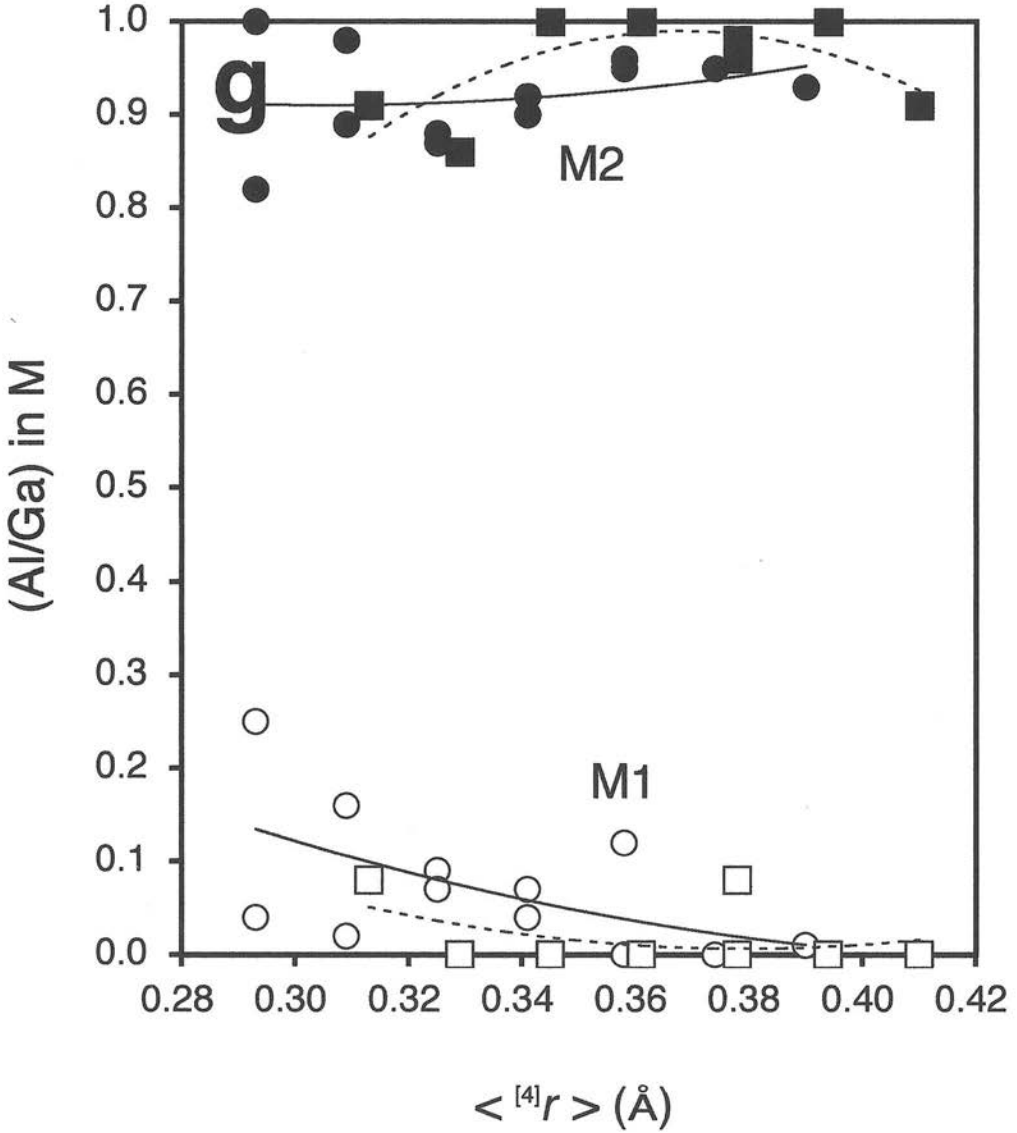
g
M2
M1
(Al/Ga) in M
1.0
0.9
0.8
0.7
0.6
0.5
0.4
0.3
0.2
0.1
0.0
0.28
0.30
0.32
0.34
0.36
0.38
0.40
0.42
< [4]r > (Å)

Fig.3g

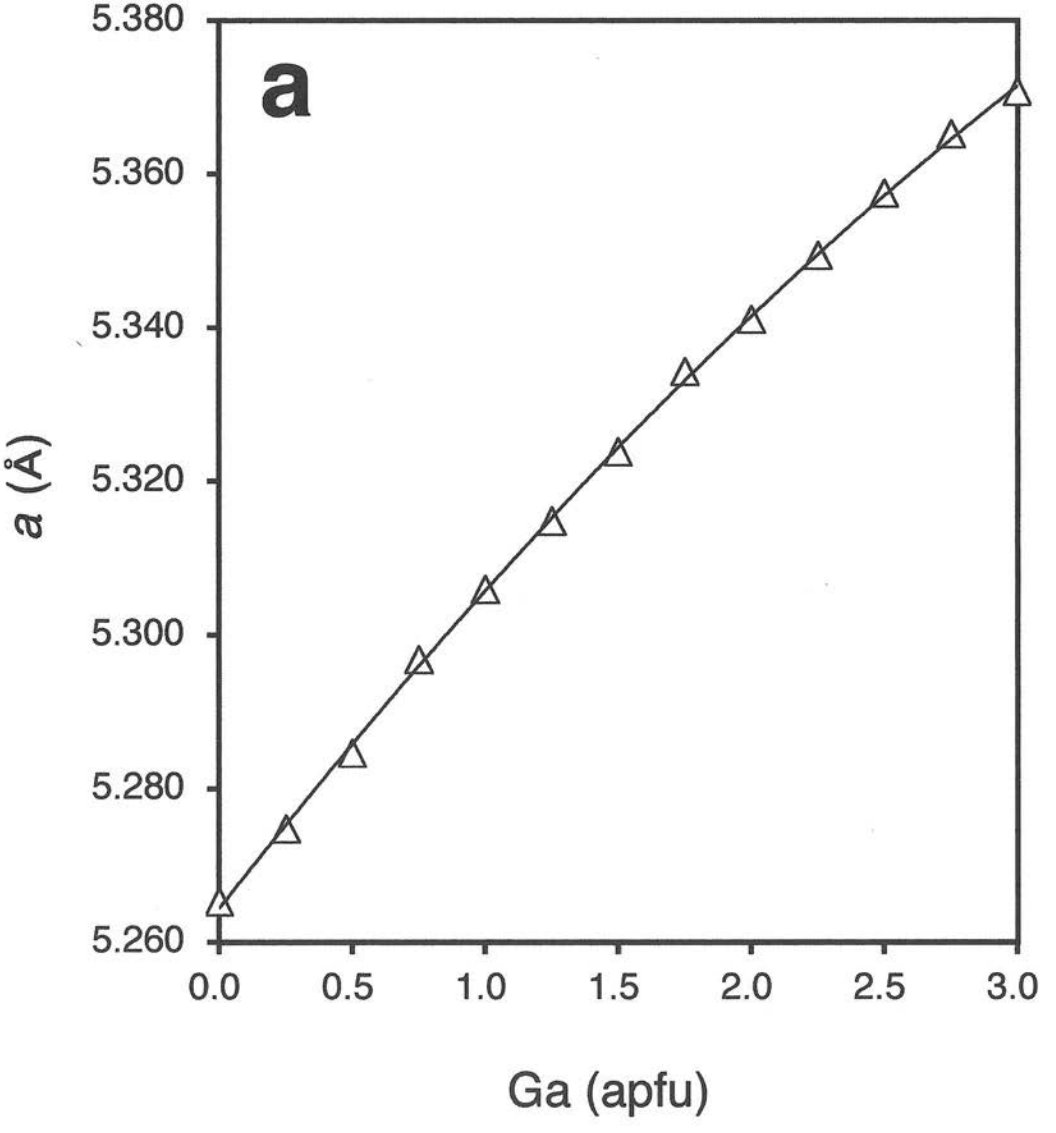
a
5.380
5.360
5.340
5.320
5.300
5.280
5.260
a (Å)
0.0
0.5
1.0
1.5
2.0
2.5
3.0
Ga (apfu)

Fig. 4a

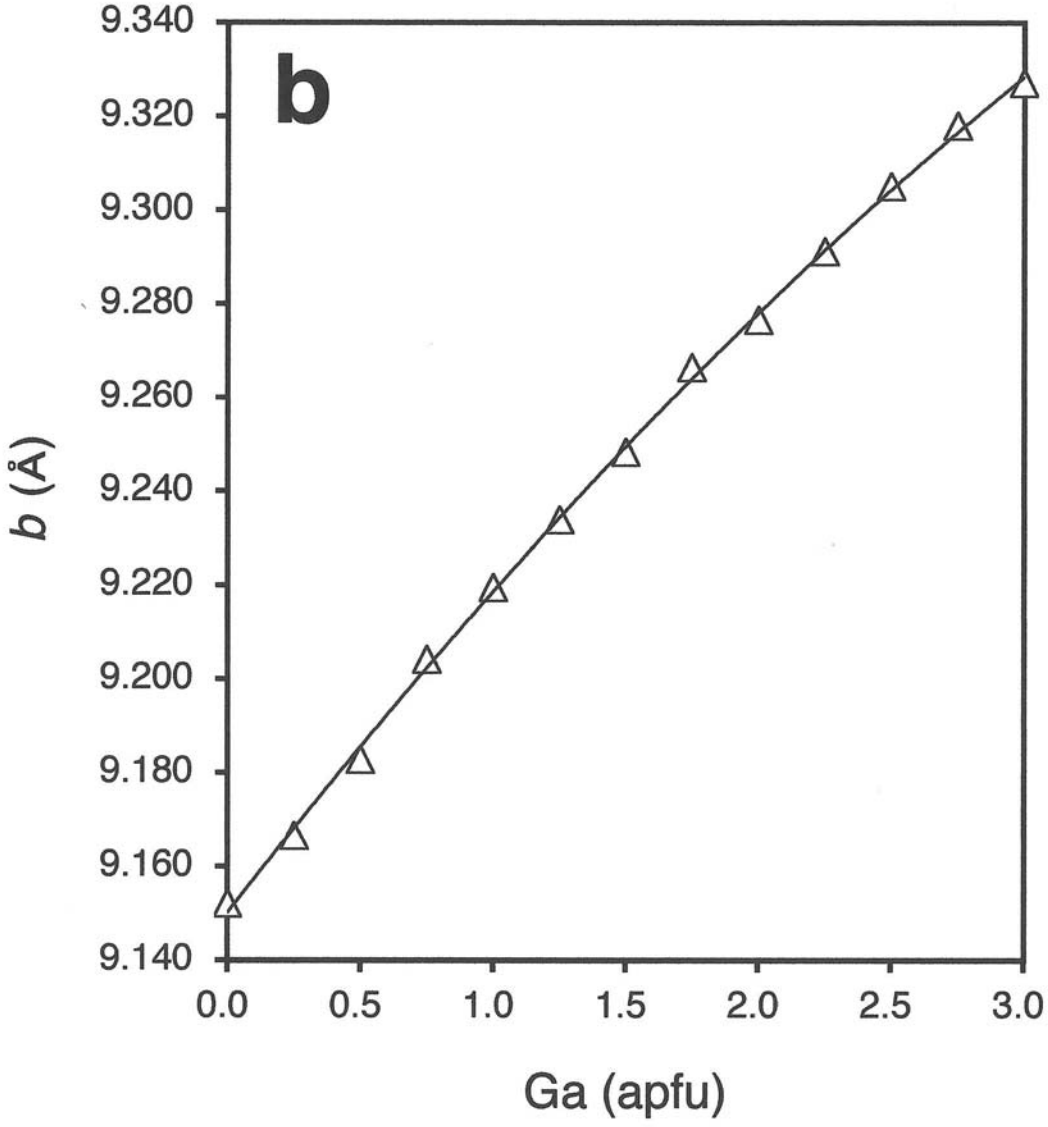
b
9.340
9.320
9.300
9.280
9.260
9.240
9.220
9.200
9.180
9.160
9.140
b (Å)
0.0
0.5
1.0
1.5
2.0
2.5
3.0
Ga (apfu)

Fig. 4b

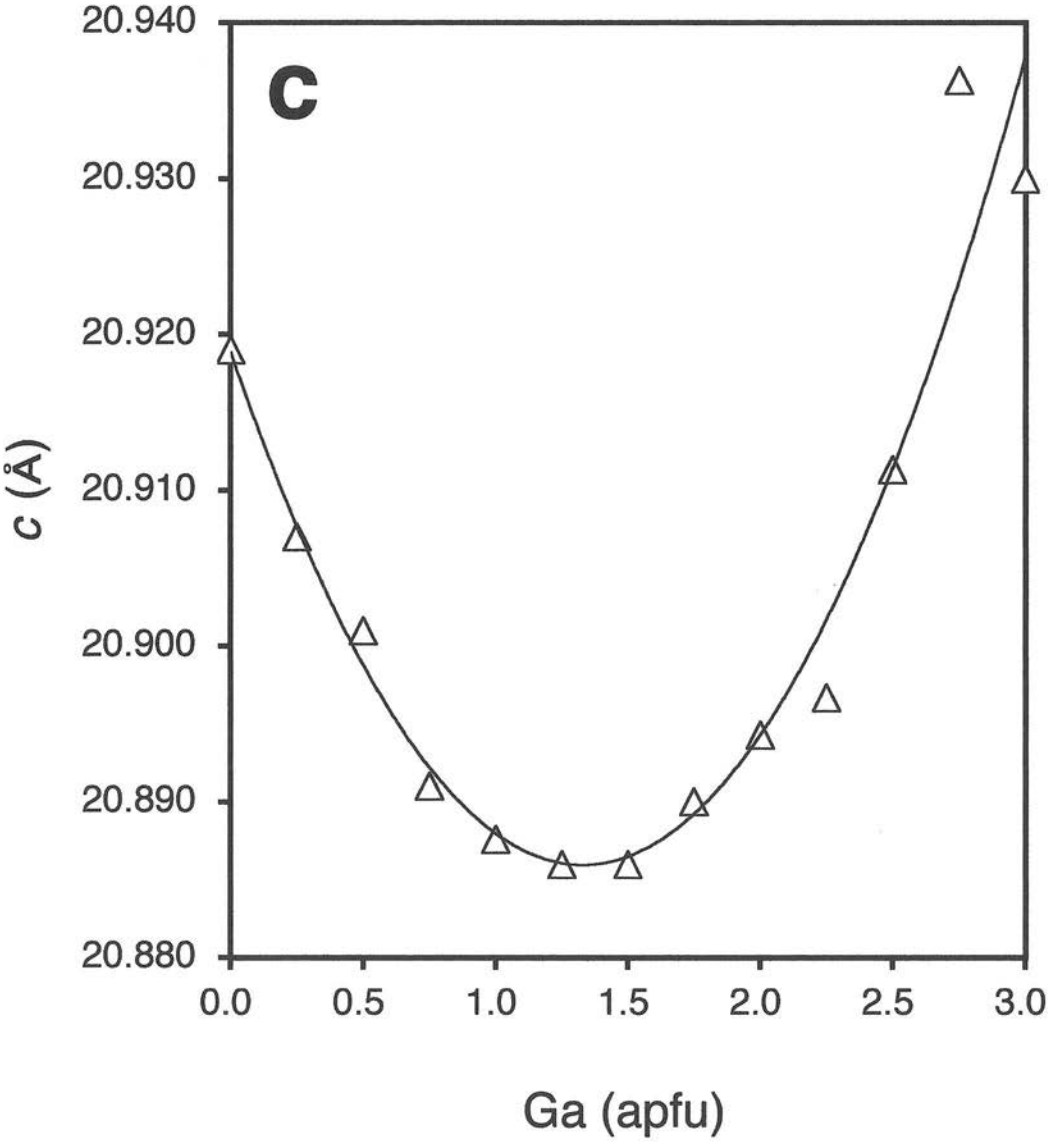
c
20.940
20.930
20.920
20.910
20.900
20.890
20.880
c (Å)
0.0
0.5
1.0
1.5
2.0
2.5
3.0
Ga (apfu)

Fig.4c

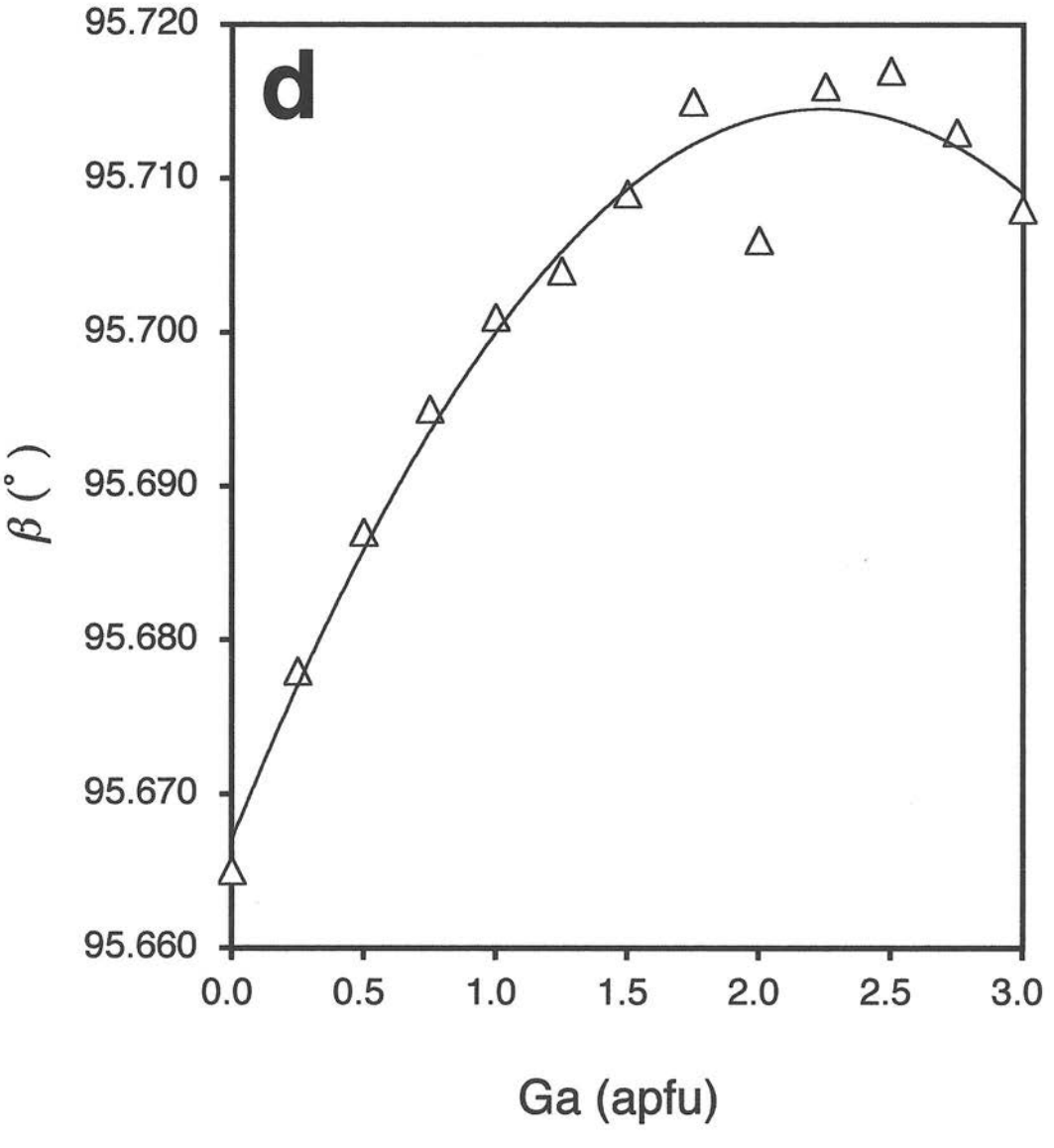
d
95.720
95.710
95.700
95.690
95.680
95.670
95.660
β (°)
0.0
0.5
1.0
1.5
2.0
2.5
3.0
Ga (apfu)

Fig. 4d

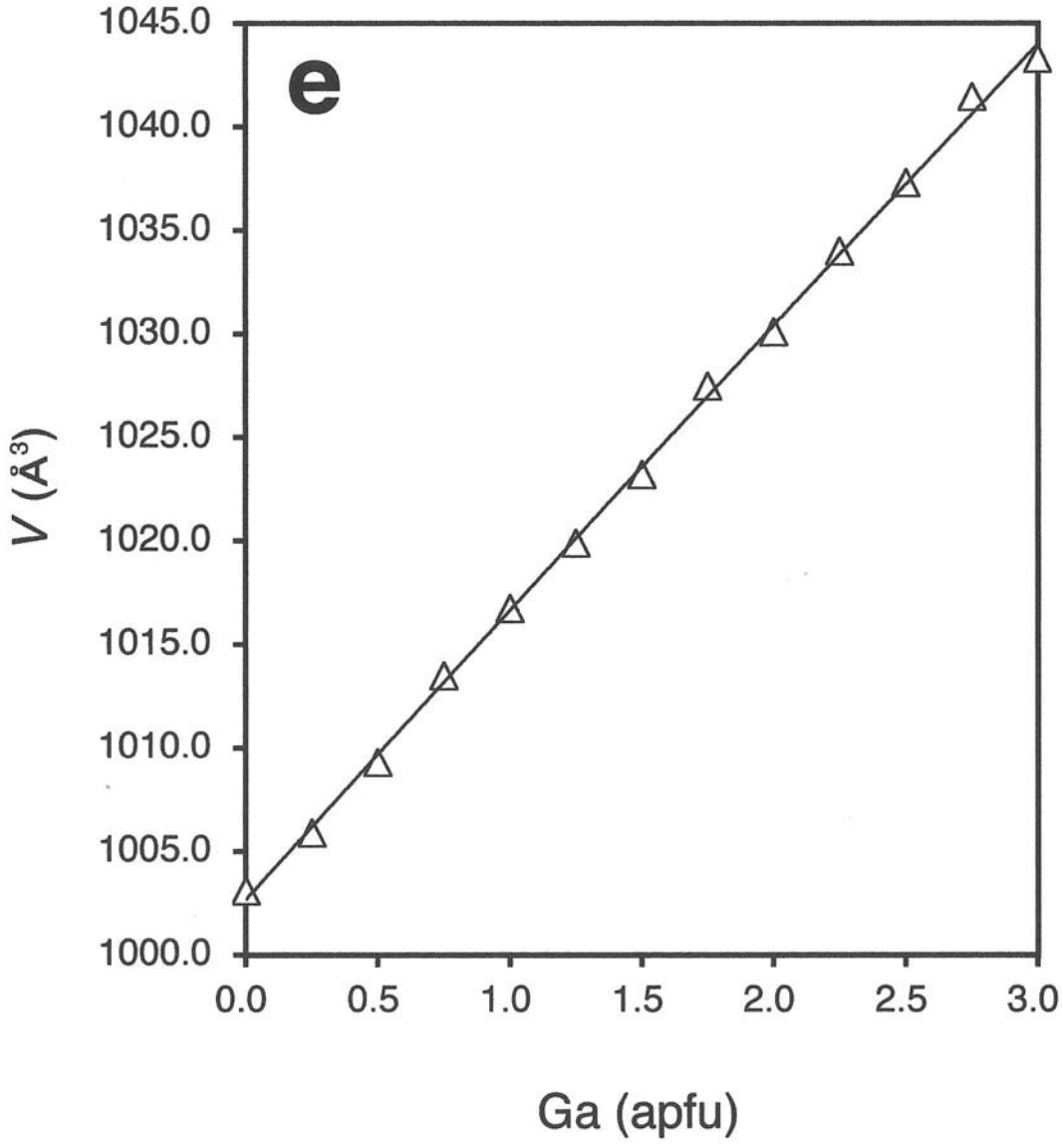
e
1045.0
1040.0
1035.0
1030.0
1025.0
1020.0
1015.0
1010.0
1005.0
1000.0
V (Å3)
0.0
0.5
1.0
1.5
2.0
2.5
3.0
Ga (apfu)

Fig. 4e

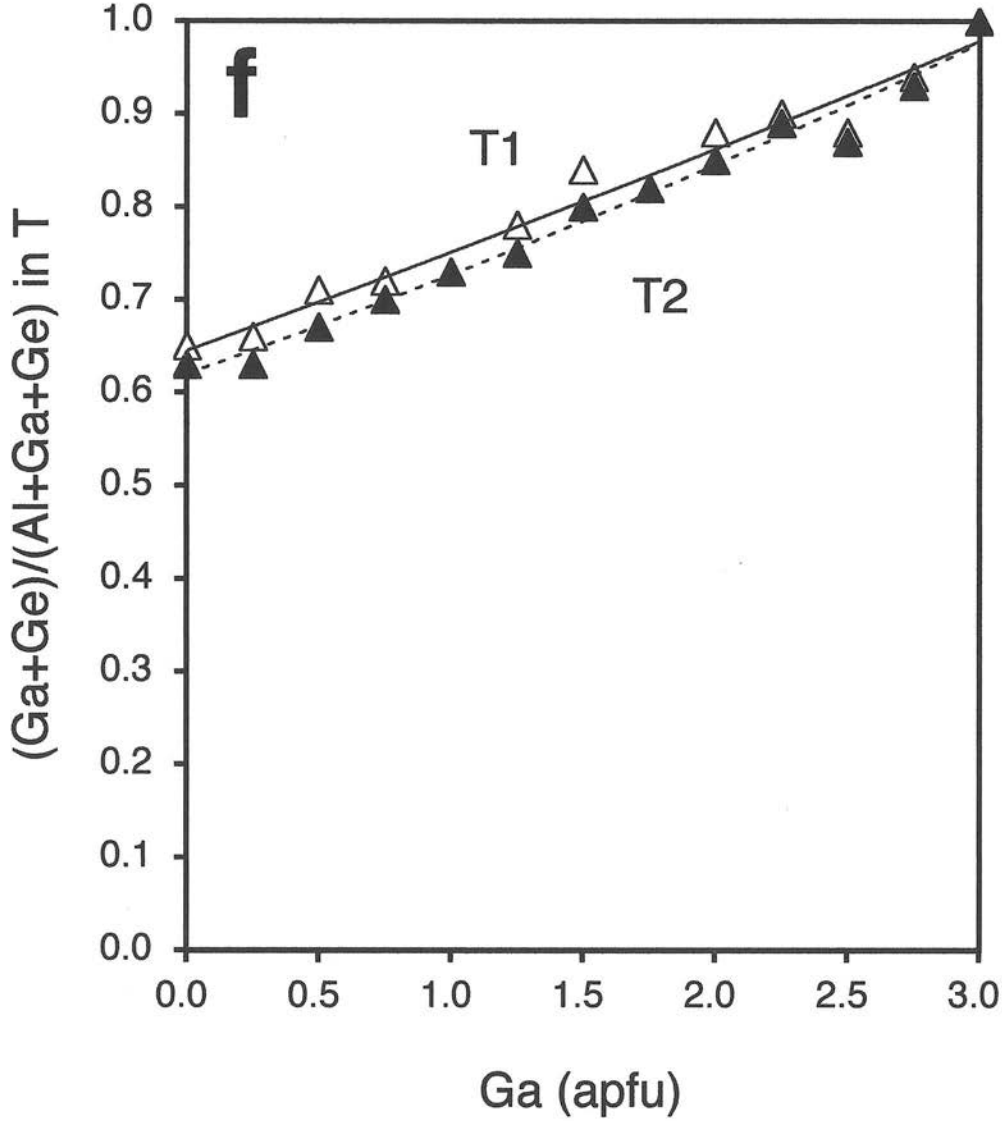
f
T1
T2
(Ga+Ge)/(Al+Ga+Ge) in T
Ga (apfu)
0.0
0.1
0.2
0.3
0.4
0.5
0.6
0.7
0.8
0.9
1.0
0.0
0.5
1.0
1.5
2.0
2.5
3.0

Fig. 4f

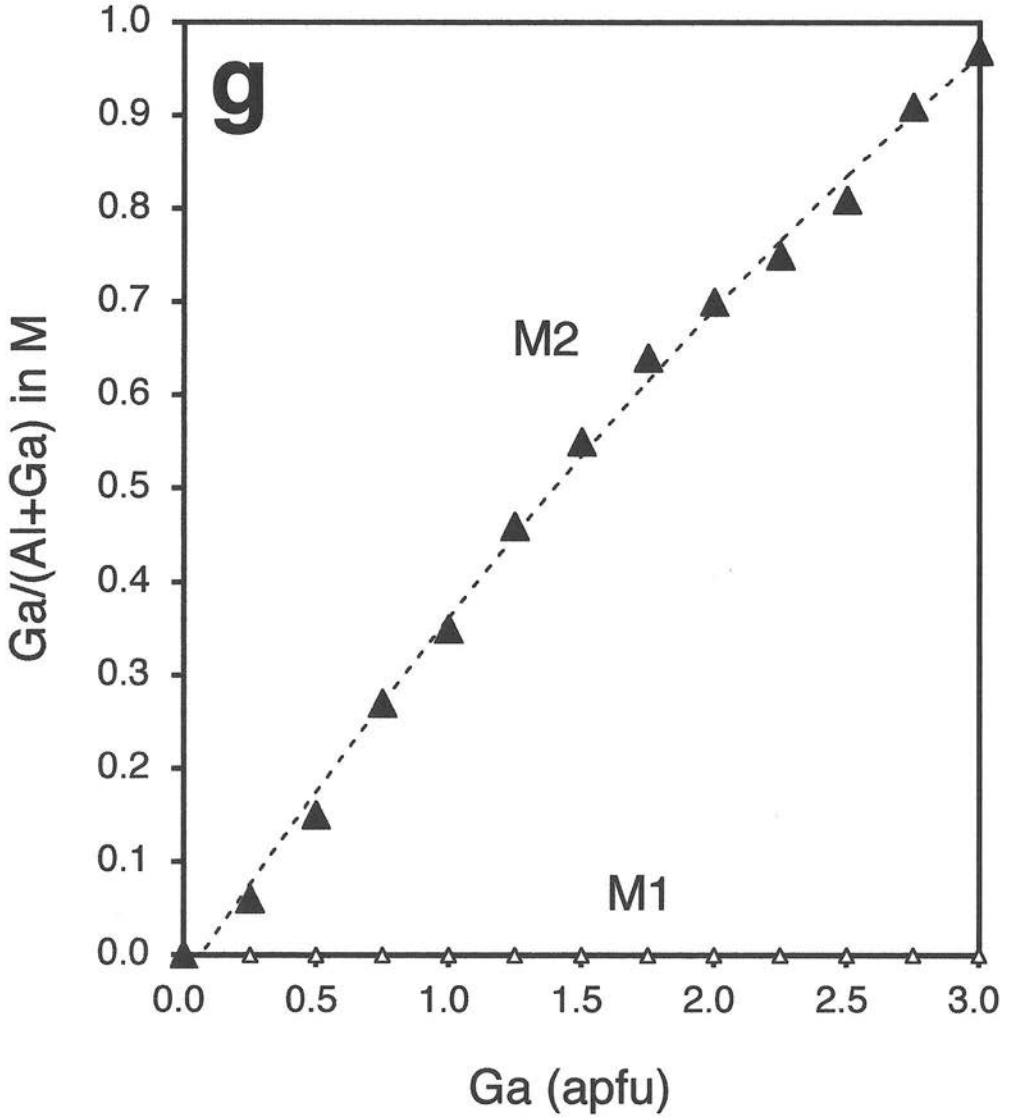
g
M2
M1
Ga/(Al+Ga) in M
Ga (apfu)
0.0
0.1
0.2
0.3
0.4
0.5
0.6
0.7
0.8
0.9
1.0
0.0
0.5
1.0
1.5
2.0
2.5
3.0

Fig.4g

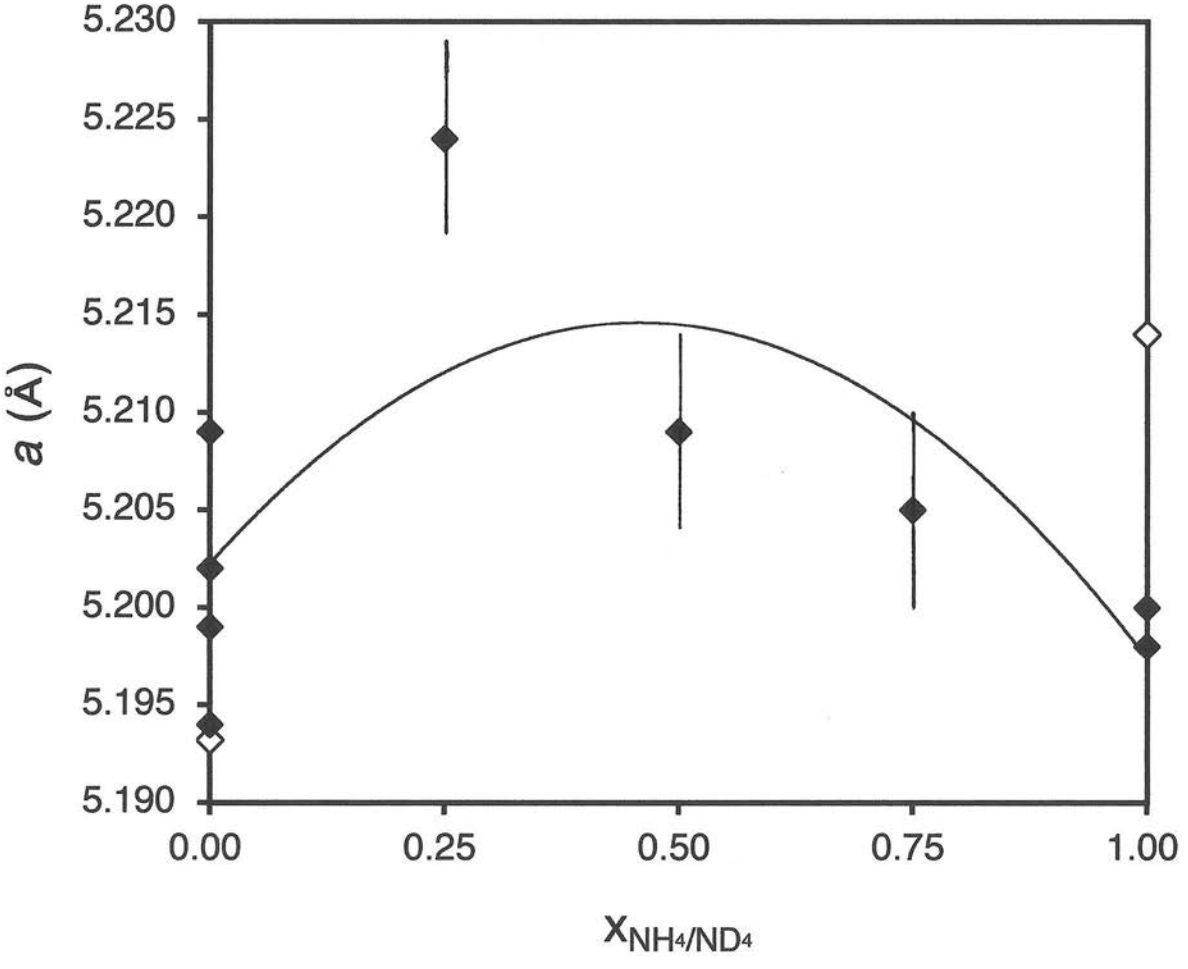
5.230
5.225
5.220
5.215
5.210
5.205
5.200
5.195
5.190
a (Å)
0.00
0.25
0.50
0.75
1.00
X_{NH_4/ND_4}

Fig. 5a

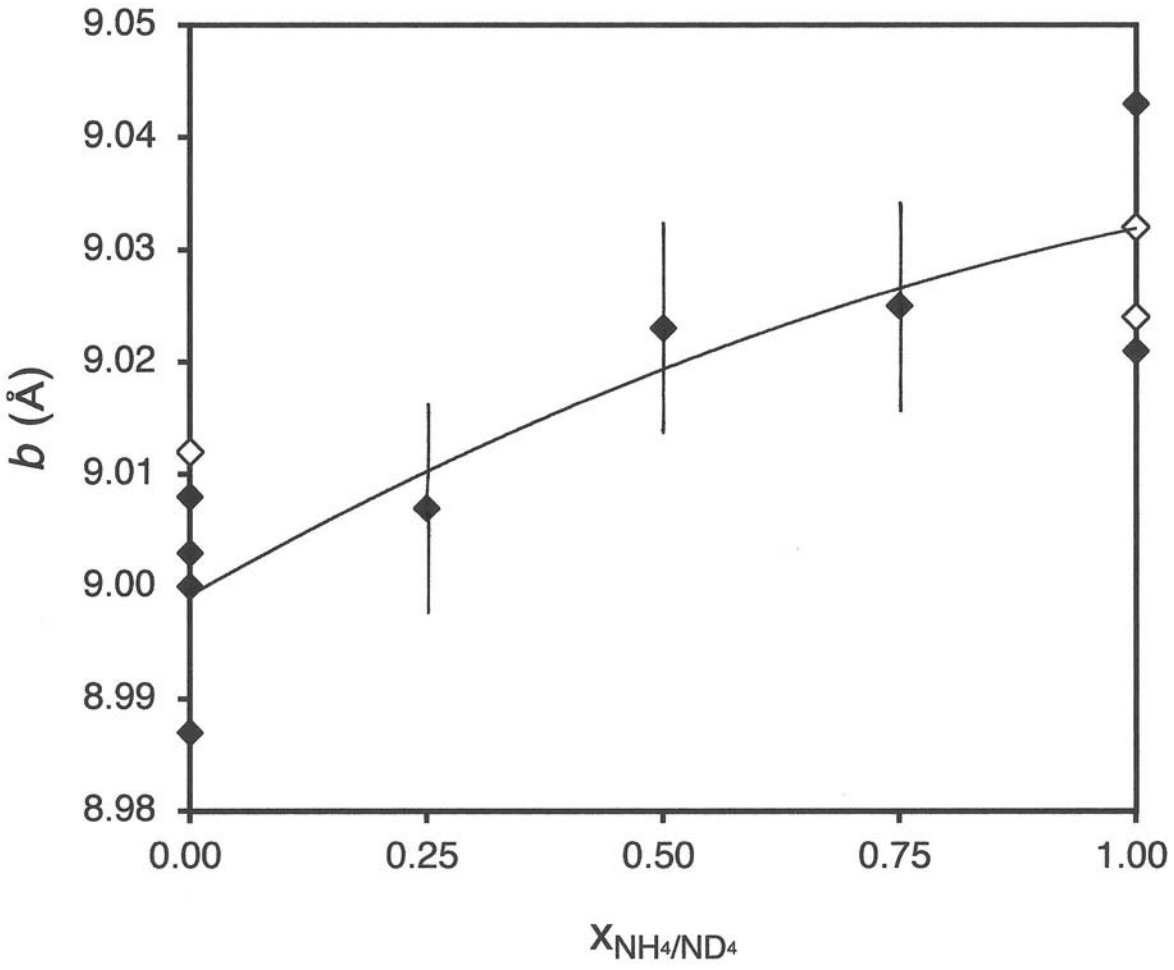

Fig. 5b

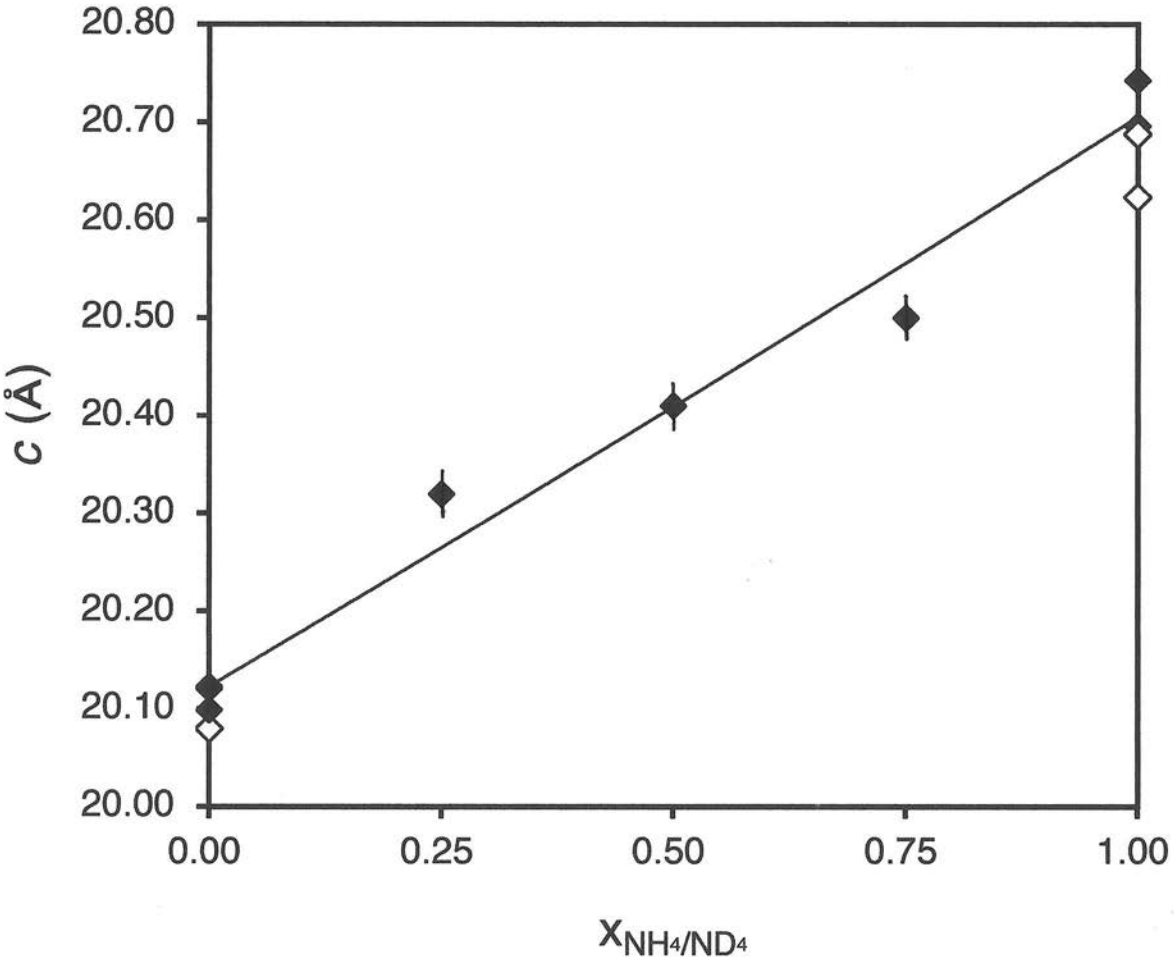
20.80
20.70
20.60
20.50
20.40
20.30
20.20
20.10
20.00
c (Å)
0.00
0.25
0.50
0.75
1.00
X_{NH_4/ND_4}

Fig.5C

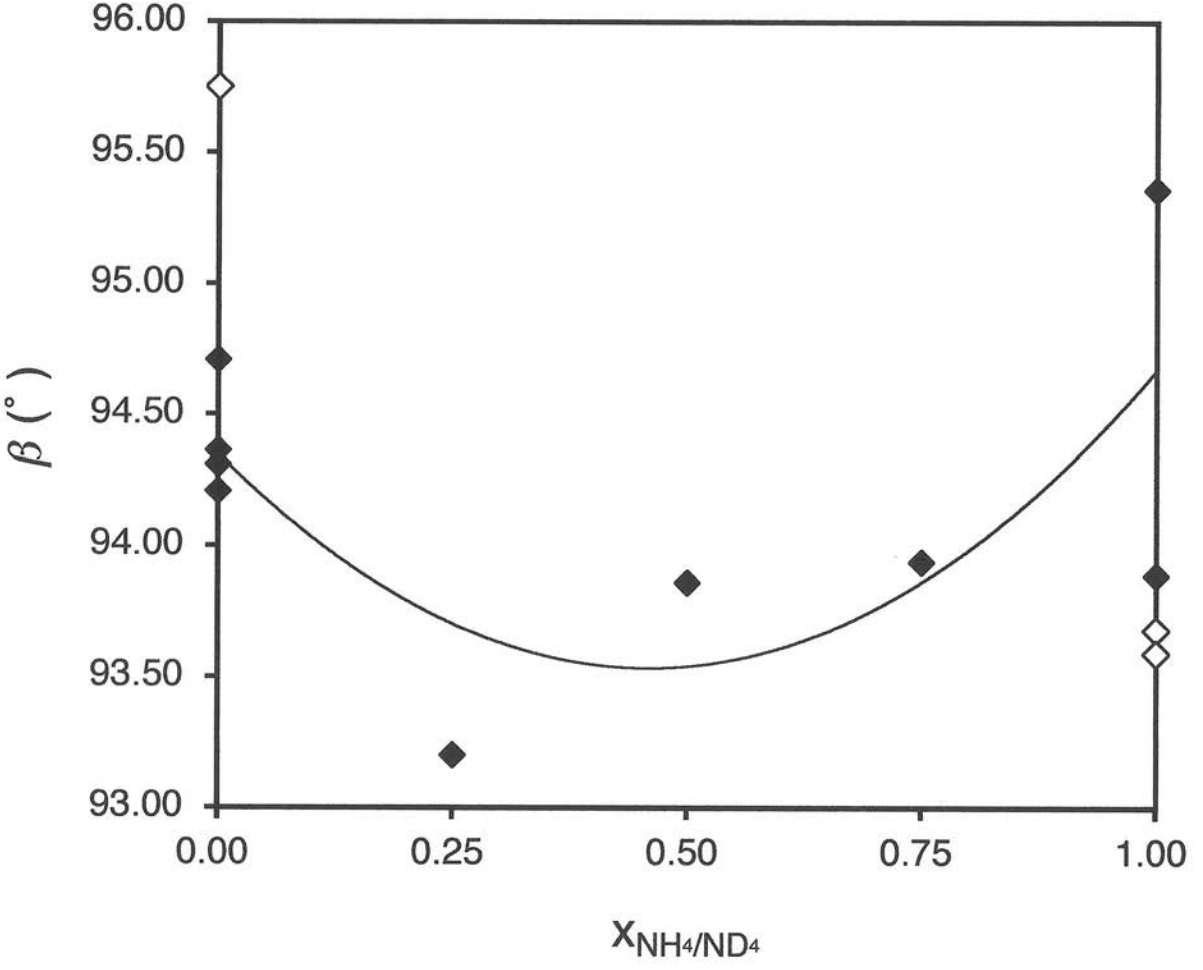
96.00
95.50
95.00
94.50
94.00
93.50
93.00
β (°)
0.00
0.25
0.50
0.75
1.00
X_{NH_4/ND_4}

Fig. 5 d

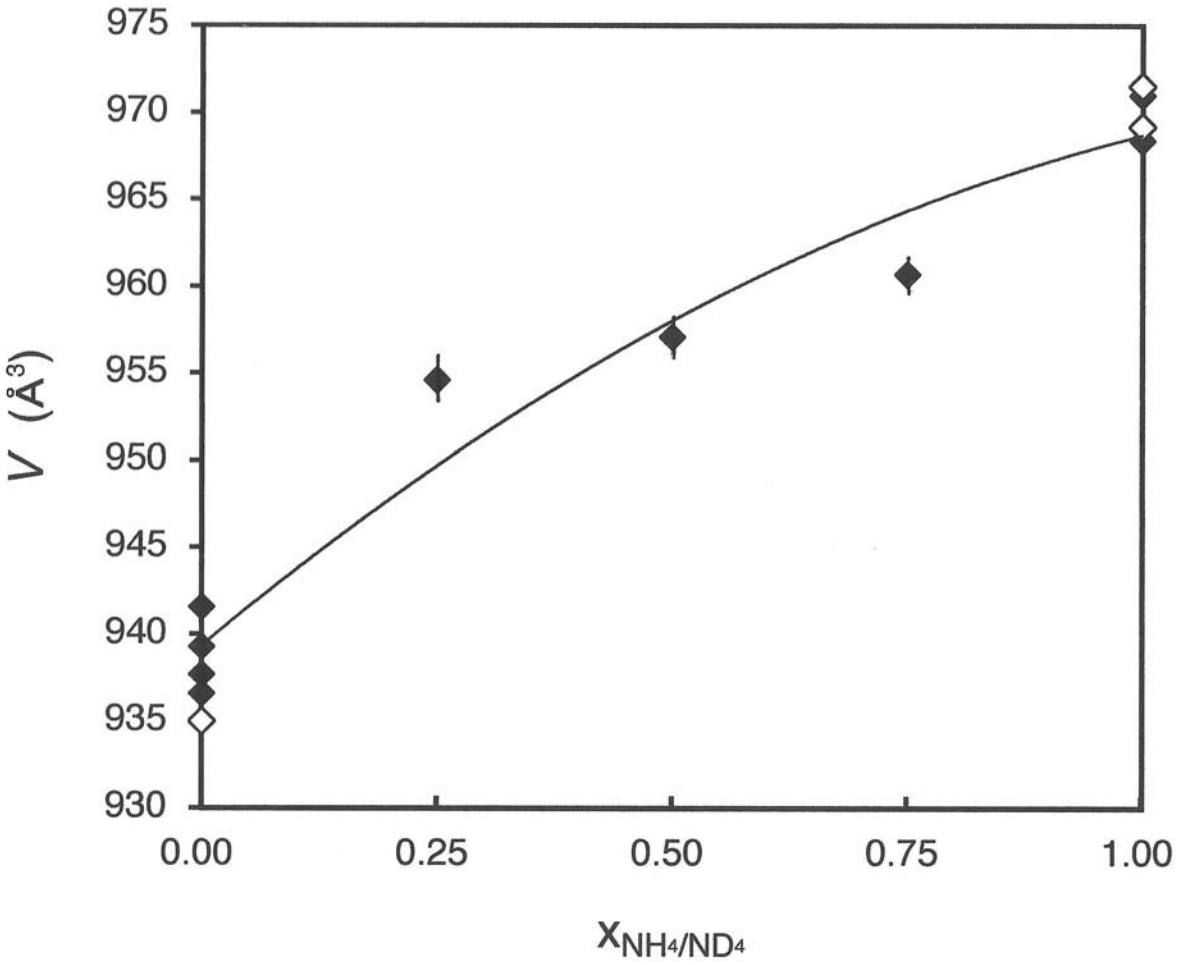
975
970
965
960
955
950
945
940
935
930
V (Å3)
0.00
0.25
0.50
0.75
1.00
XNH4/ND4

Fig. 5e

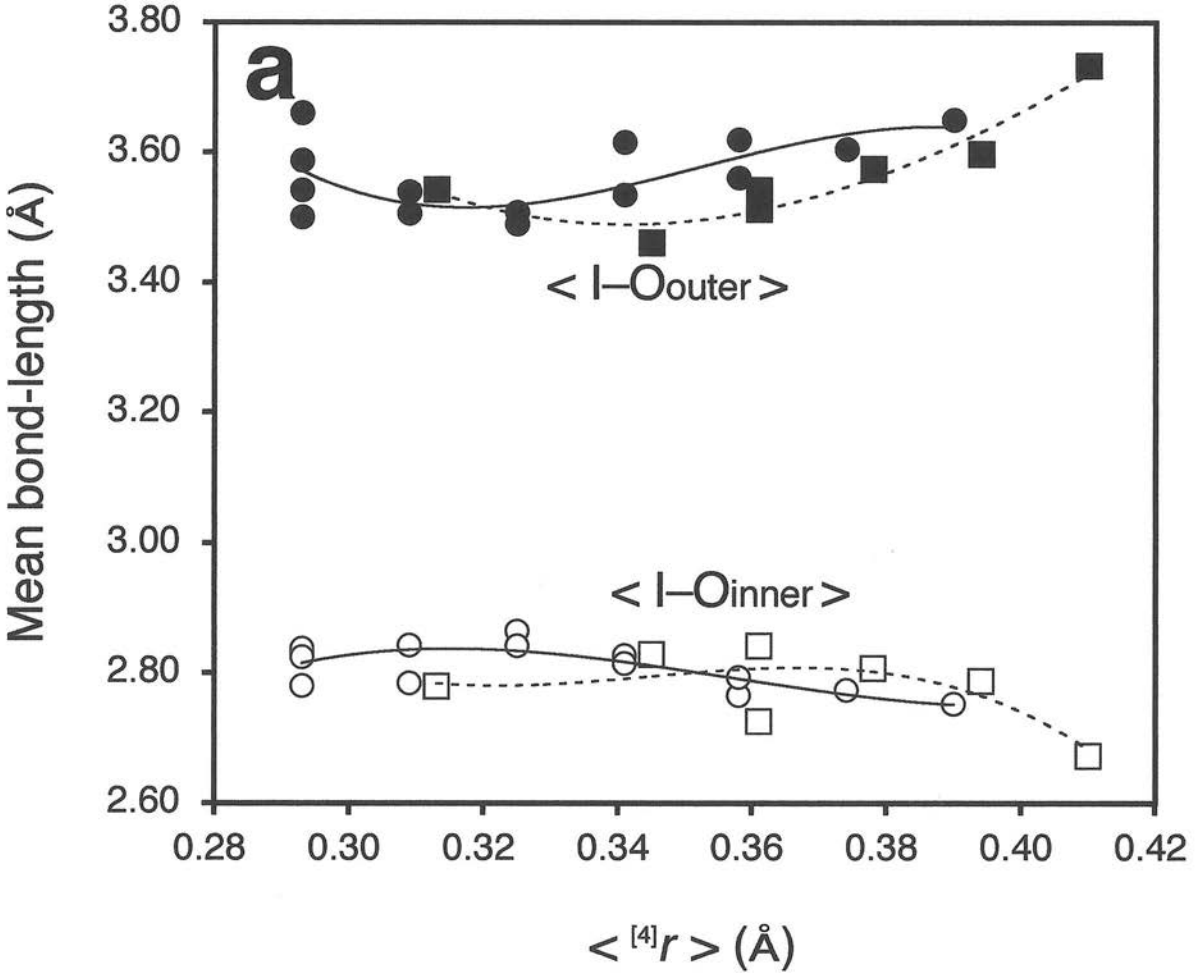
a
Mean bond-length (Å)
3.80
3.60
3.40
3.20
3.00
2.80
2.60
< I–Oouter >
< I–Oinner >
0.28
0.30
0.32
0.34
0.36
0.38
0.40
0.42
< [4]r > (Å)

Fig. 6a

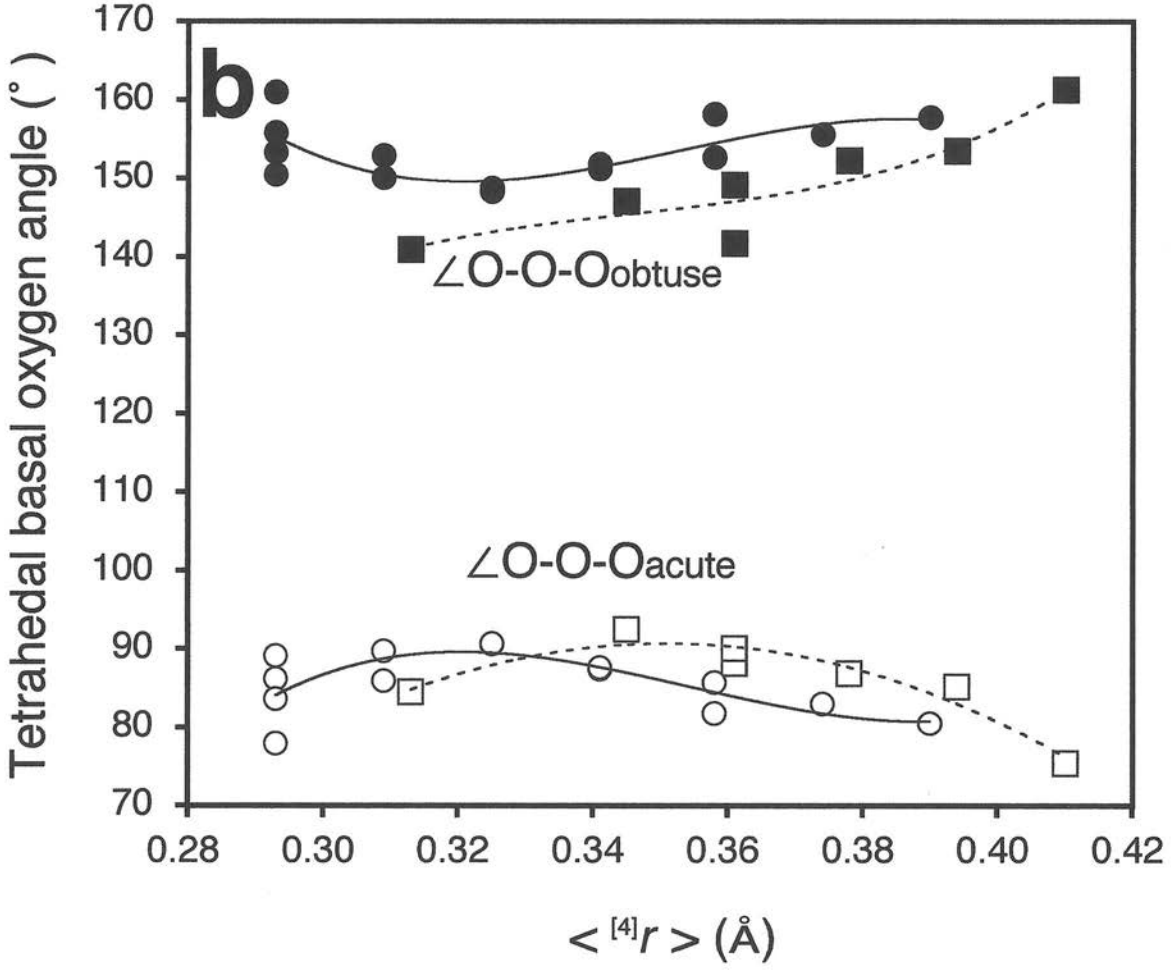
b
Tetrahedal basal oxygen angle (°)
170
160
150
140
130
120
110
100
90
80
70
∠O-O-Oobtuse
∠O-O-Oacute
0.28
0.30
0.32
0.34
0.36
0.38
0.40
0.42
< [4]r > (Å)

Fig.6b

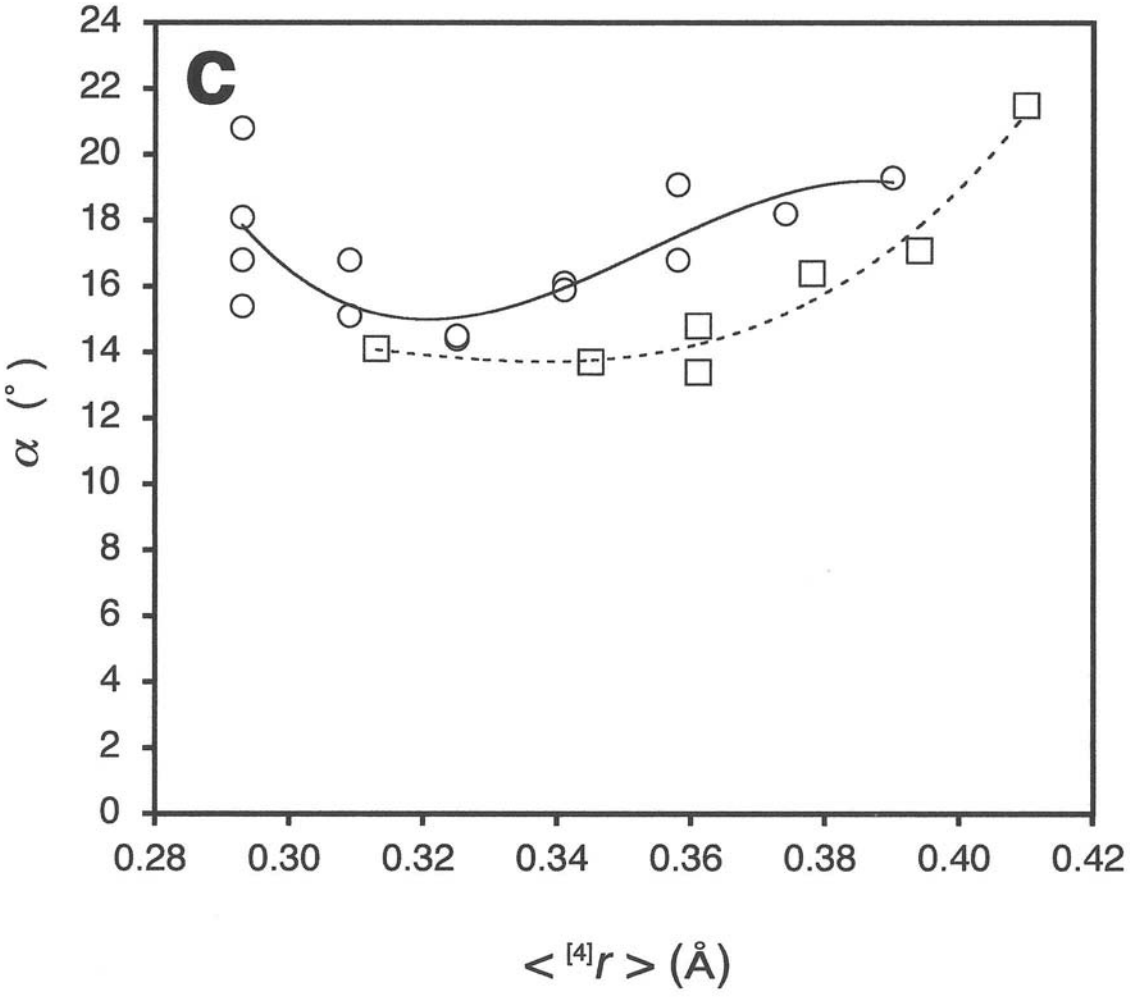
c
24
22
20
18
16
14
12
10
8
6
4
2
0
α (°)
0.28
0.30
0.32
0.34
0.36
0.38
0.40
0.42
< [4]r > (Å)

Fig. 6c

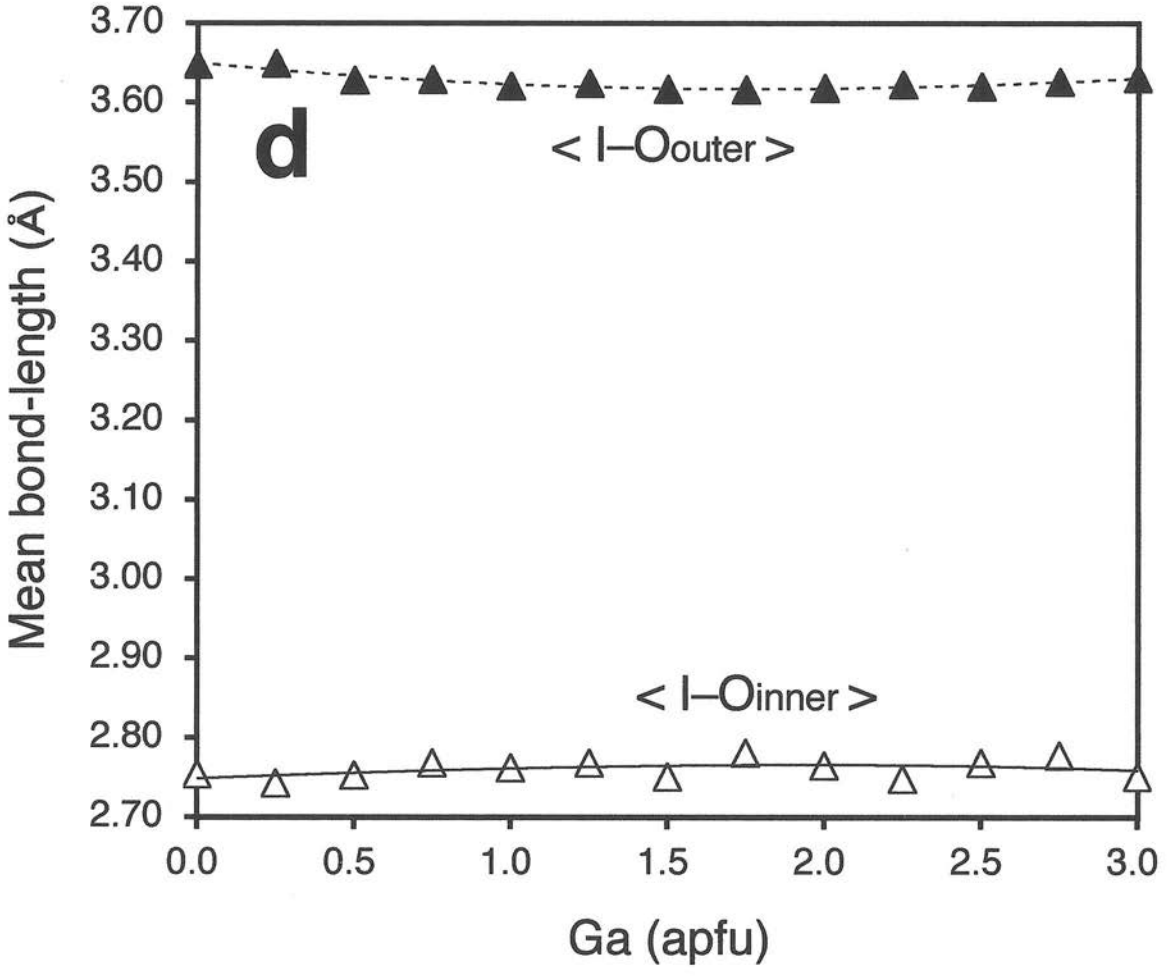
d
< I–Oouter >
< I–Oinner >
Mean bond-length (Å)
3.70
3.60
3.50
3.40
3.30
3.20
3.10
3.00
2.90
2.80
2.70
0.0
0.5
1.0
1.5
2.0
2.5
3.0
Ga (apfu)

Fig. 6d

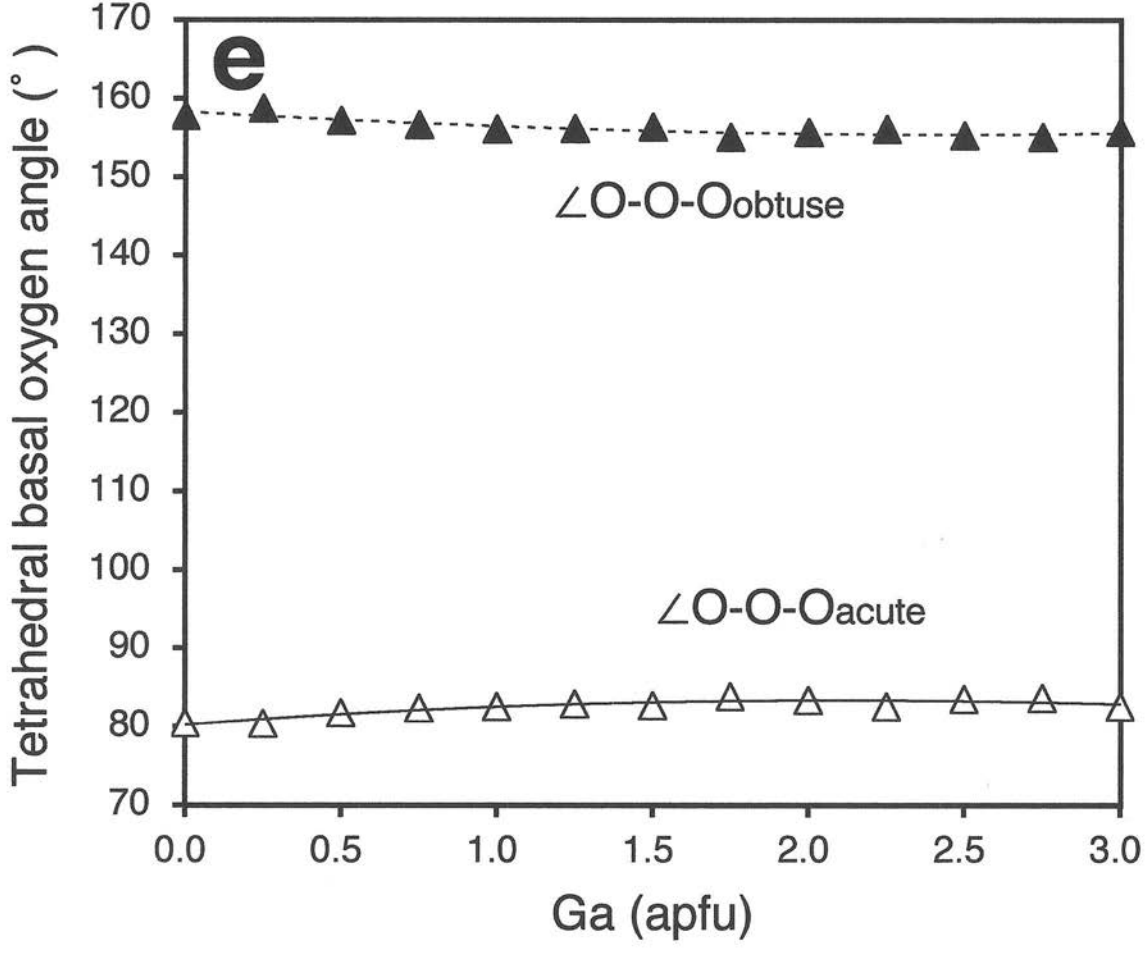
e
Tetrahedral basal oxygen angle (°)
170
160
150
140
130
120
110
100
90
80
70
∠O-O-Oobtuse
∠O-O-Oacute
0.0
0.5
1.0
1.5
2.0
2.5
3.0
Ga (apfu)

Fig. 6e

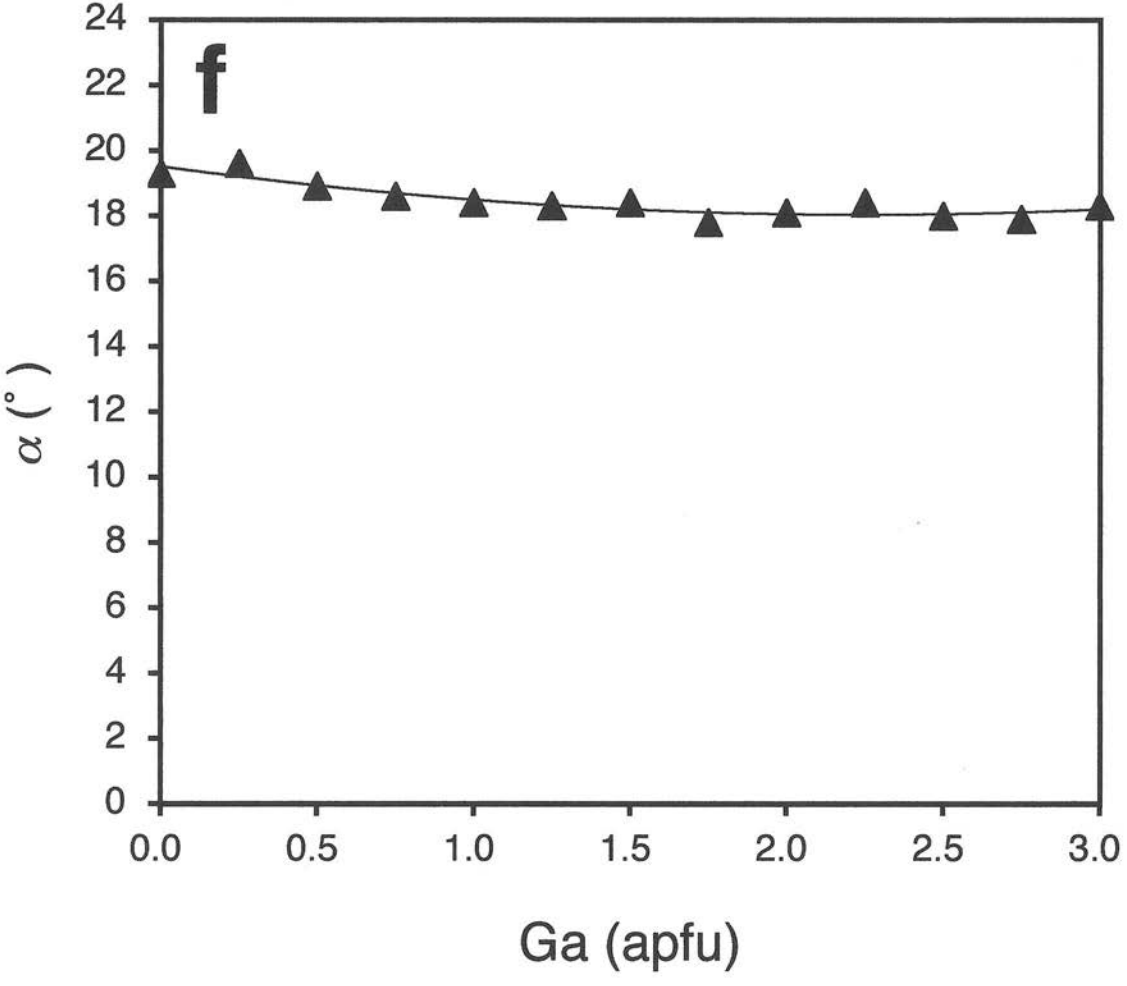

Fig. 6f.

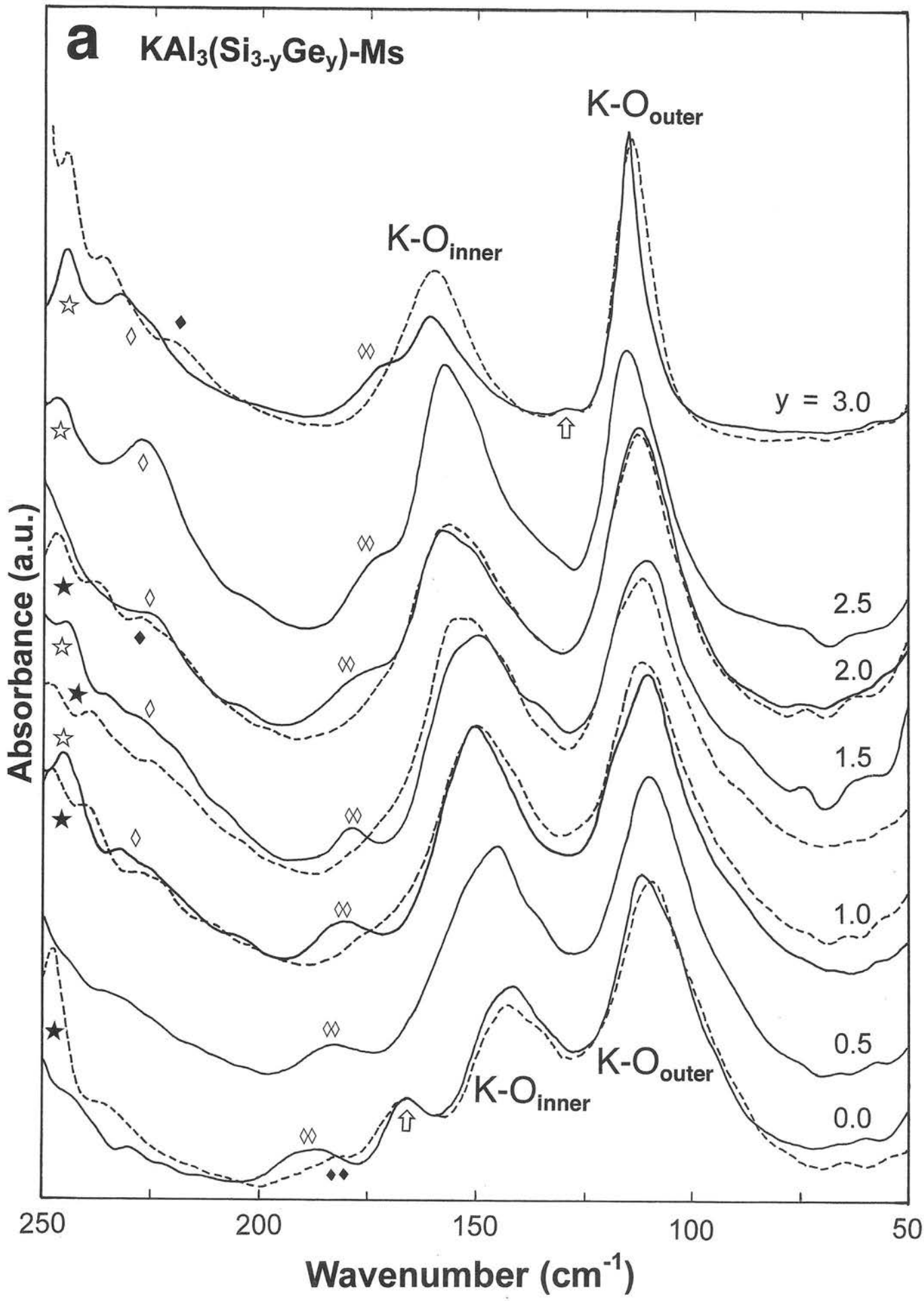
a
KAl3(Si3-yGey)-Ms
K-Oouter
K-Oinner
y = 3.0
2.5
2.0
1.5
1.0
0.5
0.0
Absorbance (a.u.)
250
200
150
100
50
Wavenumber (cm-1)

Fig. 7a

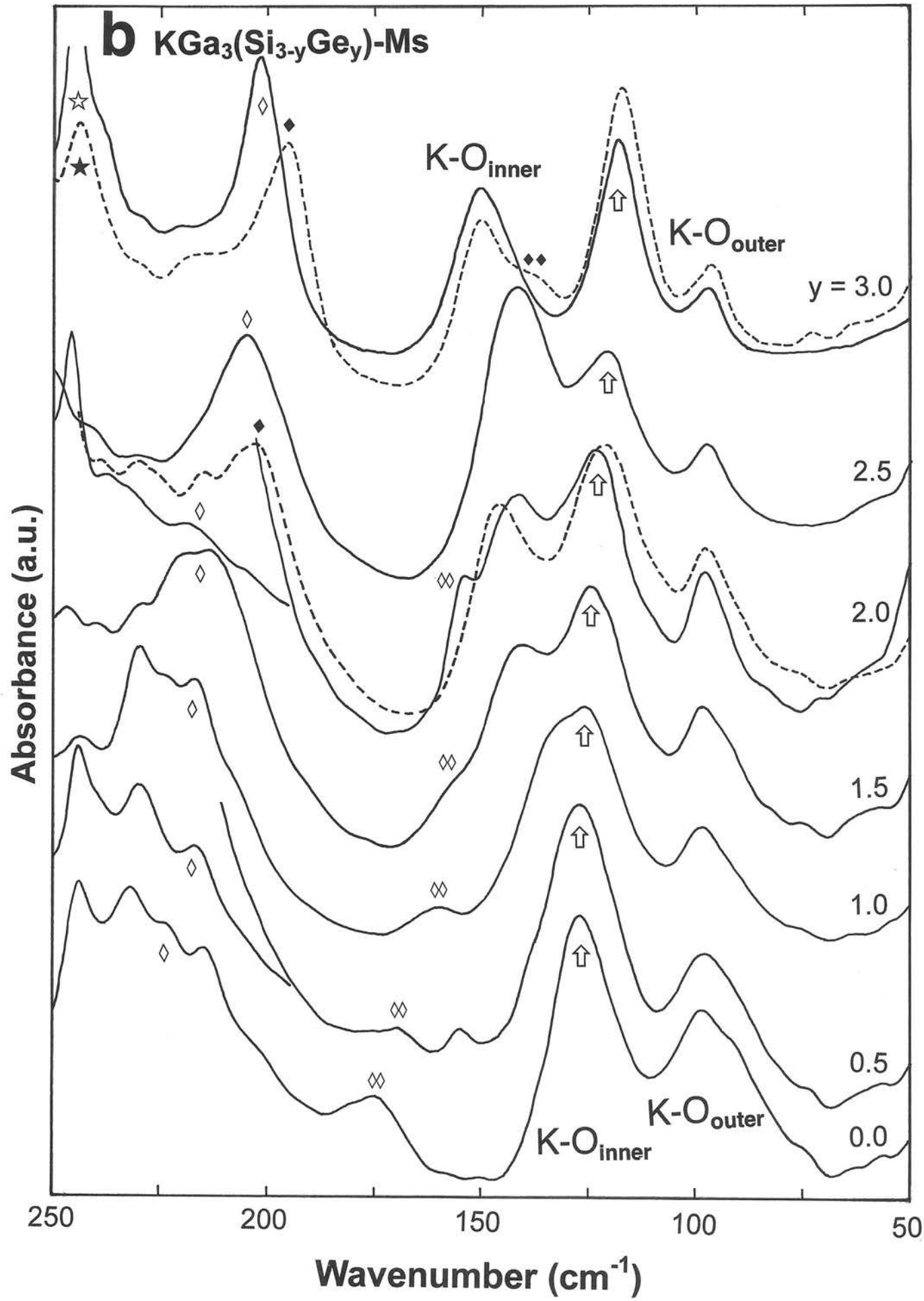
b KGa3(Si3-yGey)-Ms
K-Oinner
K-Oouter
y = 3.0
2.5
2.0
1.5
1.0
0.5
0.0
Absorbance (a.u.)
250
200
150
100
50
Wavenumber (cm-1)

Fig.7b

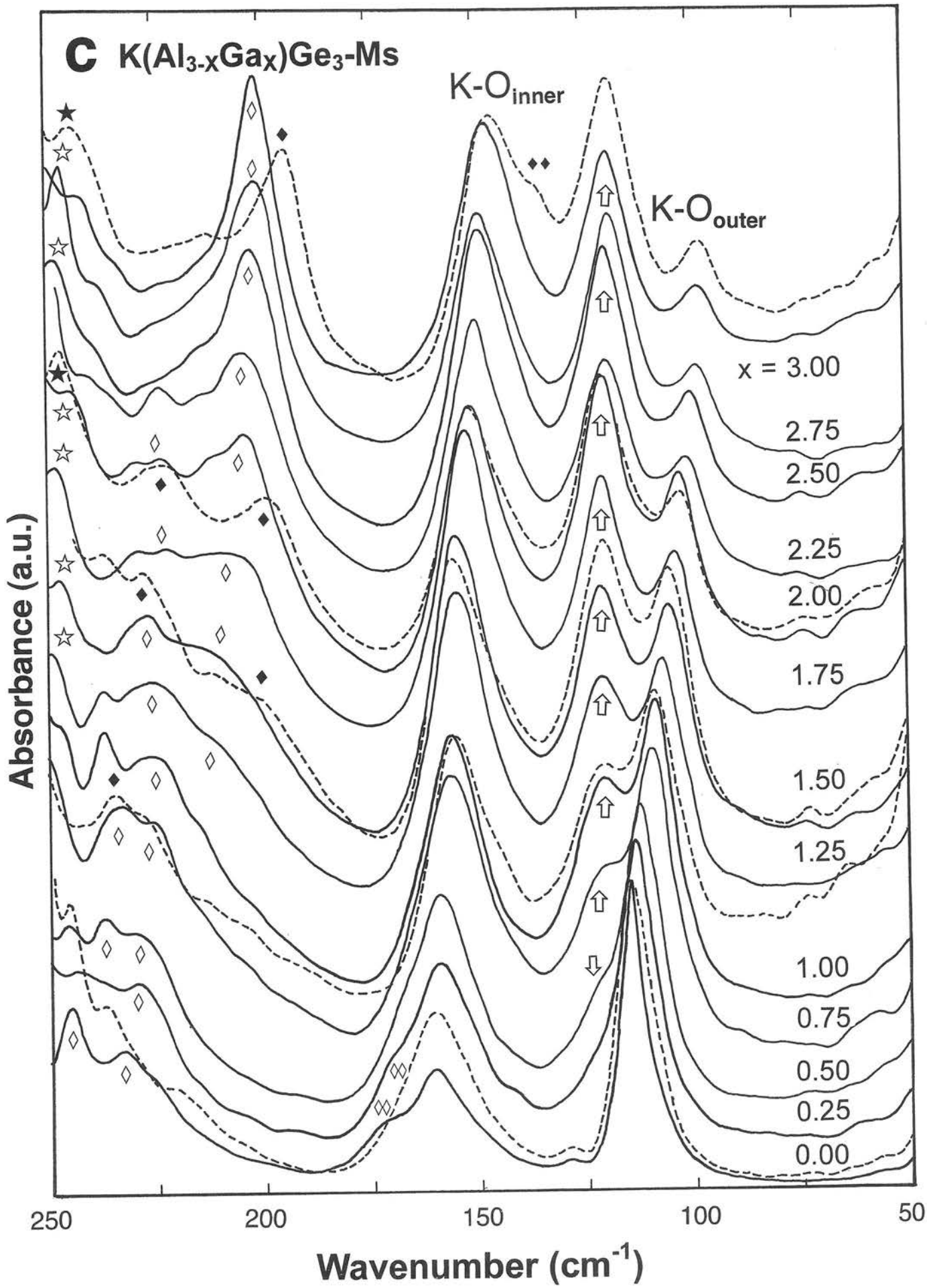
C K(Al3-xGax)Ge3-Ms
K-Oinner
K-Outer
x = 3.00
2.75
2.50
2.25
2.00
1.75
1.50
1.25
1.00
0.75
0.50
0.25
0.00
Absorbance (a.u.)
250
200
150
100
50
Wavenumber (cm-1)

Fig. 7c

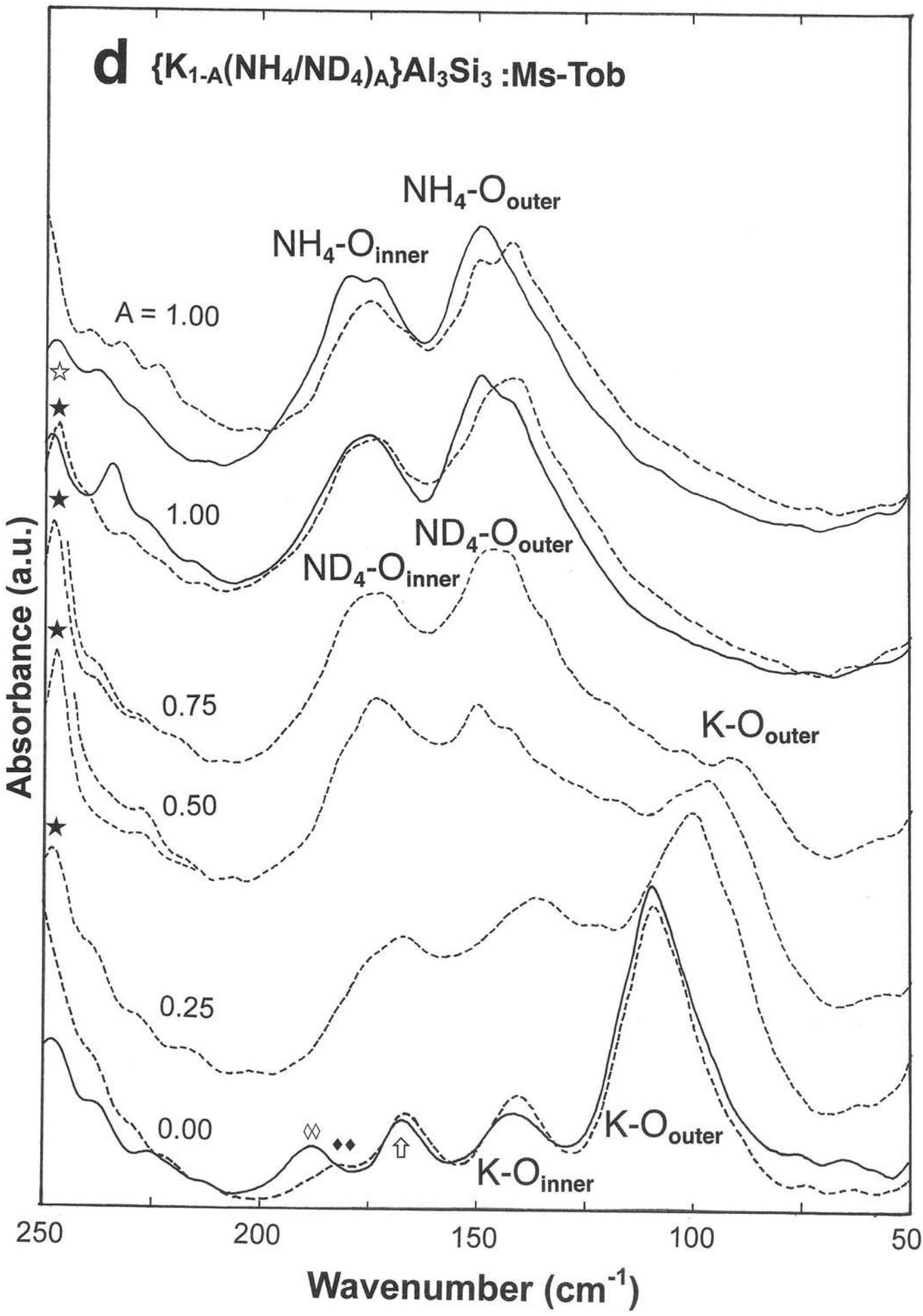
d {K1-A(NH4/ND4)A}Al3Si3 :Ms-Tob
NH4-Oouter
NH4-Oinner
A = 1.00
1.00
ND4-Oouter
ND4-Oinner
0.75
K-Oouter
0.50
0.25
0.00
K-Oouter
K-Oinner
Absorbance (a.u.)
250
200
150
100
50
Wavenumber (cm-1)

Fig. 7d

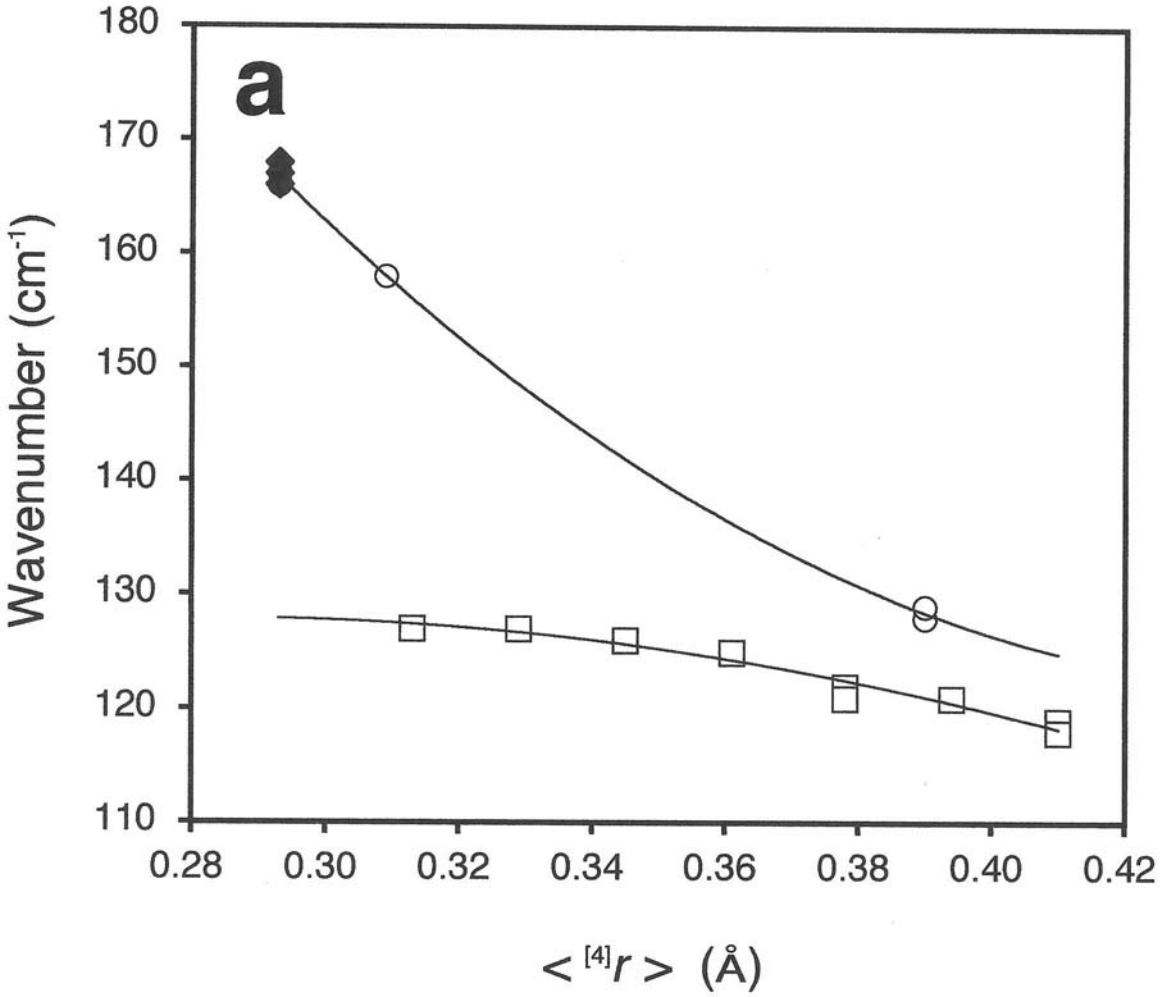
a
180
170
160
150
140
130
120
110
Wavenumber (cm-1)
0.28
0.30
0.32
0.34
0.36
0.38
0.40
0.42
< [4]r > (Å)

Fig 8a

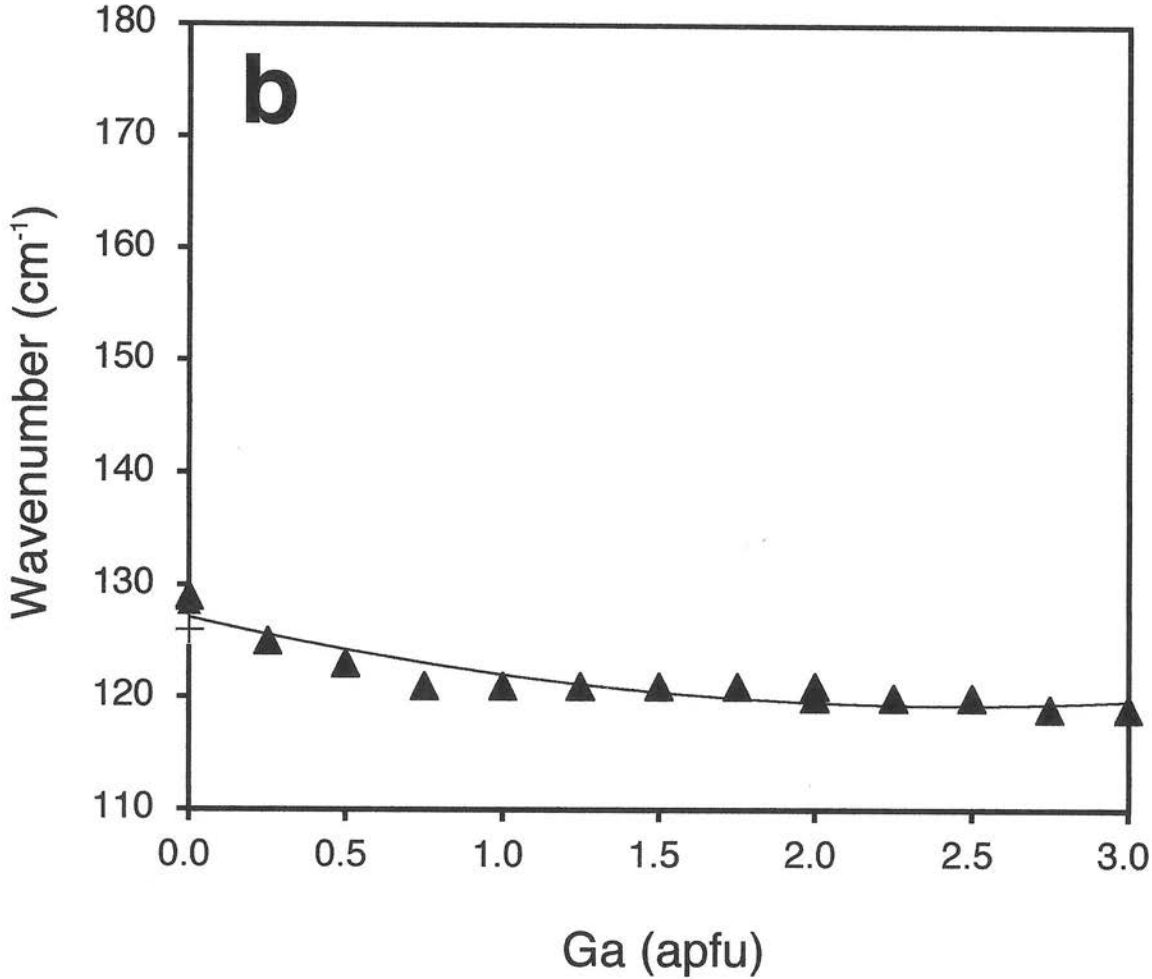
b
180
170
160
150
140
130
120
110
Wavenumber (cm-1)
0.0
0.5
1.0
1.5
2.0
2.5
3.0
Ga (apfu)

Fig.8b

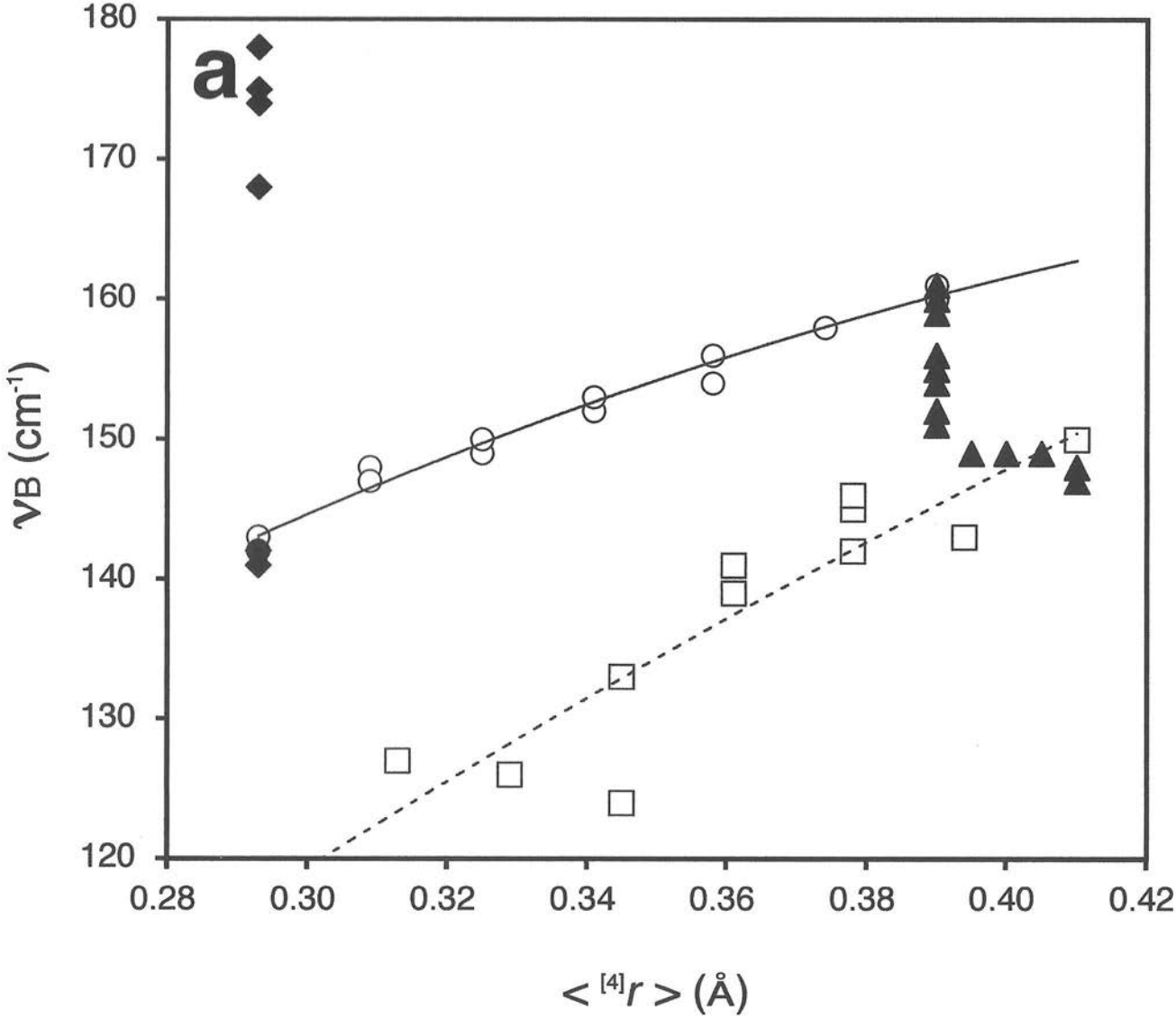
a
180
170
160
150
140
130
120
ν_B (cm^{-1})
0.28
0.30
0.32
0.34
0.36
0.38
0.40
0.42
$< {}^{[4]}r >$ (Å)

Fig-9a

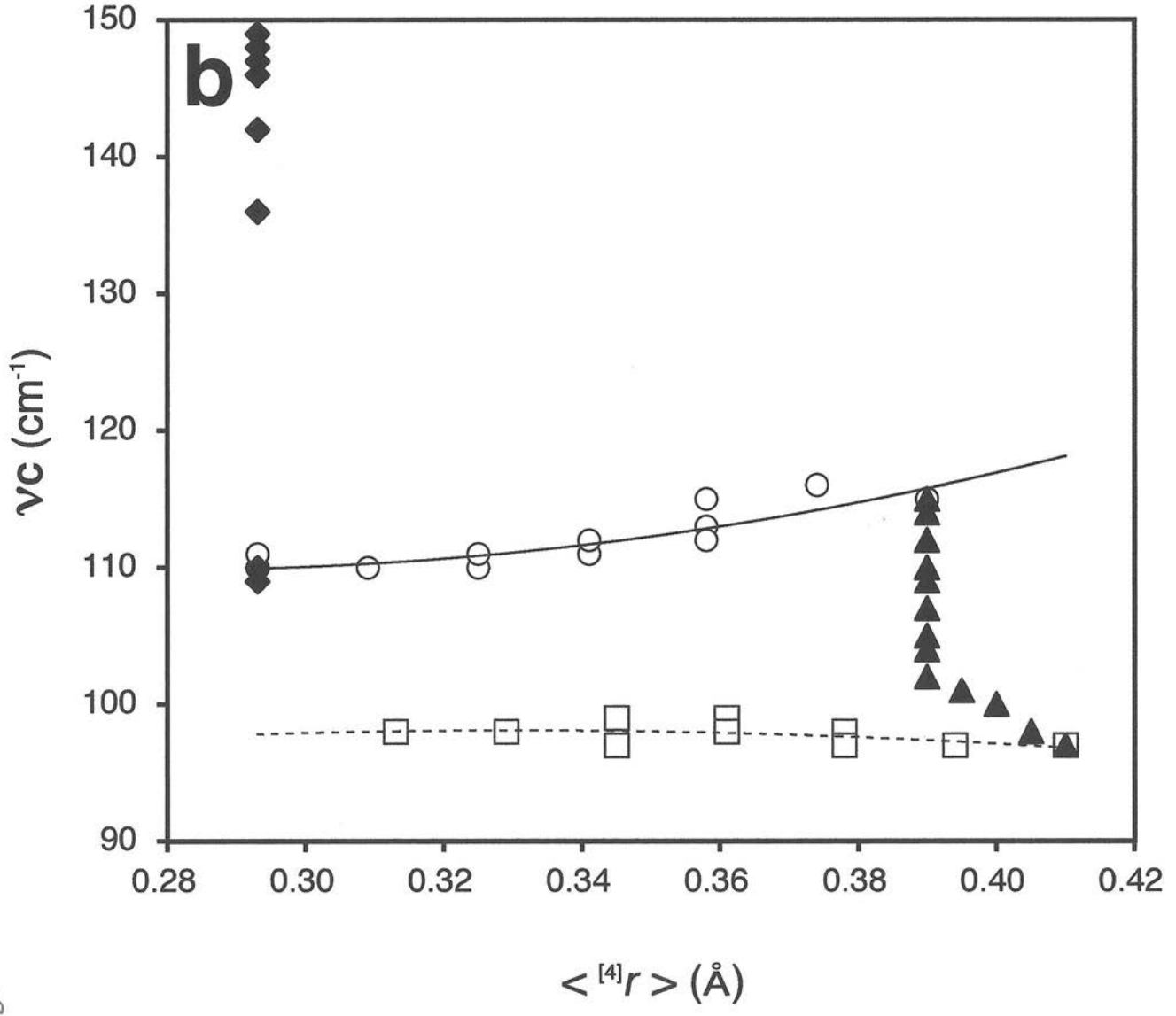
b
150
140
130
120
110
100
90
νc (cm-1)
0.28
0.30
0.32
0.34
0.36
0.38
0.40
0.42
< [4]r > (Å)

Fig. 9b

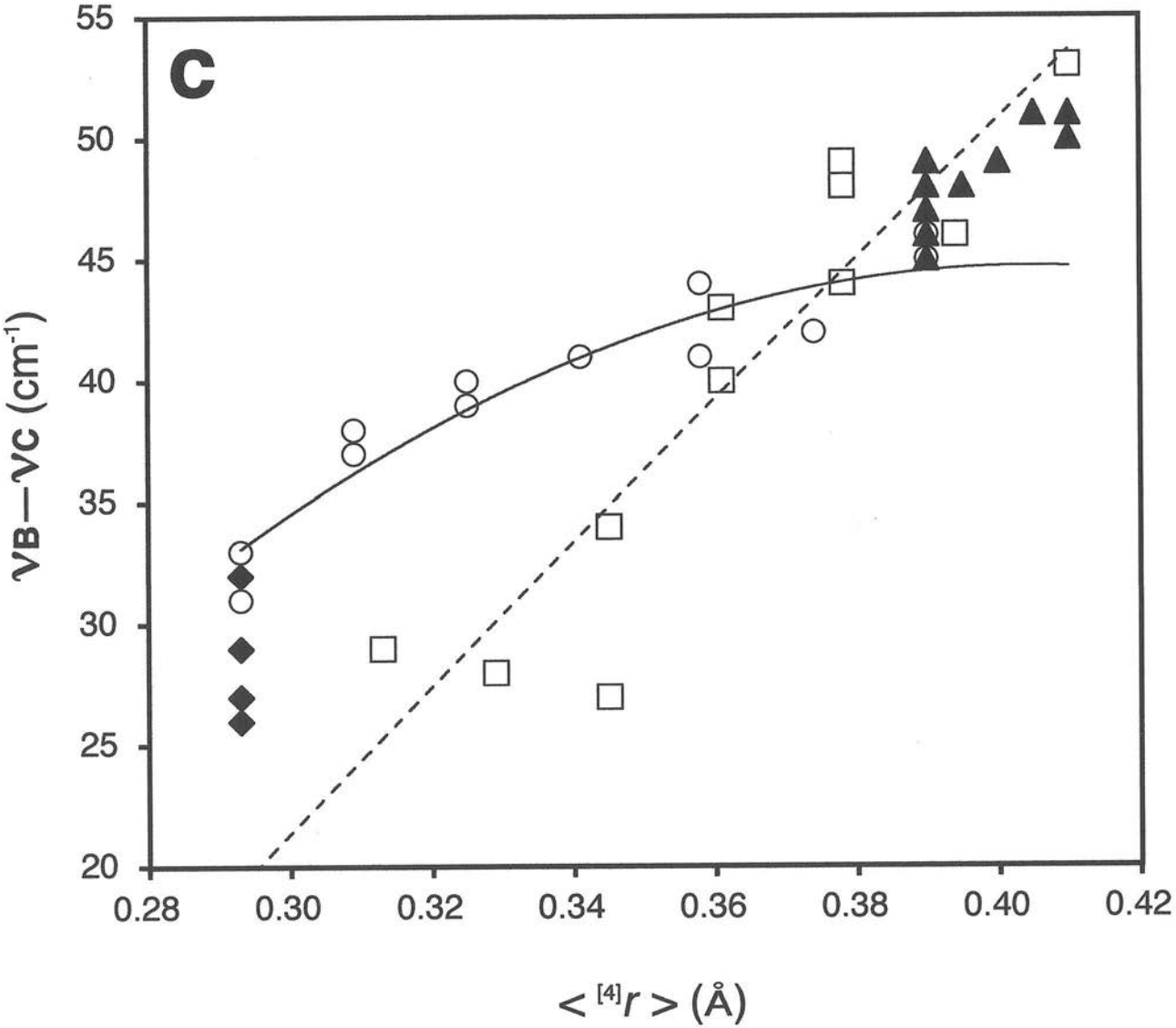
C
55
50
45
40
35
30
25
20
0.28
0.30
0.32
0.34
0.36
0.38
0.40
0.42
νB—νC (cm-1)
< [4]r > (Å)

Fig. 9c

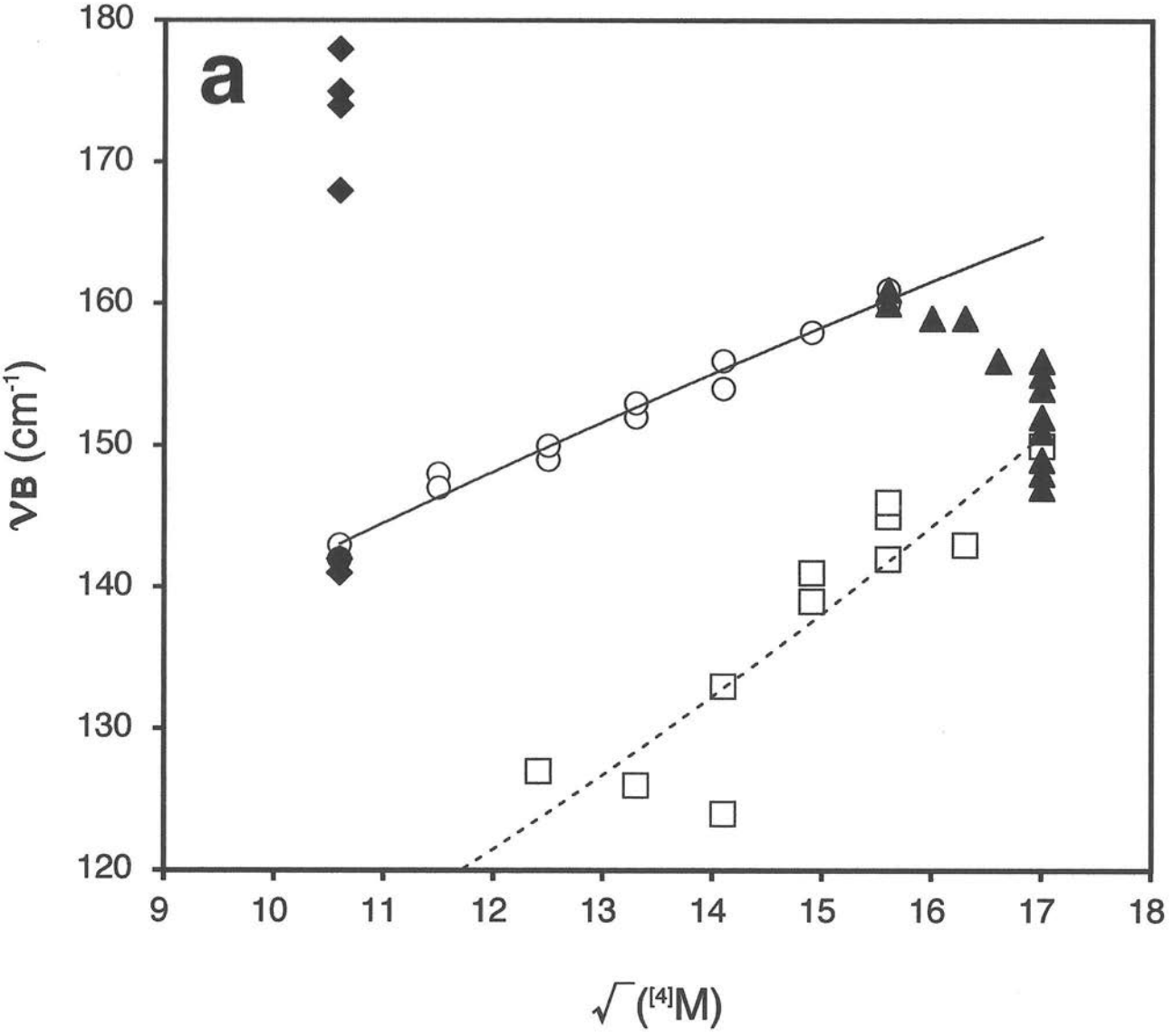

Fig. 10a

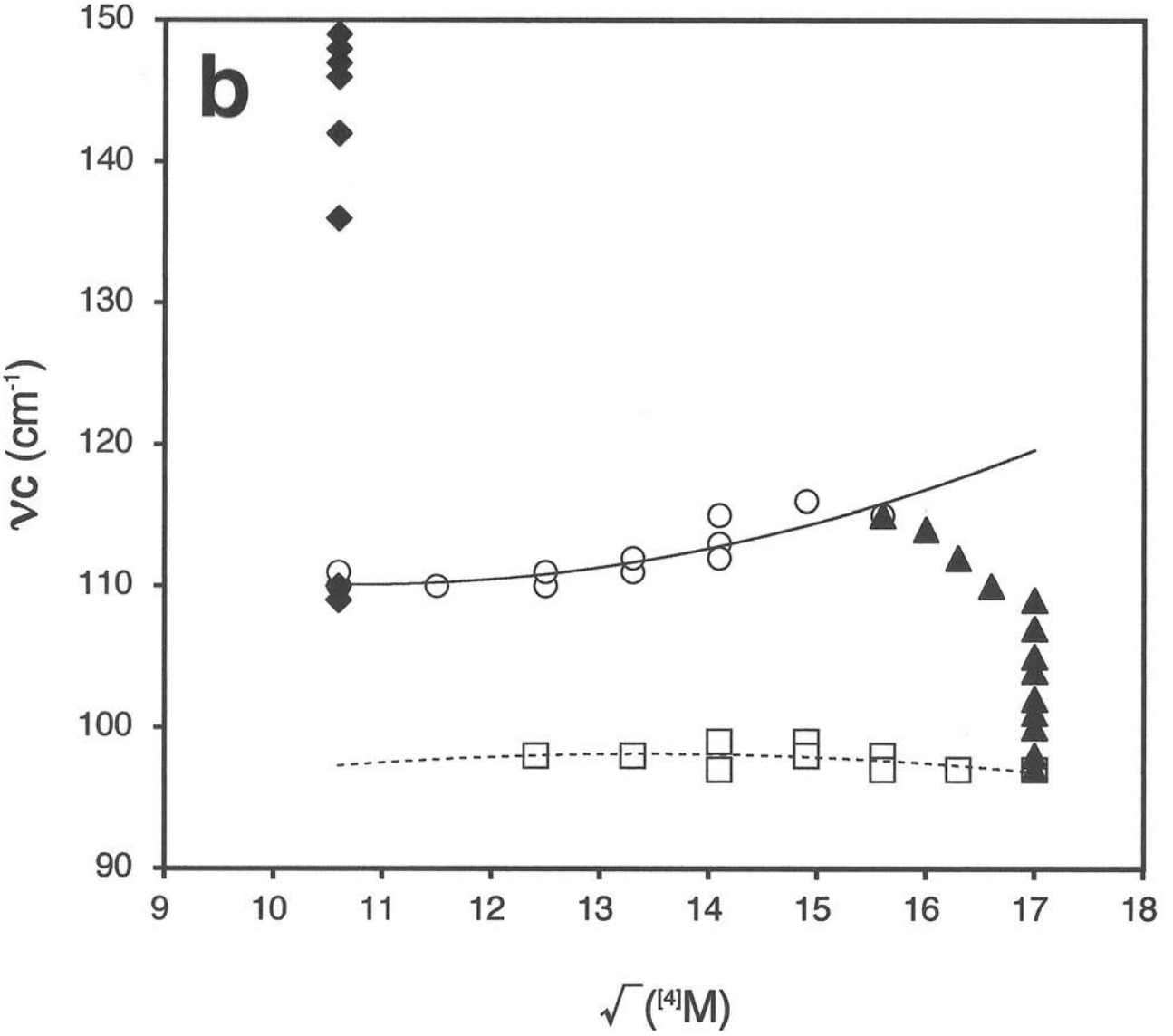

Fig. 10b

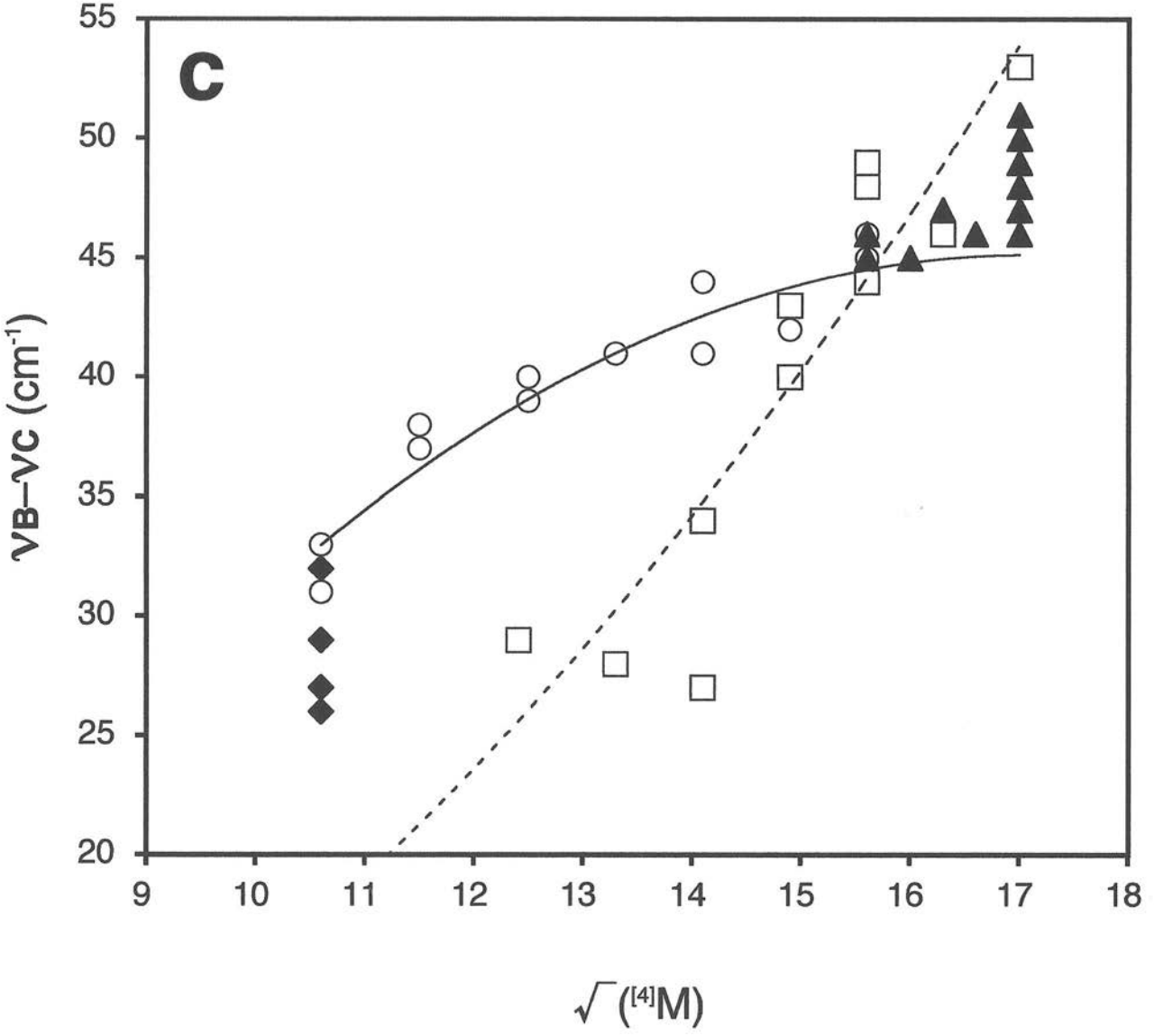

Fig. 10C

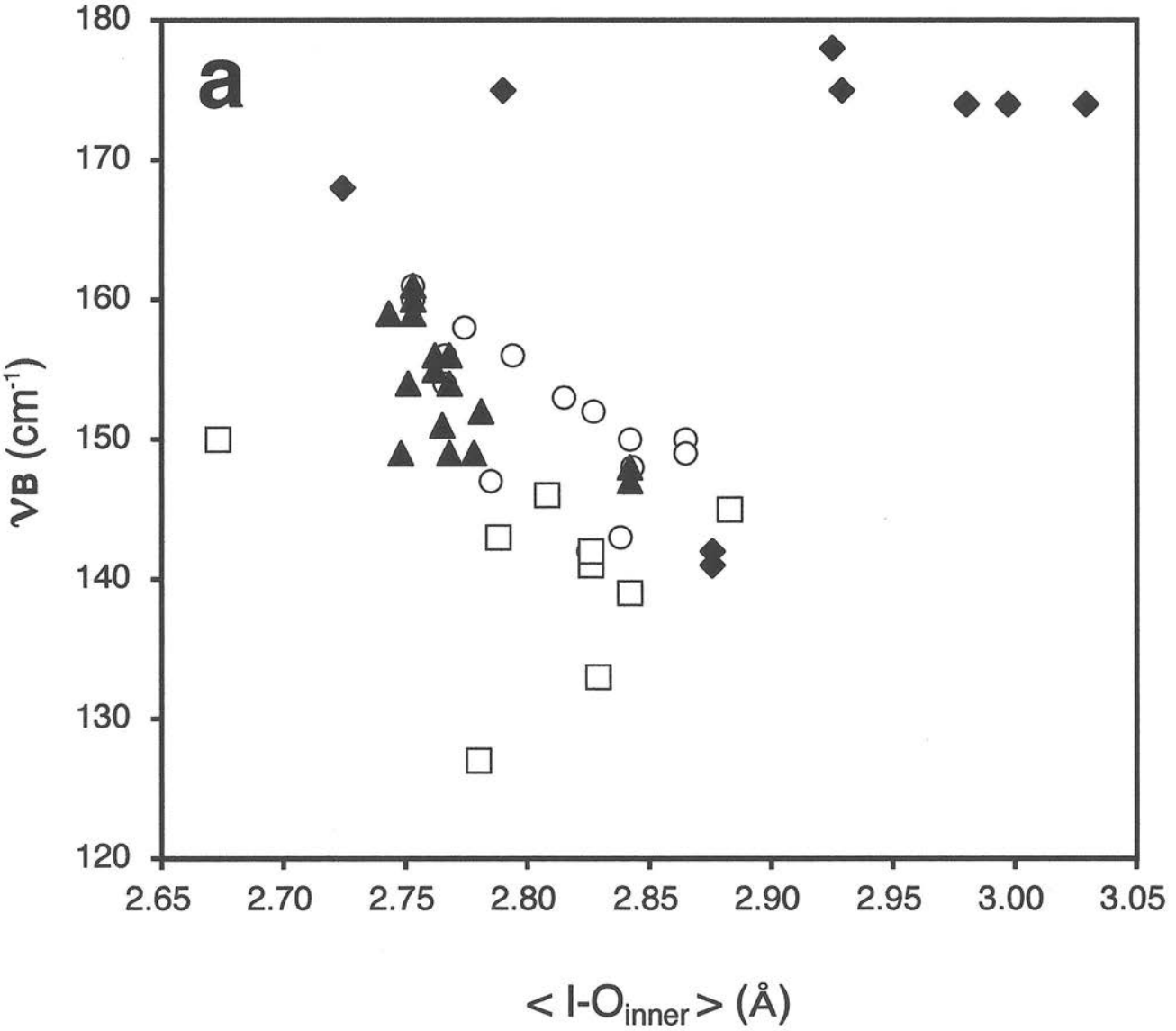
a
180
170
160
150
140
130
120
ν_B (cm^{-1})
2.65
2.70
2.75
2.80
2.85
2.90
2.95
3.00
3.05
< I-O$_{inner}$ > (Å)

Fig. 11a

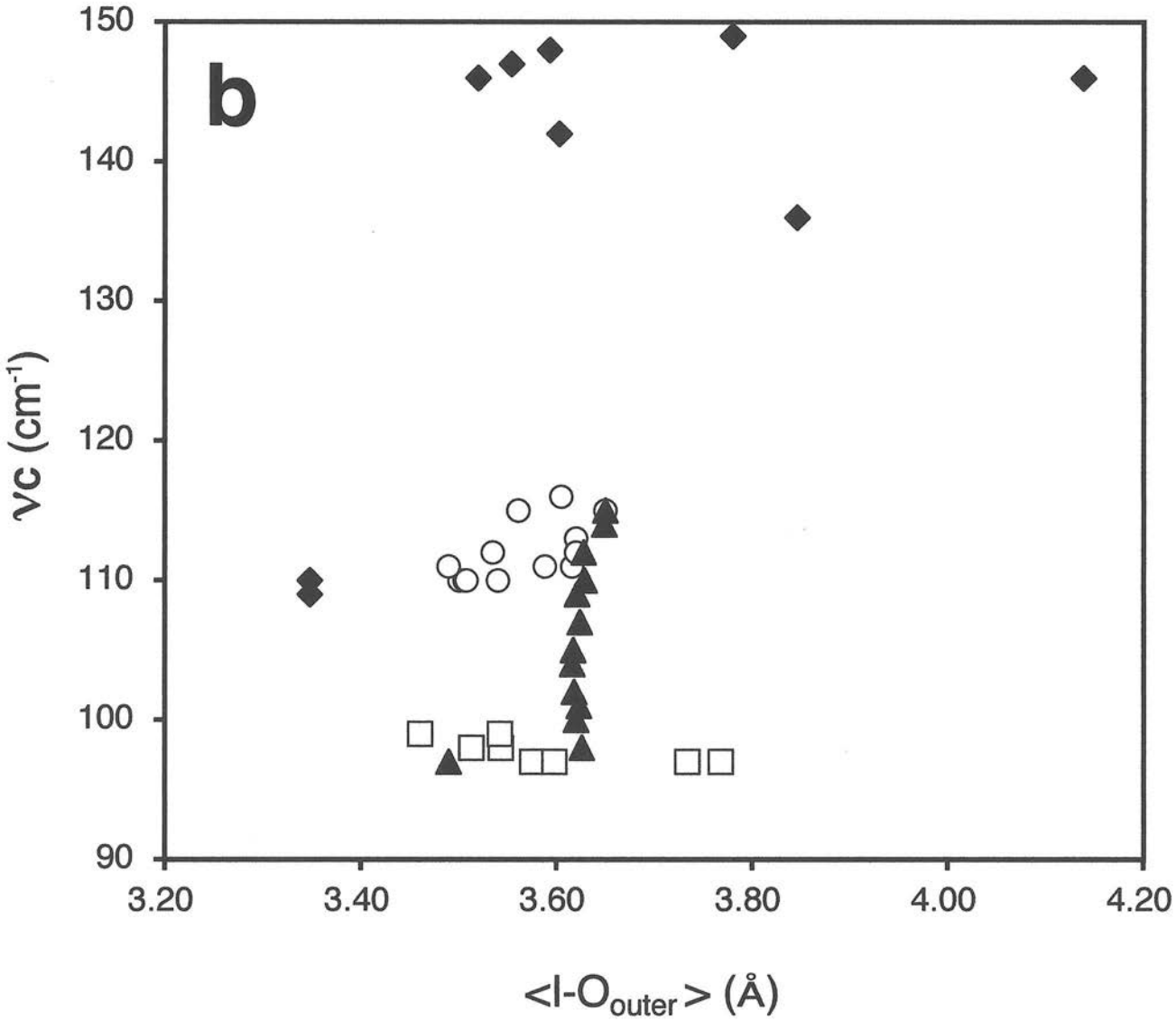
b
150
140
130
120
110
100
90
νc (cm-1)
3.20
3.40
3.60
3.80
4.00
4.20
<I-Oouter> (Å)

Fig 11b

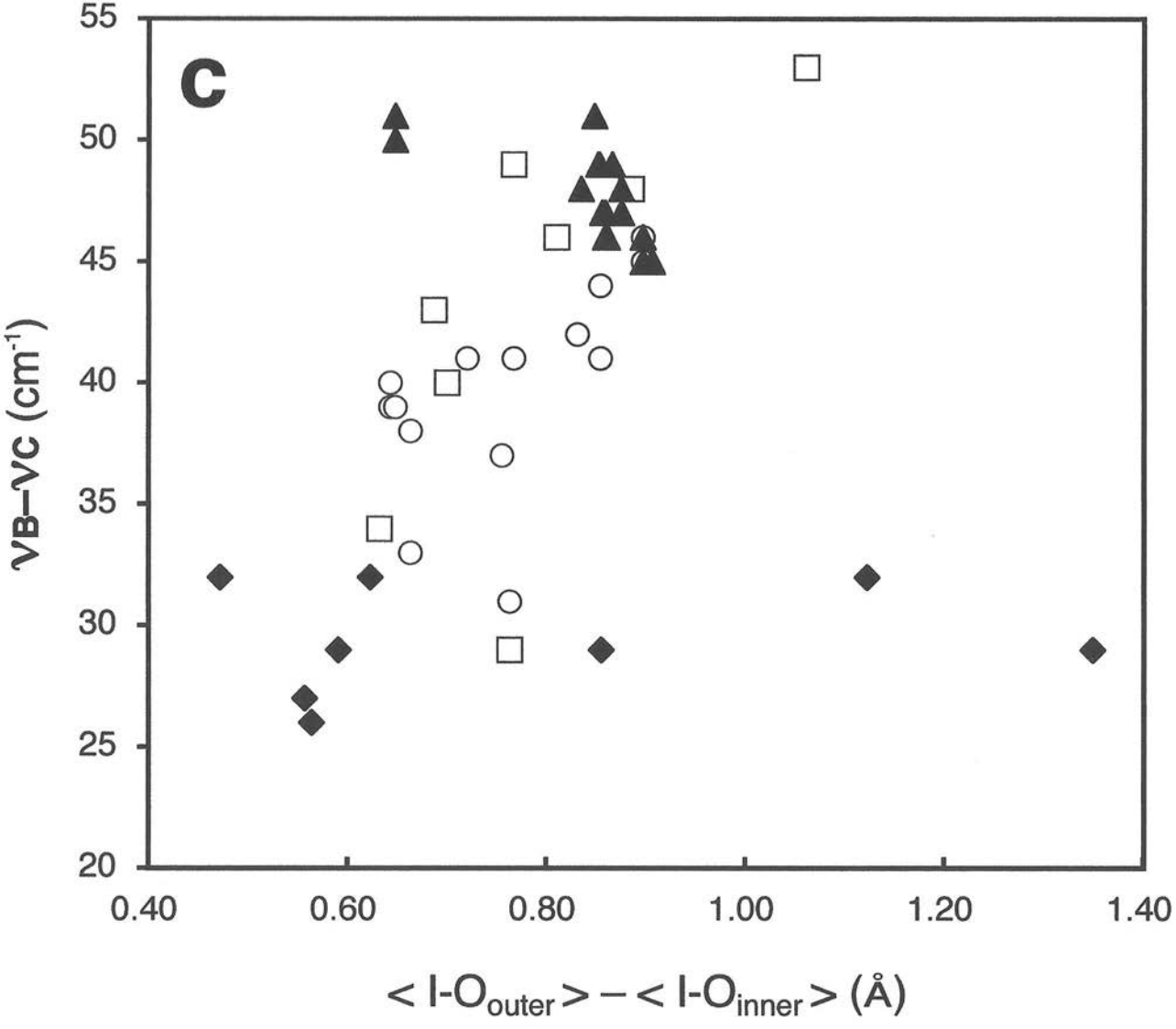
C
55
50
45
40
35
30
25
20
0.40
0.60
0.80
1.00
1.20
1.40
νB–νC (cm-1)
< I-Oouter > – < I-Oinner > (Å)

Fig. IIc

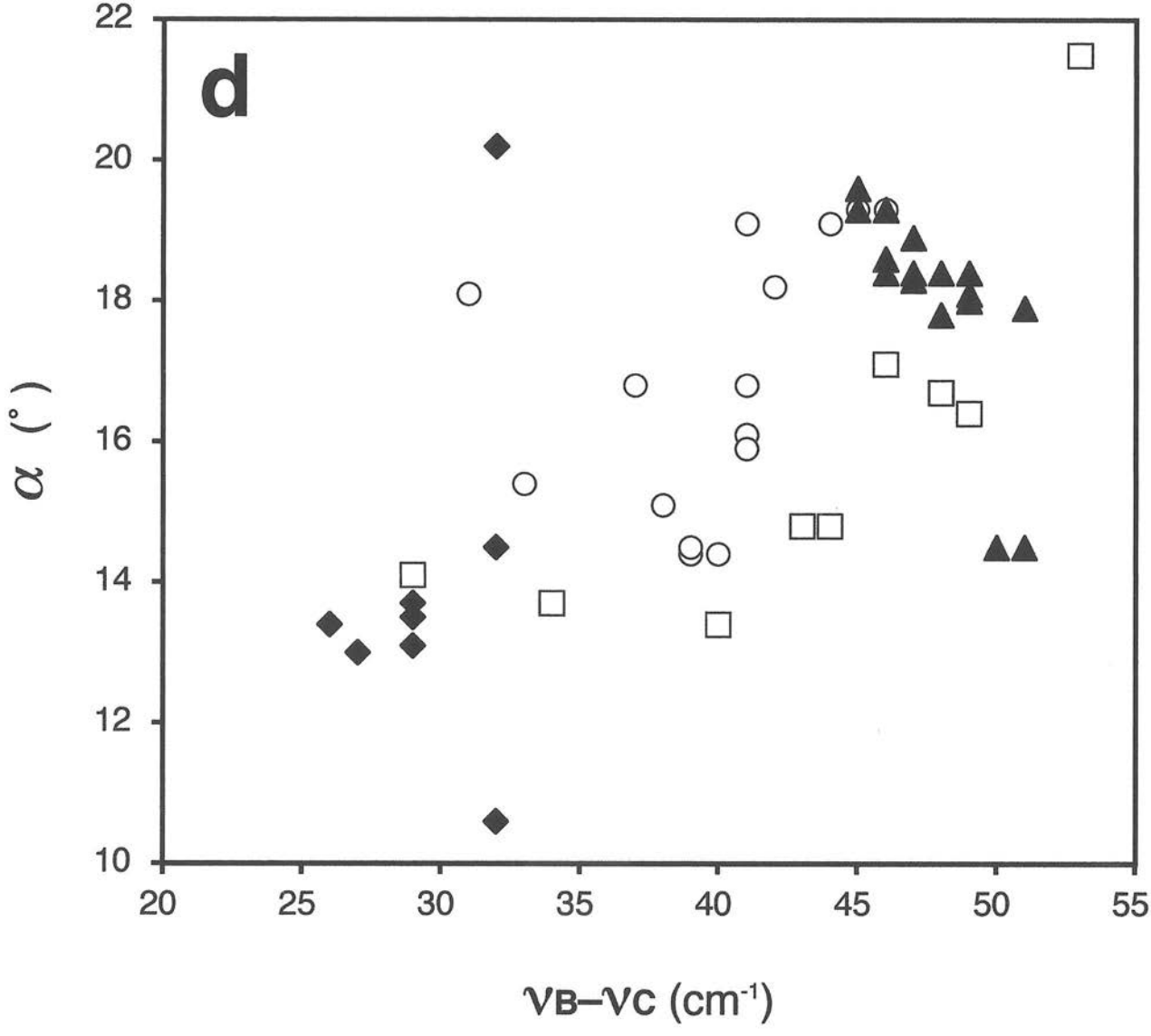

Fig. 11d